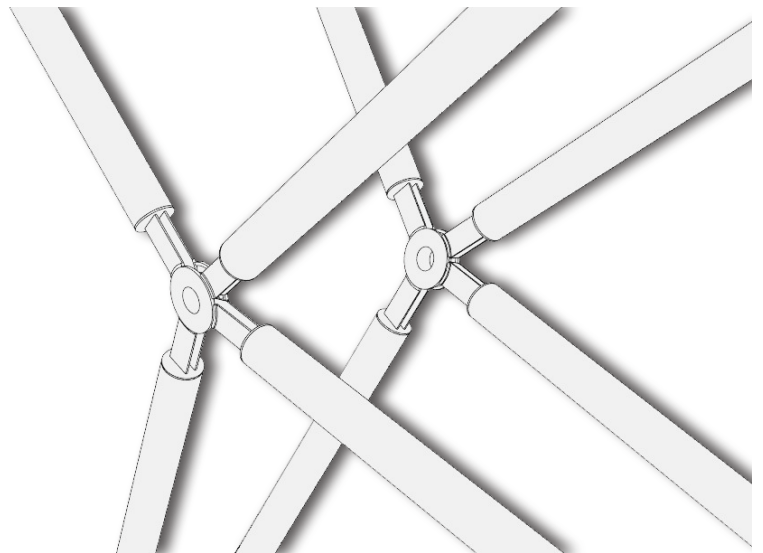
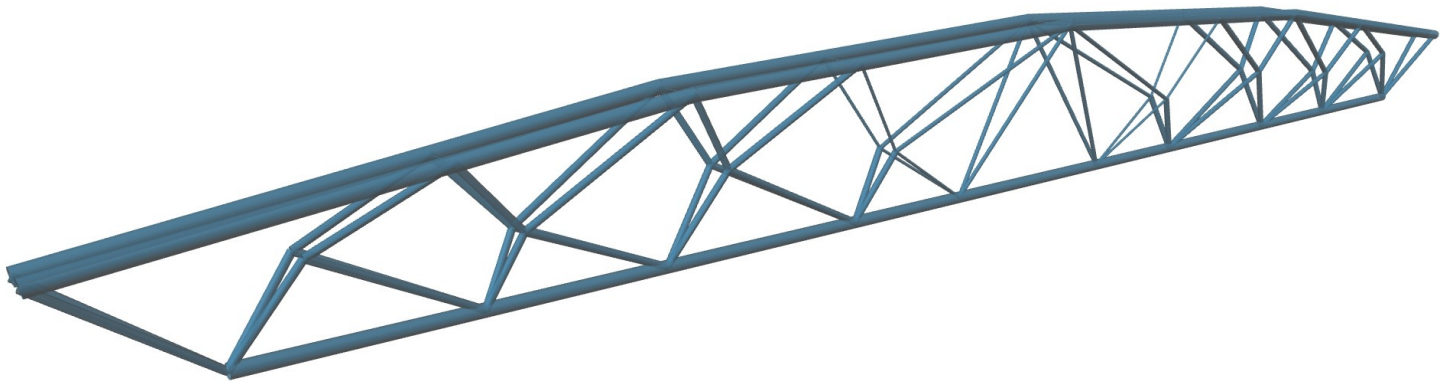


# Design, analysis and Application of Innovative Connections for Optimized Steel Trusses

**Structural behavior of innovative joints based on snap-fit connection**



# DESIGN, ANALYSIS AND APPLICATION OF INNOVATIVE CONNECTIONS FOR OPTIMIZED STEEL TRUSSES

Structural behavior of innovative joints based on snap-fit connection

by

JOSÉ ABAD GONZÁLEZ

To obtain the degree of  
**Master of Science**  
in Civil Engineering, track Building Engineering  
October 2020

at the Delft University of Technology  
to be defended publicly on Friday October 16, 2020 at 15:00.

Student number:	4898427	
E-mail:	jose.abadgon1@gmail.com	
Graduation committee:	Dr.ir. H.R. Schipper	TU Delft
	ir. LPL van der Linden	TU Delft
	Dr. F. Messali	TU Delft

## COMMITTEE INFORMATION

### STUDENT

**Name:** J.A. Abad Gonzalez  
**Institution:** Delft University of Technology  
**Address:** Hugo de Grootstraat 124  
2613TX, Delft  
**Telephone:** 06 30332389  
**E-mail:** jose.abadgon1@gmail.com  
**Student Nr:** 4898427

### GRADUATION COMMITTEE

**Name:** Dr.ir. H.R. Schipper  
Committee chair  
**Institution:** Delft University of Technology  
**Section:** Applied Mechanics  
**Address:** Stevinweg 1, Office 6.48  
2628 CN, Delft  
**Telephone:** +31 1527 89933  
**E-mail:** H.R.schipper@tudelft.nl

**Name:** Dr. F. Messali  
**Institution:** Delft University of Technology  
**Section:** Applied Mechanics  
**Address:** Stevinweg 1, Office 6.50.1  
2628 CN, Delft  
**Telephone:** +31 1527 82529  
**E-mail:** F.Messali@tudelft.nl

**Name:** Ir. LPL van der Linden  
**Institution:** Delft University of Technology  
**Section:** Applied Mechanics  
**Address:** Stevinweg 1, Office 6.48  
2628 CN, Delft  
**Telephone:** +31 1527 89933  
**E-mail:** L.P.L.vanderLinden@tudelft.nl

## PREFACE

This report is the result of my graduation research project "Design, Analysis and Application of Innovative Connections for Optimized Steel Trusses". This is the last step towards fulfilling the requirements needed to obtain the title Master of Science in Civil Engineering (Building Engineering track) at the Faculty of Civil Engineering at Delft University of Technology.

This research project was conducted at the Department of Building Engineering from TU Delft.

Firstly, I would like to thank the committee members for their guidance and valuable contribution throughout the whole graduation process. Thanks to Dr.ir. Roel Schipper to participate in this research as the chair of the thesis committee. I would also like to thank second the committee member Dr. Francesco Messali for his valuable input. I would like to express my special gratitude to my daily supervisor Ir. Lennert van der Linden for his interest on the topic and for conducting this research. Your comments and observations were very helpful to steer my research in the right direction.

I would like to thank all my friends for their support and companion throughout this two years and for making this academic achievement into a life experience.

I would like to thank my brother and my sister for their support and company. My greatest and most sincere thanks to my parents for their unconditional support, guidance and love throughout my entire life. Without them, any of this would have been possible.

Finally, I would like to acknowledge the funding of the Ecuadorean government throughout the Secretary of Superior Education, Science, Technology and Innovation (SENESCYT).

Delft, October 2020

José Antonio Abad González



## SUMMARY

Trusses are structures that have been used extensively for roofing and various construction purposes even centuries BC. Nowadays, due to its lightweight, the reduced deflection and its load bearing capacity, trusses are the preferred structures when large distances are required to span, such as bridges, stadiums roofs, etc. Despite the material used for trusses and the design of these structures have faced improvements during the last decades, the geometrical shape of trusses has barely changed along its history. Although nowadays with the help of computational tools more efficient designs can be achieved, the most commonly used systems are still the Pratt and the Warren truss. This is mainly due to the ease of the required structural calculations and due to the available standard manufacturing and assembly procedures.

Although a standard shape could be seen as an advantage, studies suggest that the relationship between the efficient use of material and design rationalization is not balanced, leading frequently to design-overcapacity of the structure. The use of optimization procedures provides new opportunities for architects and structural engineers. New design solutions and near-optimal structures can be achieved when implementing optimization processes in early design phases.

Optimization processes could generate economical alternatives in terms of weight reduction. Despite optimization techniques are becoming increasingly available for engineers and designers, optimized structures are not commonly used in real engineering practice due to the complex configuration an optimized structure might have, especially when using topological or layout optimization. Due to the non-conventional node-members configuration, realizing these optimized trusses in real practice with conventional joining mechanisms, such as bolted and welded connections, will probably lead to complex designs and higher costs. Therefore, innovative joining technologies are required to be implemented.

Snap-fit connections are a well known and widely used connecting mechanism for joining plastic components. Due to its simplicity and efficiency while connecting two or more elements together are suitable for different applications. Despite it is not commonly used in the building industry and it is frequently used on small scale applications, the principle based on snap-fit connections could be used to connect the structural members of optimized trusses. Considering this points, the following research question arises:

*How can innovative snap-fit joints help with the implementation of optimized steel trusses in the real engineering practice?*

First, a literature study provides a clear understanding of truss structures, focusing mainly on the importance of their joints, its influence on the assembly procedure and on final cost of the structure. Structural optimization is also discussed, paying special attention on a new layout-optimization ap-

proach proposed by [1], which is based on two steps: first, the less-weight possible layout is obtained (the benchmark) without taking into account any buildable considerations. The second step consists on rationalizing the benchmark contemplating practical and buildable restrictions. Additionally, the principles and design considerations behind snap-fit connections are covered on this part of the report. Finally, a representative case-study steel truss is presented.

The second part of this research explores the structural design and the optimization procedure applied on the case-study truss. Here the layout-optimization approach is applied using Peregrine, a optimization tool plug-in for Grasshopper built into the Rhinoceros3D modelling software. After an optimized layout is generated, it is design structurally using Grasshopper's plug-in structural engineering tool Karamba3D. Finally, the case-study truss and the optimized truss are compared.

To explore the opportunity of implementing optimized trusses in practice, the conceptual design of an innovative joint based on snap-fit connections is developed. A representative internal node from the optimized truss is chosen and based on a general concept, three design concepts are created, being the last one the final design. Extensive Finite Element (FE) analyses, such as dynamic and quasi-static analysis, are carried out to study the structural behavior of the innovative joint during three main phases: the assembly of the node, the usage phase and the node disassembly phase. Based on the theoretical behavior of trusses, only axial tensile and compressive forces are considered. All FE analysis were performed using the FE software Abaqus.

Finally, important aspects such as the manufacturing of the innovative joints, the member-joint connection and the assembly of the optimized truss are discussed. To conclude, this research project is an exploratory feasibility study of the use of steel snap-fit joints as internal nodes for optimized steel trusses. Based on this study it can be concluded:

The innovative concept design will allow optimized trusses with non-conventional internal nodes and member configurations to be built and used in real engineering practice. The connecting principle based on snap-fitting elements can be implemented on larger scale connections such as structural truss internal joints. Thanks to the non-welded and non-bolted joining technology the innovative connection has, the assembly time could decrease significantly reducing the cost for both the constructor and the client. Additionally, all internal nodes have the same shape which will reduce the manufacturing cost. Nowadays, manufacturing techniques that could be used for the manufacturing of the innovative joint, such as CNC machining techniques, are available and widely used.

# CONTENTS

1	INTRODUCTION	2
1.1	Introduction	2
1.2	Research Question	3
1.2.1	Research Questions	4
1.3	Objective	5
1.4	Methodology	5
1.4.1	Part I: Theory	5
1.4.2	Part II: Structural Design and optimization	5
1.4.3	Part III: Innovative connection	6
1.4.4	Part IV: Conclusion & Recommendations	7
1.5	Structure of the report	7
1.6	Scope and limitations	7
I	THEORY	
2	BACKGROUND INFORMATION	10
2.1	Introduction	10
2.2	Steel trusses	10
2.2.1	Type of trusses	11
2.2.2	Conventional joints for trusses	12
2.2.3	Production of steel trusses	12
2.2.4	Use of robots for truss manufacturing	13
2.3	Costs of steel structures	14
2.3.1	Introduction	14
2.3.2	Cost of steel structures	15
2.4	Structural optimization	17
2.4.1	Introduction	17
2.4.2	Structural optimization	17
2.4.3	Applicability restrictions of optimized structures	19
2.4.4	Types of structural optimization	19
2.4.5	Layout optimization: Two-step approach	20
2.4.6	Conclusions	22
2.5	Snap-fit connections	23
2.5.1	Introduction	23
2.5.2	General information	24
2.5.3	Main advantages and disadvantages	24
2.5.4	Cantilever snap-fit joints	25
2.5.5	Cantilever snap-fit Design	25
2.5.6	Rules of thumb for cantilever snap-fit beam design	28
2.6	Case Study	28
2.6.1	Introduction	28
2.6.2	Wimbledon Court No.1 roof	29
2.6.3	Structure	30
2.6.4	Geometry and design considerations	30
2.7	Conclusion	32

**II STRUCTURAL DESIGN AND OPTIMISATION**

<b>3</b>	<b>STRUCTURAL DESIGN OF STEEL TRUSSES</b>	<b>35</b>
3.1	Introduction . . . . .	35
3.2	Assumed Loads . . . . .	35
3.2.1	Variable load ( $Q$ ) . . . . .	37
3.2.2	Permanent load ( $G$ ) . . . . .	45
3.2.3	Load combinations . . . . .	46
3.2.4	Maximum deflection . . . . .	48
3.3	Assumptions for structural analysis . . . . .	48
3.3.1	Assumed loading scheme . . . . .	48
3.3.2	Assumed mechanical scheme . . . . .	49
3.4	Structural analysis with Karamba3D . . . . .	49
3.4.1	Size optimisation . . . . .	50
3.4.2	Model definition . . . . .	51
3.4.3	Results . . . . .	51
3.5	Conclusion . . . . .	53
<b>4</b>	<b>OPTIMIZATION OF STEEL TRUSS FROM CASE STUDY</b>	<b>54</b>
4.1	Introduction . . . . .	54
4.2	Layout optimization . . . . .	54
4.3	Structural optimization with Peregrine . . . . .	55
4.3.1	Peregrine workflow . . . . .	55
4.3.2	Peregrine validation . . . . .	56
4.4	Shape development . . . . .	59
4.4.1	Introduction . . . . .	59
4.4.2	Step 1: Benchmark . . . . .	59
4.4.3	Step 2: Post-processing . . . . .	62
4.4.4	Applied post-processes . . . . .	63
4.4.5	Final optimized layout . . . . .	63
4.5	Structural design of the optimized truss . . . . .	66
4.5.1	Assumed loading scheme . . . . .	66
4.5.2	Assumed mechanical scheme . . . . .	66
4.5.3	Structural analysis with Karamba3D . . . . .	66
4.5.4	Results and comparison . . . . .	67
4.5.5	Chosen internal node . . . . .	68
4.6	Comparison . . . . .	69
4.7	Conclusion . . . . .	71

**III INNOVATIVE JOINTS**

<b>5</b>	<b>CONCEPTUAL JOINT DESIGN BASED ON SNAP-FIT CONNECTIONS</b>	<b>73</b>
5.1	Introduction . . . . .	73
5.2	Methodology . . . . .	74
5.3	Snap-Fit principles . . . . .	75
5.3.1	Components . . . . .	75
5.3.2	Phases . . . . .	76
5.4	Innovative joint: general concept . . . . .	78
5.5	Numerical analyses . . . . .	79
5.5.1	Material models . . . . .	80
5.5.2	Geometry and boundary conditions . . . . .	81
5.5.3	Finite element mesh . . . . .	82

5.5.4	Loading . . . . .	83
5.5.5	Contact . . . . .	83
5.6	Design concepts . . . . .	84
5.6.1	Design concept 1 . . . . .	84
5.6.2	Design concept 2 . . . . .	87
5.7	Design concept 3: Final Design . . . . .	89
5.7.1	Inserting Unit . . . . .	89
5.7.2	Retaining Unit . . . . .	90
5.8	Final Design concept: Phases FEA . . . . .	91
5.8.1	Assembly phase . . . . .	91
5.8.2	Usage phase . . . . .	97
5.9	Conclusion . . . . .	109
6	REFLECTION . . . . .	110
6.1	Introduction . . . . .	110
6.2	First steps . . . . .	110
6.2.1	The challenge . . . . .	110
6.2.2	Idea generation . . . . .	110
6.2.3	Developing concepts . . . . .	111
6.2.4	Analyzing the concepts . . . . .	111
6.2.5	Final result . . . . .	111
6.3	Next steps . . . . .	112
6.3.1	Results validation . . . . .	112
6.3.2	Manufacturing . . . . .	113
6.3.3	Assembly . . . . .	115
6.3.4	Member - Tip connection . . . . .	117
6.4	Conclusion . . . . .	118
IV CONCLUSION & RECOMMENDATIONS		
7	CONCLUSION AND DISCUSSION . . . . .	121
7.1	Introduction . . . . .	121
7.2	Conclusions . . . . .	121
7.3	Discussion . . . . .	123
7.4	Recommendations . . . . .	124
7.5	Future outline and research . . . . .	125
Bibliography . . . . .		129
A	STRUCTURAL DESIGN: ASSUMPTIONS . . . . .	130
A.1	Wind load . . . . .	130
A.1.1	Wind load coefficients . . . . .	130
A.1.2	Load combinations . . . . .	130
B	DESIGN . . . . .	132
B.1	Structural design . . . . .	132
B.1.1	Grasshopper model definition . . . . .	132
B.1.2	Forces Case-study truss . . . . .	133
B.1.3	Forces Case-study truss . . . . .	134
B.1.4	Forces Optimized truss . . . . .	136
B.1.5	Forces Optimized truss . . . . .	137
B.1.6	Cross sections Optimized truss . . . . .	138
B.2	Optimization . . . . .	140
C	INNOVATIVE JOINT . . . . .	142

c.1	Design Concept 1 . . . . .	142
c.2	Design Concept 2 . . . . .	143
c.3	Design Concept 3: Final design . . . . .	145
c.3.1	Innovative joint dimensions . . . . .	145
c.4	Assembly phase . . . . .	147
c.5	Usage phase: tensile forces . . . . .	153
c.5.1	Resistance to tensile forces . . . . .	153
c.5.2	Resistance to compressive forces . . . . .	154
c.6	Input data for material models in Abaqus . . . . .	157
c.6.1	Assembly phase: sliding insertion . . . . .	157
c.6.2	Usage phase: retention to axial tensile forces . . . . .	158
c.6.3	Usage phase: retention to axial compressive forces . . . . .	159

## LIST OF FIGURES

Figure 1.1	Layout optimized truss [1]. . . . .	2
Figure 2.1	conventional types of trusses . . . . .	11
Figure 2.2	Pratt truss. . . . .	11
Figure 2.3	Warren truss. . . . .	11
Figure 2.4	Common member section of a lightweight truss. . . . .	12
Figure 2.5	Joint types on steel trusses . . . . .	12
Figure 2.6	Manufacturing process of structural hollow sections [2].	13
Figure 2.7	ETH Zurich robotic timber frame construction [3] . . . .	14
Figure 2.8	Cost distribution of steel structures [4]. . . . .	15
Figure 2.9	Workmanship and materials cost in different phases of the building process [5]. Brown color indicates the material cost and blue color indicates the workman- ship costs. . . . .	16
Figure 2.10	Costs related to joints of a steel structure [5]. . . . .	16
Figure 2.11	Structural optimization system [6]. . . . .	18
Figure 2.12	Types of structural optimization. . . . .	20
Figure 2.13	Two step approach [1]. . . . .	20
Figure 2.14	Example of a Michell truss [7] . . . . .	21
Figure 2.15	Numerical layout optimisation steps [1]. . . . .	22
Figure 2.16	Case study of a transfer truss [1]. . . . .	23
Figure 2.17	Snap-fit and buckle clip connecting mechanism. . . . .	24
Figure 2.18	Cantilever Snap-fit beam [8]. . . . .	25
Figure 2.19	Sides of a cantilever Snap-fit beam [8]. . . . .	26
Figure 2.20	Cantilever Snap-fit beam dimensions and angles [9]. . .	26
Figure 2.21	Stress concentration of a snap-fit cantilever beam with a constant and tapered cross section [10]. . . . .	27
Figure 2.22	Wimbledon No. 1 Court roof. . . . .	29
Figure 2.23	Wimbledon Court No.1 retractable roof. . . . .	29
Figure 2.24	Geometry of Wimbledon Court No.1 roof truss (dis- tances in meters). . . . .	31
Figure 2.25	Wimbledon roof truss bolted joint. . . . .	31
Figure 2.26	Support conditions of truss [11]. . . . .	32
Figure 3.1	Load factor for ULS EQU. Reproduced from BS-EN 1990:2002. . . . .	36
Figure 3.2	Load factor for ULS STR. Reproduced from Bs-EN 1990:2002. . . . .	36
Figure 3.3	Top view of the Wimbledon Court No.1 roof. . . . .	40
Figure 3.4	Pressure coefficient for case study roof for wind situ- ation 1. . . . .	41
Figure 3.5	Pressure coefficient for case study roof for wind situ- ation 2. . . . .	42
Figure 3.6	Internal pressure coefficient. . . . .	43

Figure 3.7	Wind force on the central trusses of the roof for wind situation 1 (not influence by roof zone F). . . . .	43
Figure 3.8	Snow load shape coefficients - pitched roofs. EN 1991-1-3. . . . .	44
Figure 3.9	Snow load distribution on a internal truss for undrifted and drifted load arrangement. . . . .	45
Figure 3.10	Permanent equipment on steel trusses. . . . .	46
Figure 3.11	Assumed mechanical scheme. . . . .	49
Figure 3.12	Structural design workflow. . . . .	49
Figure 3.13	3D model of analyzed truss with Karamba3D . . . . .	50
Figure 3.14	Conventional truss: structural design . . . . .	52
Figure 3.15	Forces diagrams from the design case study truss . . . . .	53
Figure 4.1	Optimization software. . . . .	55
Figure 4.2	Optimization process workflow. . . . .	56
Figure 4.3	Michell-like truss design domain. . . . .	57
Figure 4.4	Original Michell truss vs Michell-like truss obtained using Peregrine. . . . .	57
Figure 4.5	Michell-like truss benchmark and post-process . . . . .	58
Figure 4.6	Different layouts volume vs number of nodes: results after limiting the numbers of nodes per layout. . . . .	58
Figure 4.7	Optimization methodology steps. . . . .	59
Figure 4.8	Optimized benchmark layout for design domain 1. . . . .	60
Figure 4.9	Optimized benchmark layout for design domain 2. . . . .	61
Figure 4.10	Optimized benchmark layout for design domain 3. . . . .	61
Figure 4.11	Types of post-processes within Peregrine . . . . .	63
Figure 4.12	Post-process workflow. . . . .	64
Figure 4.13	Final layout. . . . .	65
Figure 4.14	Structural design workflow. . . . .	66
Figure 4.15	3D model of analyzed truss with Karamba3D. . . . .	66
Figure 4.16	Solution 1: no members grouped. . . . .	67
Figure 4.17	Solution 2: Top chord and bottom chord grouped into 2 different groups. . . . .	68
Figure 4.18	Solution 3: Top chord, bottom chord and some diagonal members grouped into different groups. . . . .	68
Figure 4.19	Internal node. . . . .	68
Figure 4.20	Normal Forces (kN) of the chosen internal node. Analysis made in OasysGSA. . . . .	69
Figure 4.21	Cross sections of the structural members connected at the chosen node. . . . .	69
Figure 5.1	Internal node . . . . .	73
Figure 5.2	Inserting part (red) and retaining part (blue) at different positions. . . . .	75
Figure 5.3	Von Mises stresses on a snap-fit assembly procedure. . . . .	76
Figure 5.4	Von Mises tresses on a steel snap fit after disassembly. . . . .	78
Figure 5.5	Parts of the inserting unit. . . . .	78
Figure 5.6	General concept of the innovative connection. . . . .	79
Figure 5.7	Innovative general concept components. . . . .	79
Figure 5.8	Steel s355 bi-linear stress-strain relationship. . . . .	80
Figure 5.9	Steel S355 material curve used in Abaqus. . . . .	81



Figure 5.10	General boundary conditions for inserting unit. . . . .	82
Figure 5.11	Boundary conditions for retaining unit (fully fixed). . .	82
Figure 5.12	Inserting unit mesh . . . . .	83
Figure 5.13	Custom loading amplitude function. . . . .	83
Figure 5.14	Design concept 1. . . . .	85
Figure 5.15	Von Mises stresses ( $N/mm^2$ ) of design concept 1. . . .	85
Figure 5.16	Stress-strain behaviour of design concept 1. . . . .	86
Figure 5.17	Design concept 2. . . . .	87
Figure 5.18	Von Mises stresses ( $N/mm^2$ ) for axial tensile loading condition for design concept 2. . . . .	88
Figure 5.19	Design concept 3: inserting unit. . . . .	89
Figure 5.20	Design concept 3: retaining unit. . . . .	90
Figure 5.21	Final design: connection between inserting unit and retaining unit. . . . .	91
Figure 5.22	3D models of the inserting and the retaining unit with boundaty conditions. . . . .	92
Figure 5.23	Meshing of the 3D model. . . . .	92
Figure 5.24	Stress strain relationship at the base of the beam. . . .	93
Figure 5.25	Von Mises stresses during the assembly of the joint. . .	94
Figure 5.26	Assembly force. . . . .	94
Figure 5.27	Stress-strain behaviour at the tips from the inserting unit. . . . .	95
Figure 5.28	Manual Assembly . . . . .	95
Figure 5.29	Different beams configurations . . . . .	96
Figure 5.30	Snap-beam deflection shape. . . . .	97
Figure 5.31	Forged u-frame press. . . . .	97
Figure 5.32	Von Mises stresses for 80 kN tensile load. . . . .	99
Figure 5.33	Stress-strain behaviour at the tips from the inserting unit. . . . .	99
Figure 5.34	Stress-strain relationship at the inserting and retain- ing unit. . . . .	100
Figure 5.35	Vertical displacement of the end-tip of the inserting unit. . . . .	101
Figure 5.36	Applied force vs vertical displacement of the inserting unit tip. . . . .	101
Figure 5.37	First buckling mode of a fixed-free strut [12]. . . . .	102
Figure 5.38	Load at the retention block. . . . .	104
Figure 5.39	Buckling shape. . . . .	104
Figure 5.40	FE model of with boundary conditions. . . . .	105
Figure 5.41	Resulting vertical displacement after FEA (colored im- age) and first buckling mode of a fixed-pinned strut [13] (white and black top image). . . . .	106
Figure 5.42	Von Mises stress distribution of the innovative con- nection under compressive loading. . . . .	106
Figure 5.43	Stress-strain behaviour at the tips from the inserting unit. . . . .	107
Figure 5.44	Von Mises stresses vs compressive force. . . . .	107
Figure 5.45	Failure behavior under compressive loads. . . . .	108

Figure 5.46	Vertical displacement ( $mm$ ) at a compressive load of 92 $kN$ . . . . .	108
Figure 5.47	Force vs displacement at bowing zone of inserting unit.	109
Figure 6.1	Optimized truss 3D assembly process. . . . .	112
Figure 6.2	FEA validation procedure. . . . .	113
Figure 6.3	CNC milling machine during operation [14]. . . . .	114
Figure 6.4	Optimized truss 2D assembly process. . . . .	116
Figure 6.5	Optimized truss 3D assembly process. . . . .	116
Figure 6.6	Assembly of the V-shaped optimized truss. . . . .	117
Figure 6.7	Possible connections between the inserting unit and the steel member. . . . .	118
Figure A.1	Wind coefficients and wind loads calculations. . . . .	130
Figure B.1	Case study truss Grasshopper script. . . . .	132
Figure B.2	3D model of the case-study truss. . . . .	132
Figure B.3	Case-study truss elements ID. . . . .	135
Figure B.4	Forces diagrams from the design case study truss . . .	135
Figure B.5	Optimized truss elements ID. . . . .	139
Figure B.6	Bending moment diagram on optimized truss . . . . .	139
Figure B.7	Shear forces diagram on optimized truss . . . . .	139
Figure B.8	Normal forces diagram on optimized truss . . . . .	139
Figure B.9	Post-process workflow on Grasshopper. . . . .	140
Figure B.10	Complete optimization process on Grasshopper. . . . .	140
Figure B.11	Grasshopper script for the structural design of the optimized truss. . . . .	141
Figure B.12	3D model of the optimized truss. . . . .	141
Figure C.1	Stress concentration ( $N/mm^2$ ) at the perforation in design concept 1. . . . .	142
Figure C.2	Vertical displacement ( $mm$ ) of the inserting unit from design concept 1. . . . .	142
Figure C.3	Stress vs time curve at the perforation in design concept 1. . . . .	143
Figure C.4	Von Mises stresses ( $N/mm^2$ ) at a cut-view plane of inserting unit from design concept 1. . . . .	143
Figure C.5	Reaction forces ( $N$ ) at each tip of design concept 2. . .	144
Figure C.6	Reaction forces at each tip of design concept 2. . . . .	144
Figure C.7	Insertion tip dimensions. . . . .	145
Figure C.8	Retaining unit dimensions. . . . .	146
Figure C.9	Plastic strains and contact stresses of the snap-beam. .	147
Figure C.10	Node at the round-edge: Strain vs time . . . . .	147
Figure C.11	Von Mises stress at node at the round edge. . . . .	148
Figure C.12	Vertical displacement of each tip during the assembly phase. . . . .	148
Figure C.13	Manual disassembly procedure. . . . .	149
Figure C.14	Safety mechanism for the manual disassembly procedure. . . . .	149
Figure C.15	Von Mises stresses ( $kN/mm^2$ ) on the inserting unit tip. Top view. . . . .	153
Figure C.16	Plastic strains (-) at the retaining unit. . . . .	153
Figure C.17	Plastic strains (-) at the inserting unit. . . . .	154

Figure C.18	Von Mises stresses ( $kN/mm^2$ ) vs applied force ( $kN$ ). . . . .	154
Figure C.19	Buckling shape for a compressive force. . . . .	155
Figure C.20	Strain at the inserting unit. . . . .	155
Figure C.21	Stresses at retaining unit . . . . .	155
Figure C.22	Von Mises stresses vs strain at retaining unit. . . . .	156
Figure C.23	Von Mises stress distribution ( $kN/m^2$ ) of the innovative connection at a compressive load of 92 $kN$ . . . . .	156

## LIST OF TABLES

Table 3.1	Terrain categories. Reproduced form Table 4.1 EN 1991-1-4:2005. . . . .	39
Table 3.2	External pressure coefficients for flat roofs (assumed with sharp edges). Table NA.5 BS-EN 1991-1-4:2005. . .	41
Table 3.3	Permanent and variable loads acting on a central truss (including wind situation 1). . . . .	46
Table 3.4	Permanent and variable loads acting on a central truss (including wind situation 2). . . . .	46
Table 3.5	Coefficients for LC1. . . . .	47
Table 3.6	Coefficients for LC2. . . . .	47
Table 3.7	Coefficients for LC3. . . . .	47
Table 3.8	Coefficients for LC4. . . . .	47
Table 3.9	Coefficients for LC5. . . . .	47
Table 3.10	Loads for load combination 4. . . . .	48
Table 3.11	Steel S355 material properties. . . . .	51
Table 3.12	Cross section names for the structural members. . . . .	52
Table 4.1	Cross section names for the structural internal members. . . . .	69
Table 4.2	Relative efficiency of the various analysed types of trusses compared to the case-study truss . . . . .	70
Table 4.3	Number of different cross sections. . . . .	70
Table 5.1	Stress and strain conversions. . . . .	81
Table 5.2	FEA characteristics for design concept 1. . . . .	84
Table 5.3	FEA characteristics for design concept 2. . . . .	87
Table 5.4	Tips load-carrying contribution. . . . .	88
Table 5.5	FEA characteristics for the final design concept. . . . .	92
Table 5.6	Height and beam configuration study. . . . .	96
Table 5.7	FEA characteristics for axial tensile force. . . . .	98
Table 5.8	Fixed-free edges steel plate buckling behaviour. . . . .	103
Table 5.9	Euler buckling load comparison. . . . .	103
Table 5.10	FEA characteristics for axial tensile force. . . . .	105
Table A.1	Loads for load combination 1. . . . .	130
Table A.2	Loads for load combination 2. . . . .	130
Table A.3	Loads for load combination 3. . . . .	131
Table A.4	Loads for load combination 4. . . . .	131
Table A.5	Loads for load combination 5. . . . .	131

## 1.1 INTRODUCTION

Since the beginning of civilizations to modern times different elements have been used to withstand the load of roofs. Archaeological remains of wooden triangulated compositions have been found as evidence of the use of structures that served as roof supports. The first timber trusses were already used in the Greek temples in the 6<sup>th</sup> century BC [15]. After that point, wooden truss were extensively used for roofing and for other various construction purposes. It was not until the early 19<sup>th</sup> century that the design of trusses was forced to improved and developed in order to be applicable to truss bridges. Metallic materials, such as cast iron and wrought iron, became popular as main material for trusses, succeeded now by hot or cold-rolled steel members.

Despite all the material and design improvements trusses have faced during the last decades, the geometrical shape of trusses has barely changed along its history. Although nowadays with the help of computational tools more efficient designs can be achieved, the most commonly used systems are still the Pratt and the Warren truss. This is mainly due to the ease of the required structural calculations and due to the available standard manufacturing and assembly procedures [16].

Although a standard shape could be seen as an advantage, studies suggest that the relationship between material-efficiency and design rationalization is not balanced, leading frequently to design-overcapacity of the structure [17]. By implementing optimization procedures in early design phase of the design of a structure near-optimal structures can be achieved [18].

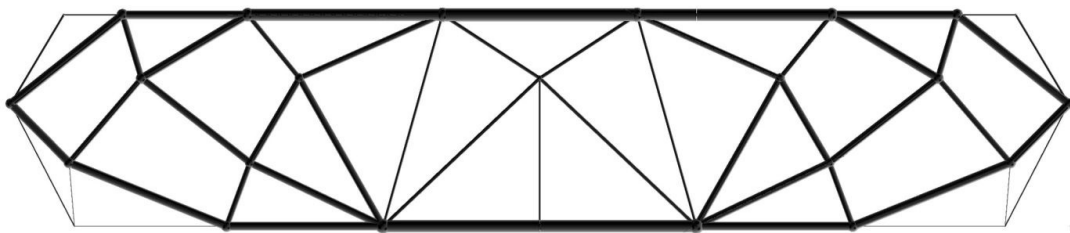


Figure 1.1: Layout optimized truss [1].

Despite optimization techniques and optimization packages are becoming increasingly available for engineers and designers, optimized structures are not commonly used in real engineering practice due to the complex configuration an optimized structure might have, specially when using topological or layout optimization. On one hand, weight and deflection can be significantly reduced, generating a material-cost-efficient design. On the other

hand, the complex node-member configuration of the optimized truss will probably lead to higher cost than a conventional truss structure.

Once a layout optimization is applied, the resulting optimized truss structure will very likely be composed of unique nodes which is required to connect different members at unique arrival angles. This can be observed in Figure 1.1. Realising such structure with conventional joints, such as bolted or welded connections, might increase the final cost of the structure and the erection assembly might be hindered. Therefore, innovative and adaptable solutions are required. The selection of a specific type of connection has also influence on the construction and erection time of the structure of a building and thus affect the safety of the workers.

It is time to step out of the box and start thinking about different ways of connecting two or more elements together that could be applied and scaled to structural connections. Snap-fit connection-principle seems to be an easy and efficient way to connect elements together [8] [10] [19]. Despite snap-fit connections are commonly used for small scale applications, the same principle could be applied on a larger scale, such as structural connections.

Concluding, buildings can be potentially benefit from the development of innovative structural joints based on the snap-fitting principle that allow the construction of optimized trusses composed of non-conventional geometries and complex node-members configurations.

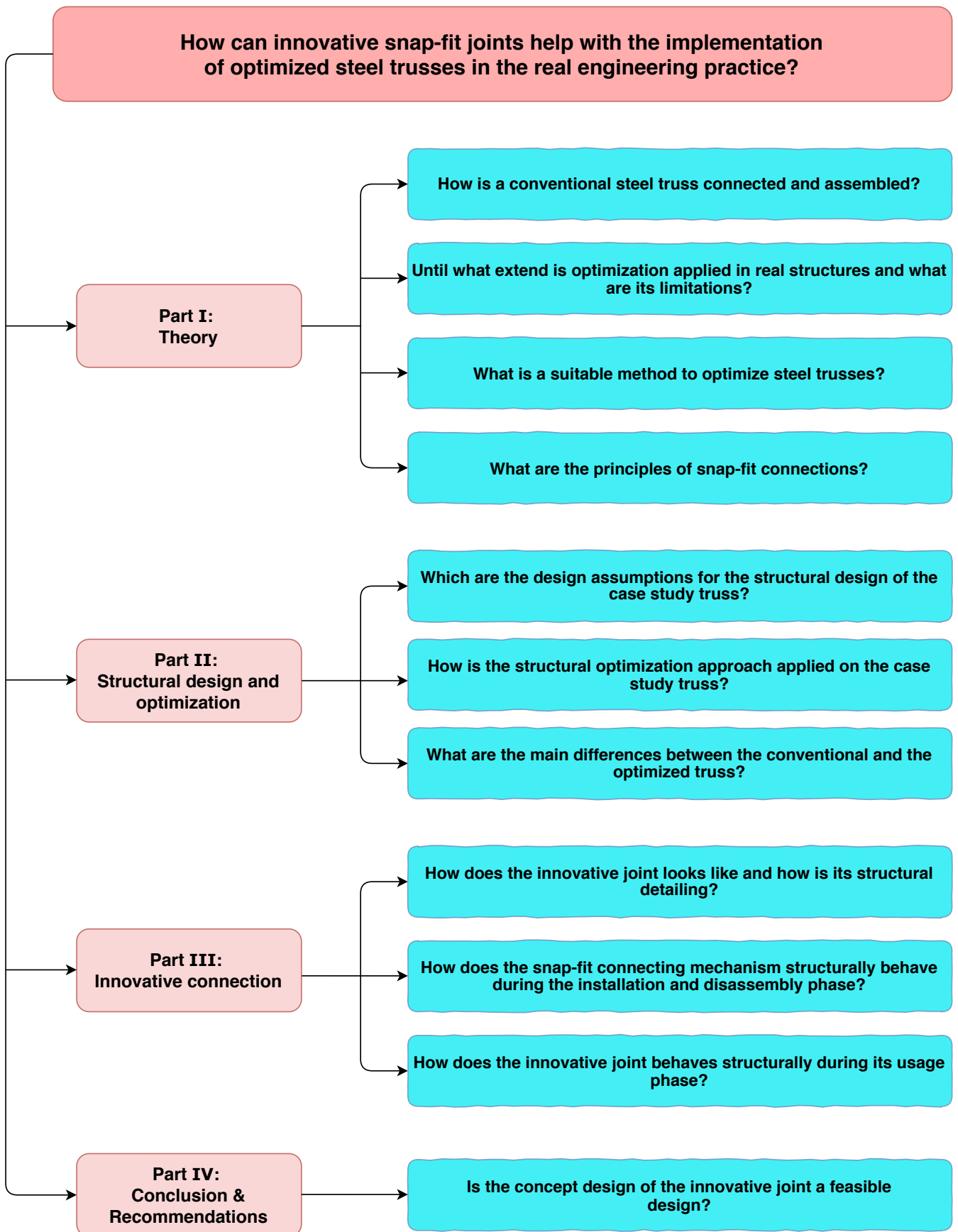
## 1.2 RESEARCH QUESTION

The aim of the thesis is to find an answer to the problems described in the previous paragraphs. The problem can be defined by a following main research question:

*How can innovative snap-fit joints help with the implementation of optimized steel trusses in the real engineering practice?*

The following chart presents the main research question including the sub-questions for each part of the thesis.

### 1.2.1 Research Questions



### 1.3 OBJECTIVE

The objective of this research is to develop, design and analyze a concept of a non-conventional innovative joint for an existing steel truss that is further optimized by layout optimization.

### 1.4 METHODOLOGY

The methodology is defined to answer each sub-question.

#### 1.4.1 Part I: Theory

*How is a conventional steel truss connected and assembled?*

This question is answered with a literature review to gain understanding on the different types of steel trusses and how are they commonly connected. This includes a brief description of the manufacturing process and information about the increasing implementation of robots in the assemble of structures. This question is answered in Section 2.2.

*What are the principles of snap-fit connections?*

A detailed literature review of the types, advantages, disadvantages applications and design principles of span-fit connections is performed to understand the state of the art of such connections in big-scale structures. This question focuses on the connecting mechanism that will be used for the innovative connections of an optimized steel truss. The investigated principles will serve as starting point for develop of the innovative joint in Part III. This question is answered in Section 2.5.

*Until what extend is optimization applied in real structure and what are its limitations?*

The state of the art of optimization applied to structures is investigated with special attention on topological optimization. The main advantages of structural optimization and its current limitations is addressed. This question is answered in Section 2.4.

*What is a suitable method to optimize steel trusses?*

A review of different optimization methods for steel trusses is carried out. The new and innovative optimization approach proposed by [1] is presented. This approach will be further applied in Part II in order to obtain an optimized steel truss. This question is answered in Section 2.4.5.

#### 1.4.2 Part II: Structural Design and optimization

*Which are the design assumptions for the structural design of the case study truss?*

An existing steel truss is chosen as case study in order to demonstrate how a truss can be further optimised. Due to lack of information about



the structural design, assumptions are made regarding to geometry, loads, material and cross-sections. The case study truss is modelled in Grasshopper, which is a visual programming language and environment within the CAD software Rhinoceros3D. The truss will be design and analyze using Grasshopper's plug-in structural engineering tool Karamba3D. This question is answered in Section 3.2 and in Section 3.3.

*How is the structural optimization approach applied on the case study truss?*

After the case study truss is realized and design, an layout-optimization procedure will be performed on it. This will be performed using a powerful structural layout optimization plug-in for Grasshopper, built into the Rhinoceros3D modelling software. This is realized by following the two-step optimization approach addressed in Part I and using the design assumptions input from Part II. This question is answered in Section 4.4.

*What are the main differences between the conventional and the optimized truss.*

The results from the previous sub-questions are presented, further discussed and compared. This show the advantages and limitations of implementing optimized structures in real engineering practice, which are further studied in Part III. This comparison aims to answer in part the main research question. This question is answered in Section 4.6.

### 1.4.3 Part III: Innovative connection

*How does the innovative joint looks like and how is the structural detailing?*

Using the input form Part I and Part II, a connection based on the connecting principle of snap-fit mechanism is realised. This connection allows multiple members to attach into a unit with different "arrival angles". This makes possible to derive and economical solution and an optimised structure in real engineering practice, answering the main research question. This question is answered in Section 5.7.

*How does the snap-fit connecting mechanism behaves structurally during the installation and disassembly phase?*

The resulting geometry and shape of the connection from the previous sub-question is 3D-modelled using Fusion 360, a CAD software from Autodesk. The final design concept model is structurally analysed using the finite element software Abaqus for the assembly of the node. This question is answered in Section 5.8.1.

*How does the innovative joint behaves structurally during the usage phase?*

Finally, a complete 3D-model of one connection, including members, is created in the FEA software Abaqus. This model is structurally analyzed using the real forces on one node belonging to the optimised truss, resulting from Part II. This question is answered in Chapter 5.

#### 1.4.4 Part IV: Conclusion & Recommendations

*Is the concept design of the innovative joint a feasible design?*

With the input from all the previous parts the main research question is answered completely. Conclusions and recommendations regarding to the feasibility and applicability of the innovative joint are presented and discussed. This question is answered in Chapter 7.

### 1.5 STRUCTURE OF THE REPORT

The report is divided in three parts, as exhibited above. Each sub question is treated and answered in various chapters. A part is composed of multiple chapters. The introductory chapter and the last chapter on conclusions and recommendations will support and complement the three parts.

### 1.6 SCOPE AND LIMITATIONS

Developing an innovative design concept of a structural connection for a optimized steel truss is a broad and complex field. Therefore, this research is restricted by some scope limitations that make this research feasible as a graduation thesis:

- This research will mainly focus on the development of a design concept of a innovative join for optimized steel trusses and its structural behaviour during some specified phases.
- A representative case study truss will be chosen.
- The structural calculations are based on the Eurocode.
- A recently developed layout optimization approach will be applied on this research using and existing optimization tool. A custom made optimization tool will not be developed. Other optimizations methods are not considered on this research.
- Numerical models of the innovative joint will be created and analysed using an existing Finite Element (FE) software Abaqus.
- The structural analyses of the innovative joints concerns only the internal nodes of the truss. Nodes at the top and bottom chord are nor considered on this research.
- Physical test are beyond the scope of this research. The numerical computer models are verified with simplified examples and calculations.
- All FE analyses were carried out with a perfect structure. No imperfections were considered.
- This research does not consider out-of-plane behaviour of the innovative joints.

- The manufacturing of the innovative joints is briefly discussed. Similarly, the manufacturing cost are not considered on this research.

Part I

THEORY

# 2 | BACKGROUND INFORMATION

## 2.1 INTRODUCTION

First of all it is required to understand the structural principles of steel trusses and what role joints play on the design and construction of these type of structures. Then, a recently developed method of layout-optimization will be used as a design tool, it is necessary to understand the method and how this will be applied on the research. Thirdly, snap-fit connection mechanism plays a very important role in the research project. Therefore, its connecting principle, its advantages and disadvantages must be studied. Finally, a case-study truss is presented which will be used to optimize and based on this result an innovative joint will be developed.

This chapter presents all relevant information about the above mentioned topics and the following research sub-questions are answered:

- *How is a conventional steel truss assembled?*
- *What are the principles of snap-fit connections?*
- *Until what extent is optimization applied in real structures and what are its limitations?*
- *What is a suitable method to optimize steel trusses?*

## 2.2 STEEL TRUSSES

A conventional truss can be explained as triangulated system usually composed of straight interconnected cold or hot-formed steel structural elements. Those elements are connected at nodes and those connections are usually assumed as fully pinned connections. Only axial tension or compression force is taken by structural elements in a truss and transferred to the supports through the nodes. A truss can be called 2D truss when all the applied forces and the elements are in the same plane [16].

Trusses are usually a preferred choice when large distances are required to span due to its lightweight, the reduced deflection and its load bearing capacity. Elements in bending require more material in order to resist that type of loading therefore, trusses are usually lighter. For these reasons, trusses are widely used in buildings, such as airports terminals, sports halls, stadiums, coliseums, auditoriums, leisure buildings, among others. Trusses are generally used to support roofs, floors and internal loading.

### 2.2.1 Type of trusses

Different trusses can be created by the arrangement of the straight structural members. As mentioned before, these members are tension and compression elements. The top and bottom chord, under gravity load, resist overall bending and the bracing resists the shear forces [16]. Each truss can vary in geometry and individual members can also be different. Figure 2.1 shows the most commonly used truss-types for steel trusses.

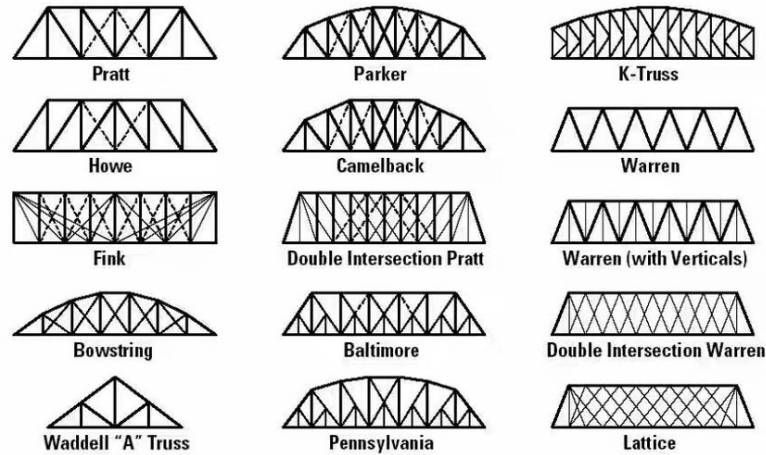


Figure 2.1: conventional types of trusses

The most conventional type of trusses used in building structures are the following:

- Pratt Truss: Composed of vertical and diagonal members distributed uniformly along the length of the truss. Usually chosen when gravity load is predominant. Diagonal members are in tension for gravity loads.

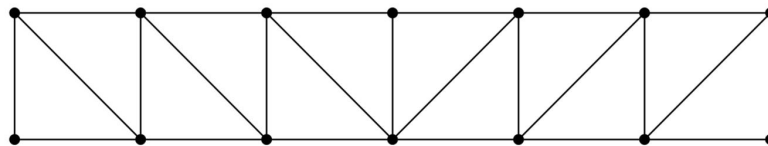


Figure 2.2: Pratt truss.

- Warren Truss: Composed of diagonal members arranged alternatively in tension and compression. The web members under tension and compression have equal length. This truss usually has fewer members than a Pratt truss.

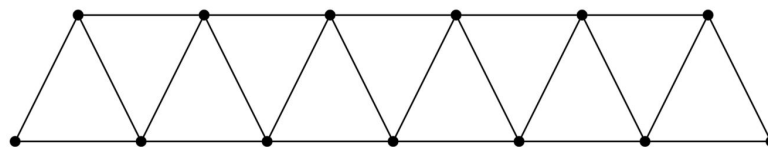


Figure 2.3: Warren truss.

For shorter spans trusses such as a Flink truss, King Post truss and North-Light truss are commonly used.

### 2.2.2 Conventional joints for trusses

Different member sections are used in steel roof/floor trusses. The most common ones are shown on Figure 2.4. For all these member sections it is possible to design either welded or bolted connections. The Eurocode EN 1993-1-8 [20] presents all design aspects and considerations for the design of steel joints. On this code the joints are checked for punching failure, chord face failure and brace failure. Generally, bolted connections are preferred in steelwork construction for economy and speed of assembly and erection. Hollow sections such as tubes are usually connected by welding, whereas open sections can be connected either by bolting or welding [16]. Different types of connections are presented on Figure 2.5.

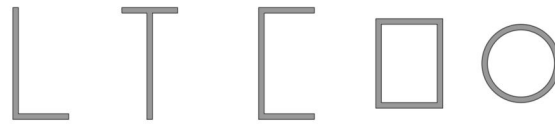


Figure 2.4: Common member section of a lightweight truss.

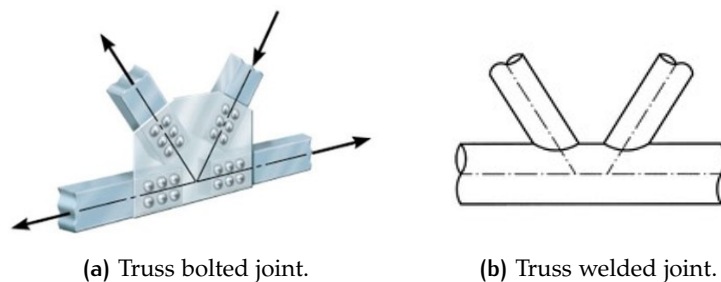


Figure 2.5: Joint types on steel trusses

### 2.2.3 Production of steel trusses

As mentioned before, steel trusses are usually composed of hollow structural section members. Tubular sections offer higher strength-to-weight ratio than others steel or timber sections. This feature results in lightweight structures that allows to reduce material and span larger distances. Hollow structural steel sections can be manufactured either by hot-finish or by cold-formed process. Hot-finished hollow sections are formed at temperatures of  $900^{\circ}\text{C}$  and produced in accordance with the standards EN10210-1. Cold-formed hollow sections are formed at room temperature and are produce under the standards EN10219-1 [2]. Figure 2.6 shows this manufacturing processes. As a result of its forming process, cold-formed hollow sections could be more susceptible to corner cracking if manufactured with tight radius corners.

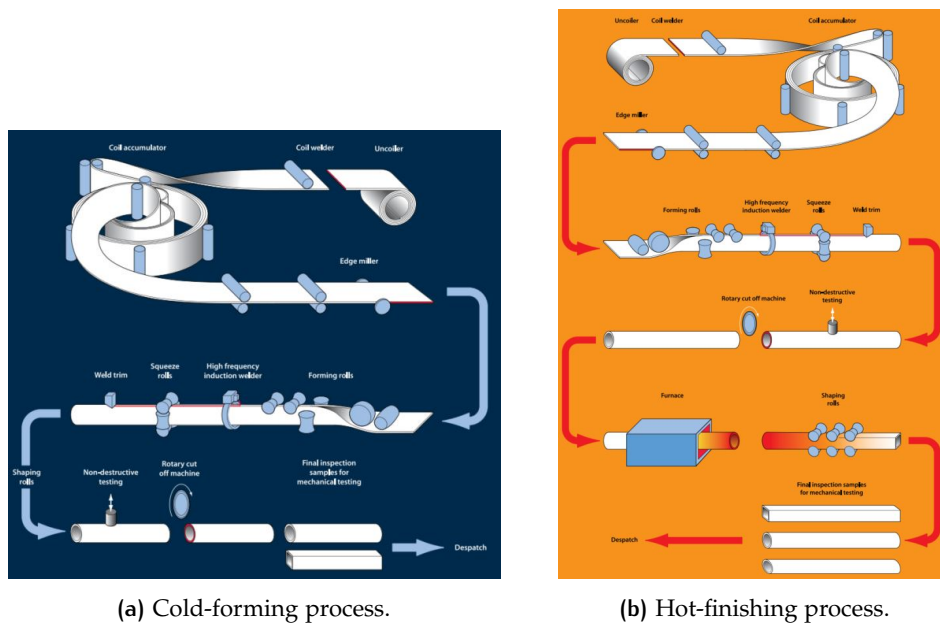


Figure 2.6: Manufacturing process of structural hollow sections [2].

After the structural hollow sections are manufactured and a truss is designed by a structural engineer or designer, a truss manufacturer assembles the elements on a workshop. Small trusses which can be transported as a whole element from the factory are usually entirely welded. In case of bigger and larger trusses that cannot be transported as one piece, sub-assemblies are required being these ones connected on site via either welding or bolting.

#### 2.2.4 Use of robots for truss manufacturing

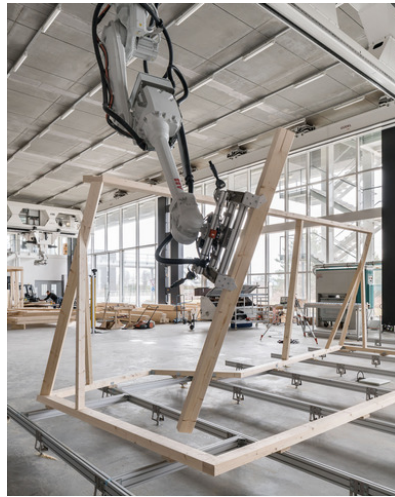
In today's reality in steel structures manufacturing, most of the assembling and welding is performed manually. However, in the steel production industry the use of robots for specific tasks is increasing rapidly. In some existing steel production factories robots are being used to perform automated sawing and drilling but a complete and automated fully assembly of a structure is not implemented yet. By implementing robots in the manufacturing process of a structural member or a whole structure:

- The risk of human error could be mitigated
- The risk of workers caused by working under dangerous circumstances could be reduced
- The assembly time could be improved
- Material savings could be achieved

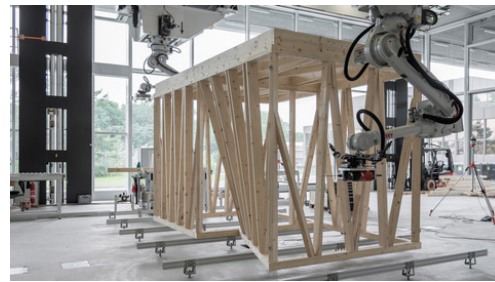
Voorman Steel Group has developed an Multi System Integration (MSI) [21] in which all the cross-transport of elements and the machines are linked together creating an intelligent production line with multiple systems. Multiple operations are carried out at the same time and are seamlessly connected to each other. This optimized process optimizes material handling and machine functions, decreases labor costs and increases efficiency.



The use of robots in the assembly or construction of structures open new possibilities to the implementation of optimised and customised structures. Researchers from ETH Zurich developed a new method for digital timber construction [3]. The timber structure is composed out of spacial modules which are prefabricated completely by robots as shown on Figure 2.7. The robots take the timber beam and guides when it is precisely-sawed. A second robot drills the required holes. In a later stage another robot moves and positions the beam into its final position. Human activity is still needed to screw the timber elements together.



(a) Robot positioning the timber element.



(b) Final stage of the timber frame constructed by robots.

Figure 2.7: ETH Zurich robotic timber frame construction [3]

Despite the increasing attempts to include robots in the building and construction industry, due to its currently limit capabilities and its high initial and indirect costs robots are not widely implemented [22]. It is expected that in the near future robots will be widely implemented and used in the complete assembly and construction of a structure.

## 2.3 COSTS OF STEEL STRUCTURES

### 2.3.1 Introduction

Structures have as main goal to ensure the safety of its occupants at all cost. It means that a structure, besides fulfilling all specified functional and aesthetic demands, have to have sufficient structural performance. A structure must be stable, strong and serviceable. Usually, when designing a structure higher loads than the possible real loads are considered into the design and different scenarios are taken into account. Additional safety factors are included into the calculations to ensure extra safety in the structure in case of unusual events or loading. As expected this safety measures increases the final cost of a structure. A good structural design should fulfil the previous requirements but also be economic in order to be competitive in the market of buildings. A design that focus mainly on safety measures will proba-

bly lead to an oversized and less economic structure. On the other hand, a economic-focused design will end with a less expensive and optimized structure but the degree of robustness of the structure may decrease.

### 2.3.2 Cost of steel structures

The costs of a structure have a major influence on the final cost of a building or a project. For a steel structures the cost distribution is presented on Figure 2.8. For a typical multi-storey office building the cost of the steel frame structure can be broken down into 6 items [4]:

- Raw material
- Fabrication
- Construction
- Fire protection
- Engineering
- Transport

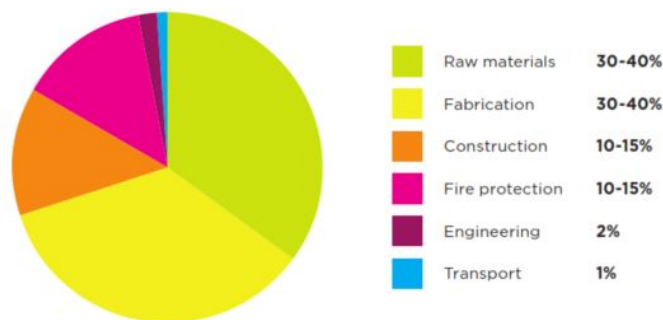


Figure 2.8: Cost distribution of steel structures [4].

Usually in order to calculate the cost of a structure, after the structural elements have been sized and selected, the length of the structural member would be multiplied by its weight, expressed as  $kg/m$ . This rate per tonne of all components includes different elements of the cost of the profile, such as the raw material, detailing, fabrication, transportation and erection [4].

Taken into account the way the costs of a structure are presented ( $kg/m$ ) it could lead to false assumptions such as thinking that a steel structure with the minimum tonnage will also have the lowest costs. As Figure 2.8 shows, the fabrication cost also accounts for around 30% of the total cost of a structure. For unusual design, such as ones with complex geometries, higher proportions of non standard sections, complex connections, etc. will have a higher fabrication costs, and the overall rate per tonne will likely be higher.

Figure 2.9 presents an overview of the workmanship and materials cost in different phases of the building process. The blue color indicates the workmanship costs whereas the material cost is indicated in brown. The yellow

area represents the stage where important decisions are taken in terms of design, type of material, production method, etc. This stage will have a great impact on the final cost of the structure. From the figure can be concluded that 88% of the total cost is determined by the end of the design phase which means that the cost of the structure is highly affected by the decisions made in the design phase [5]. The decisions taken during fabrication, erection and assembly of the structure will barely affect the final cost of the structure.

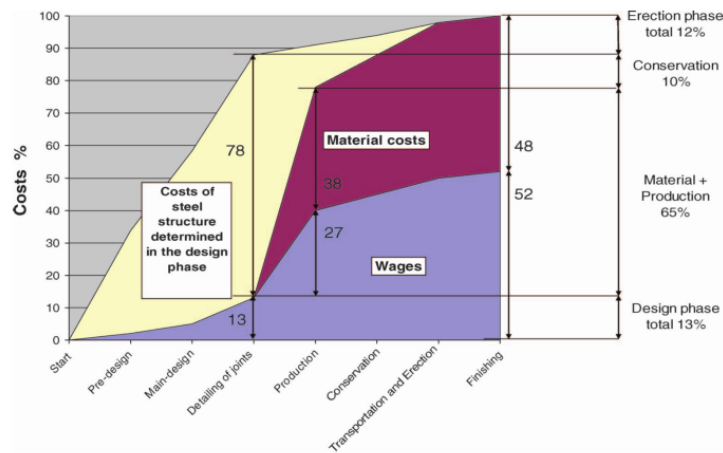


Figure 2.9: Workmanship and materials cost in different phases of the building process [5]. Brown color indicates the material cost and blue color indicates the workmanship costs.

According to [5] a large part of the cost of a steel structure is related to the joints, as shown on Figure 2.10. These costs added up together to 50% of the total cost which includes the phase of pre-design, final design, detailing and preparation work, material, fabrication, conservation and erection and transportation. The material and production cost are predominant being these 38% and 27% respectively. Then it is clear that the type of joint, its fabrication and its installation procedure have an important influence on the total cost of a steel structure.

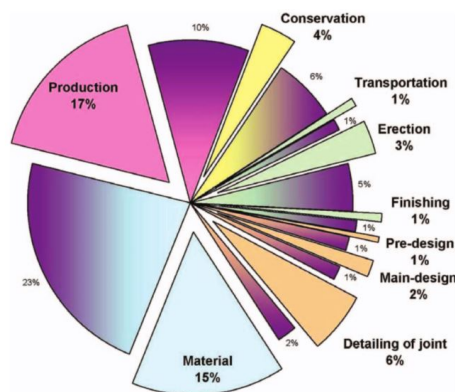


Figure 2.10: Costs related to joints of a steel structure [5].

Connections on typical multi-storey buildings usually account for 10% of the total weight of the frame structure but can account for a significant larger percentage of the total frame cost. Cost of connections is mainly based on

their complexity rather than their weight [4]. A balance between material cost and fabrication cost of the connections should be achieved.

## 2.4 STRUCTURAL OPTIMIZATION

### 2.4.1 Introduction

Structural designers often provide a certain degree of spare capacity in the structural designs in order to reduce the amount of engineering work as well as the fabrication and construction costs. Rationalization of sections types is a common engineering practice which includes several benefits such as [23]:

- repetition of details and dimensions
- interchangeable elements for easier erection
- reduced design and fabrication detailing

For example, cross sections that are design for the most loaded element is repeated and copied to less loaded elements to avoid confusions on the construction site. However, some studies suggest that often structures are too rationalized and material is not efficiently used which usually results in an overcapacity of the structure. [17] studied and analyzed the structural design of 23 steel-frame buildings to estimate how much steel could be saved. In this research it has been concluded that the average utilization rate of the steel structural members is 54% corresponding to a spare capacity of 85%.

The difference between theory and the reality on site suggests that the relationship between material minimization and design rationalization is not balanced. Therefore, considerable material savings without compromising the structural performance and without too much impact on the fabrication and construction cost can be achieved [18].

Structural optimization methods could be implemented to reach a balance between rationalization and material consumption. Implementing optimization methods can reduced the engineering work and automation can be reached. As consequence, clients, constructors and engineers could be benefited by including structural optimization methods on the design phase of a structure. A structural optimization system is described on Figure 2.11.

### 2.4.2 Structural optimization

On the recent human history the emergence and development of computational power in the last decades has opened a large amount of possibilities to design optimization of structures. New and advanced numerical optimization methods support structural designers and engineers in finding an optimal design.

In the 1940's and 1950's the availability of the digital power led to application of linear programming techniques to plastic design of frames using mathematical programming techniques. The space race in the 60's and the demand for lightweight structures led to the development of new design

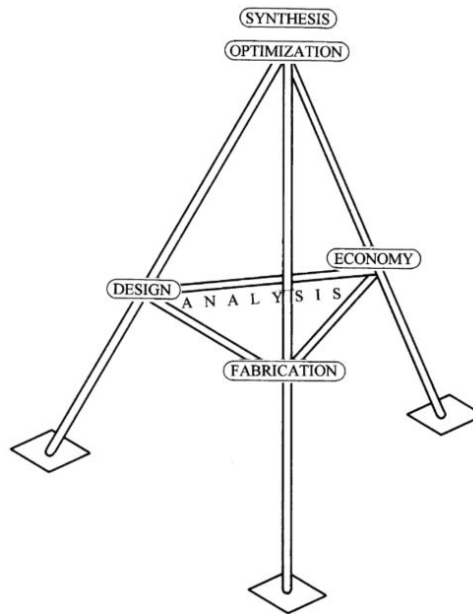


Figure 2.11: Structural optimization system [6].

techniques. Complex civil, aeronautical and space structures were analysed and designed thanks to the availability of digital computers, finite element method and more powerful mathematical programming algorithms. The “optimality criteria” approach was considered for the first time in the 70’s. This approach establishes the criterion that defines the optimum and then devise a recursive formula that, by an iterative process, leads to the desire solution. This means that if the criterion is satisfied, subject to the constrains, then the design is optimum [24].

Nowadays evolutionary algorithms are usually used for solving discrete frame optimization problems such as simulated annealing, generic algorithms, ant colony optimization, particle swarm optimization, among others [25]. The general idea behind this evolutionary algorithms is to explore a design space randomly, thereby moving forward towards a better performing design by collecting data and information from previous analyses.

Evolutionary algorithms are the most popular and widely used since they are relatively easy to understand and to implement, allowing that a non-specialist user include real-world constrains. Despite this is a powerful method and easy to implement, it has important deficiencies. This algorithms have a slow convergence and global optimality might not be reached since no conclusive convergence checks can be made [25]. The defined starting point, which is generated randomly or chosen based on intuition, will influence the results leading to sub-optimal designs. Once a solution is found it is not longer possible to know how much further benefit is available. This means that effort might have been wasted improving a design that was already efficient [1].

### 2.4.3 Applicability restrictions of optimized structures

Despite optimization techniques and optimization packages are becoming more and more available for the structural design community and despite its great potential to achieve the most efficient designs, very optimized designs are not commonly used in the engineering practice. Usually an optimized structure generated by a topological optimization will have complexity of form and geometry. This unusual-shaped structure will be a material-efficient design but its complexity will probable lead to higher costs than a convectional non-optimized structure. In other words, besides reducing its weight, deflection or optimizing all members of a structure, constructability and production cost of optimized structure should also taken into account.

### 2.4.4 Types of structural optimization

While optimizing a structure, three strategies addressing different aspects from the design can lead the optimization: size, shape and topological optimization. For each strategy different parameter or design variables steer the design. Figure 2.12 shows an example of each structural optimization type.

#### *Sizing optimization*

The layout of the structure is fixed and the design variables are usually geometrical parameters such as length, width or section area of the analysed members.

#### *Shape optimization*

A shape can be optimized by controlling its boundaries. The design variables could be the height of a truss, angle of the diagonals or the length of the members.

#### *Topological optimization*

The design domain, loads, boundary condition and amount and type of material are specified. An optimal placement of material points within a reference domain is obtained and an optimal internal member configuration is achieved.

Most topological optimization methods are usually formulated based on the ground structure approach [26], in which nodes are distributed among a design domain or design space, then connected by potential connecting bars. Usually this method leads to structures that are too difficult to fabricate in practice [27] [28]. Studies shows how structural optimization can be also performed based graphic statics, where structural optimization is conducted using design variables in the force domain or also known as the force diagram [29]. In this research topological optimization method, or layout optimization for frames, is applied on a traditional steel frame warren-type truss based on the two-step approach proposed by [1].

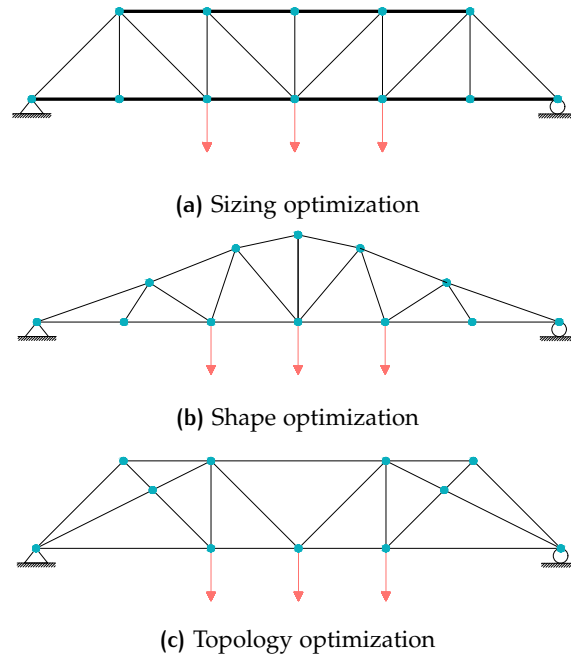


Figure 2.12: Types of structural optimization.

#### 2.4.5 Layout optimization: Two-step approach

[1] presents an optimization approach using layout optimization which will be followed on this research project. This approach could be explained as a two step method:

First, a problem is optimized and simplified accounting for only equilibrium and stress limits considerations and no limits on form complexity are imposed. As result a minimum weight structure is found. This "optimum layout" structure will be the benchmark. For the second step the benchmark design is gradually rationalized through the solution space taking into account buildable and practical considerations. Figure 2.13 shows how the two-step approach works.

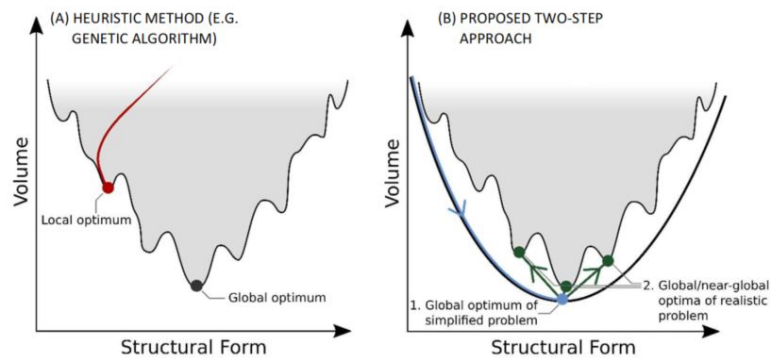


Figure 2.13: Two step approach [1].

The optimum layout resembles a Michell truss [30], who was the first to discuss optimal layout of trusses for different types of loading. A Michell structure is an optimal structure composed of a arrangement of bars of infinitesimal lengths. The bars of the truss follow logarithmic spirals that inter-



sect the radial lines under  $\pm 45^\circ$ . Although this structure does not represent a practical design, a structure in which no allowable stresses are exceeded and the minimum weight is found [7] [30]. Figure 2.14 shows an example of a Michell truss for the transmission of a point load  $P$  to the foundation.

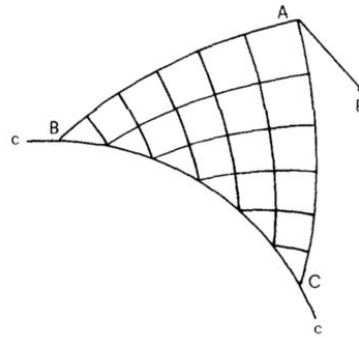


Figure 2.14: Example of a Michell truss [7]

Continuum based topology optimisation methods are generally used to determine a structure with a minimum weight. This method is commonly used in the aerospace and automotive industry rather than civil and building industry due to the fact that building structures are composed of the assembly of discrete elements and its occupied volume inside the design domain is low. For this reason [1] applied numerical layout optimisation methods which uses a ground structure. Similar as [7] did on his research, by restricting the position of the nodes within the design space in a grid of rectangular meshes and interconnecting the nodes with potential members, a truss conformed of finite numbers of joints can be obtained.

[1] used a case study of a transfer basement truss which spans  $50m$ , to demonstrate how this two-step optimisation procedure performs and how could be implemented on real engineering practice.

**Step 1:** taking into account real boundary conditions, support conditions, stress and equilibrium considerations, a global optimum ground structure based on layout optimisation method was found. This structure has the minimum volume and complexity of shape or geometry are not considered for its design. Figure 2.16c shows the generated optimum structure.

**Step 2:** by rationalizing manually the optimum structure (benchmark) a simpler structure was generated. For this step the number of members and nodes were reduced, some complex nodes were removed, cross sections were standardized as much as possible and a more intuitive or common layout shape was found. The final rationalised optimised truss structure can be observed in Figure 2.16b.

For the same established pattern of loads and constrains a conventional-shaped truss, similar to a Warren truss was design and analyzed, shown on Figure 2.16a. A comparison taking into consideration final weight and shape/geometry between the mentioned truss designs is presented on Figure 2.16.

Since this was an exploratory study and in order to make it comparable to convectional truss strictures, some assumptions and considerations were taken within the case study:



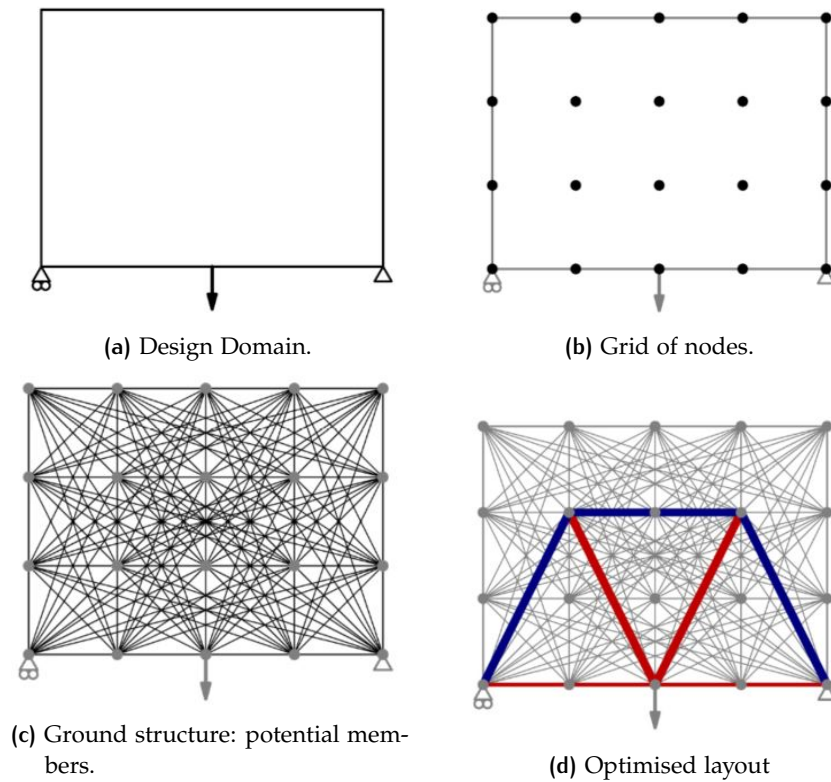


Figure 2.15: Numerical layout optimisation steps [1].

The structure was generated using hollow square sections made of S355 steel plate. The permissible strength in compression was reduced to the effect of member buckling. All unrestrained nodes were modelled as pin-joints. Deflection on this study was not considered as a main constrain, instead only the ultimate limit state restrictions such as stress limits were considered. The LimitState:FORM software was implemented to edit manually the optimised solution in order to produce a simpler structure taking into account also buildable considerations. This software allows to second-optimize the problem and adjust it within a few seconds.

#### 2.4.6 Conclusions

As presented on Figure 2.16, considerable weight reduction of a truss structure could be achieved by implementing this two-step layout optimisation procedure. In the case study presented by [1], an optimised and rationalised structure (Figure 2.16b) presented a weight reduction of almost 50% compared to a Warren-like truss (Figure 2.16a). It is mentioned that the convectional-shaped truss presented 32% more deflection than the optimised ones.

Structural optimisation can be a powerful tool that could help structural engineers developing material-efficient structures. Considerable reduction and savings on material, embodied carbon and/or costs could be achieved. The two-step optimisation approach proposed by [1] will be followed in this research project in order to find a optimised truss structure. Potential advantages of layout optimisation were also presented on this section.

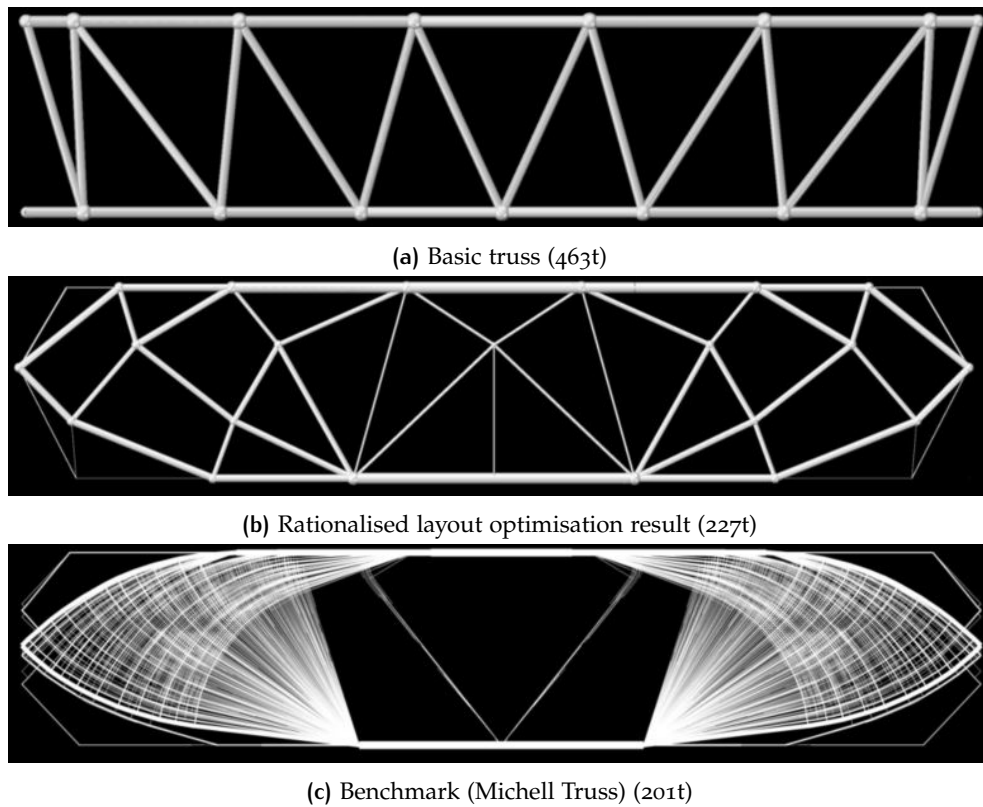


Figure 2.16: Case study of a transfer truss [1].

Despite all the potential advantages this method could contribute to a design, the complexity of form of the structure and unusual joint configuration are still important factors that influence the applicability of this optimisation techniques in real engineering practice. The cost related to the material that could be saved by optimising a structure can be overshadowed by the complex-joint configuration.

## 2.5 SNAP-FIT CONNECTIONS

### 2.5.1 Introduction

As presented on the previous section 2.4, an structurally-optimized structure could have several benefits compared to a conventional non-optimized one. One of the main difficulties and disadvantages of such structures is the complex-joint configuration that is generated after the optimized process. For that reason, a design concept of an innovative non-conventional joint for an layout-optimized truss is developed in this research project. This innovative connection is based on connecting different elements to one node using the snap-fit connecting principle.

In this section a review of different types of snap-fit connections and its application is presented. Similarly, some basic design considerations are presented which will be used in Part iii.

### 2.5.2 General information

Snap-fit and buckle clips mechanisms are very simple, quick and cost effective method to of assembly two parts through an interlocking configuration. In this fastening mechanism a protrusion on one part is slightly deflected during assembling to catch in a depression or undercut molded into the other part [10]. Snap-fit are usually used for joining dissimilar plastics, or plastics to metal. This joining mechanism can be design for permanent fastening or for repeated assembly and disassembly.

Due to its nature, snap-fit methods require more attention to engineering design than other mechanical fastening methods. If a snap-fit is not properly design and analyzed fail could occur during assembly or during use. Stress analysis and stress concentrations are important factors that need to be studied with hand calculations and if require using finite element analysis for accurate results. Snap-fits can be design with many materials. Due to its high flexibility, thermoplastic materials are preferred [8].

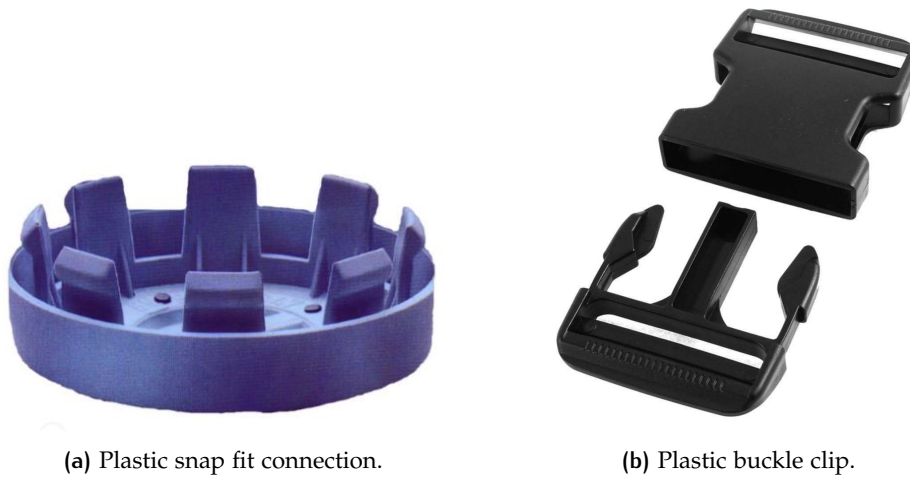


Figure 2.17: Snap-fit and buckle clip connecting mechanism.

### 2.5.3 Main advantages and disadvantages

This mechanism has an easy and intuitive assembly procedure. The purely state of a snap-fit connection does not require any inclusion of additional materials such as adhesives, fasteners or bolts. Since these connections are usually made of plastic materials and manufactured using mold injections, the production rate is relatively high and minimal tooling is needed. Snap-fits allow to connect effectively similar and dissimilar materials, such as a metal-to-plastic connection. As mentioned before, a snap-fit connection could be design as a permanent fastening devise or for repeated disassembly [10] [19].

Although it seems that snap-fits connections could be a highly effective and an infallible way to connect two elements, are also vulnerable and very difficult to repair in case of fracture. Fatigue of the component is a major case of failure and fracture of the part and could led to irreversible damage leaving the connection unusable. For this reason, ductile materials are preferred for a snap-fit part. Other factors, such as thermal expansion, moisture

uptake and environmental impacts, could influence its performance and are important to consider [10].

A snap-fit connection could have different designs and shapes. The most important and common designs are cantilever snap joint, U-shaped snap joints, torsion snap joints and annular snap joints [19]. For this research cantilever snap joints will be studied and developed further.

#### 2.5.4 Cantilever snap-fit joints

A cantilever snap joint or cantilever beam snap-fit consist on a hook-and-groove joint in which a protrusion or overhang from one part interlocks with a groove on the other part [10]. This is the most common snap-fit design and after insertion provides good retention and the joint is usually stress-free. Figure 2.18 shows the a conventional cantilever snap-fit beam.

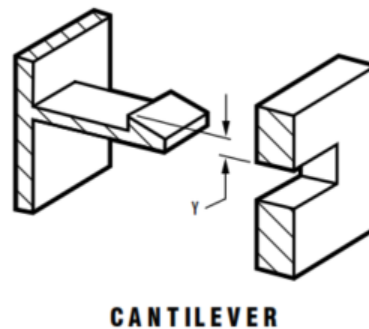


Figure 2.18: Cantilever Snap-fit beam [8].

#### 2.5.5 Cantilever snap-fit Design

As mentioned before, a cantilever snap-fit consist can be simplified as a cantilever beam with an overhang at the end of the beam and the depth of this overhang will define the amount of deflection during its insertion. Figure 2.19 presents the different sides of the overhang of the beam. Usually this overhang has a gentle angle on the side that will have the first contact with the other part. This angle on the entrance side will be called  $\alpha$  from now on. This angle  $\alpha$  helps to reduce the assembly effort while the angle on the retraction side ( $\beta$ ) makes disassembly possible or impossible depending on the intended use of the connection. Assembly and disassembly forces can be optimized by changing these angles [8].

Integrity of the assembly and strength of the beam are main design considerations. The amount of required deflection and so the integrity of the assembly is governed by the stiffness ( $k$ ) of the beam. The product of the modulus of elasticity ( $E$ ) and the cross sectional moment of inertia ( $I$ ) of the beam will determine the total rigidity of the beam [8].

A perfect balance between the overhang depth and allowed deflection is a key factor for the design of a cantilever snap-fit beam. By increasing the overhang depth, the deflection has to increase and the beam stress also increases. The shape and geometry of the beam has to be optimized in order

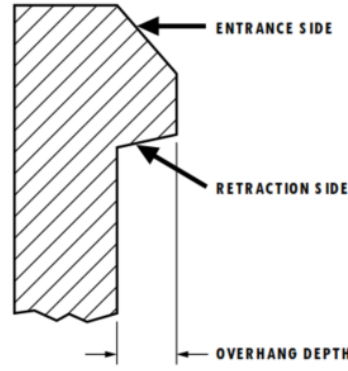


Figure 2.19: Sides of a cantilever Snap-fit beam [8].

to achieve the desired deflection without exceeding the strain limit of the material.

The amount of deflection and the involved forces can be calculated using the classical beam theory based on Castigliano's second theorem. It assumes that beam is rigidly fixed to the base and the deflection is due only bending stress part [10].

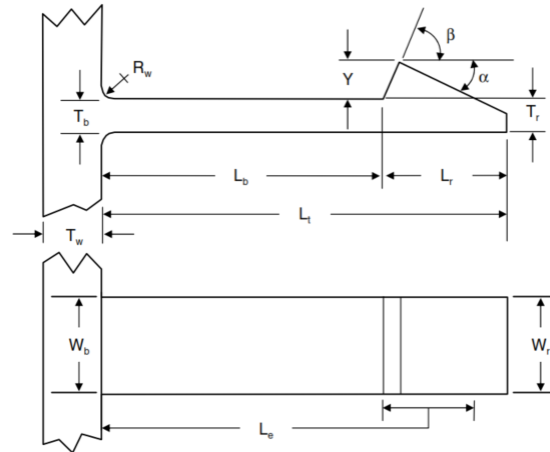


Figure 2.20: Cantilever Snap-fit beam dimensions and angles [9].

Figure 2.20 shows a rectangular cantilever beam with constant cross section. For these beams, the permissible deflection depends on the overhang height ( $Y$ ), the thickness ( $T_b$ ), the length ( $L_b$ ), and the maximum strain of the material ( $\epsilon$ ):

$$Y = \frac{2\epsilon L_b^2}{3T_b}$$

Permissible strains for snap-joints that are design for a repeated assembly are usually 40% lower than for permanent assembly joints. However, safety factors should be applied since the most damage occurs after the initial deformation. For conventional materials used in snap-fit joints the deflection should be less or equal to 0.5 times the length of the beam. The length/thick-

ness ratio influences allowable strain. A typical length/thickness ratio used in snap-fit cantilever beams is 5.4 [10].

The deflection force ( $P$ ) needed to bend the end of the cantilever equal to the overhang ( $Y$ ) depends on the geometry and the secant modulus of the material ( $E_s$ ) [10]:

$$P = \frac{W_b T_b^2}{6} \times \frac{E_s \epsilon}{L_b}$$

The secant modulus of the material ( $E_s$ ) is recommended to use instead of the elastic modulus in order to obtain more accurate estimates of the deflection on the momentary high-stress application.

The assembly or engagement force ( $F$ ) depends on the deflection force ( $P$ ), the entrance side angle ( $\alpha$ ) of the overhang and the coefficient of friction ( $\mu$ ) of the material [10]:

$$F_i = P \left[ \frac{\mu + \tan \alpha}{1 - \mu \tan \alpha} \right]$$

For a snap-fit cantilever beam that has constant cross-section the stress distribution is not equally distributed along its length. The stress is concentrated at the base of the beam. A radius on the root or base should be added to reduce stress concentrations. The ratio radius/height has a major influence on the stress concentration. It is recommended that this ratio should be close to 0.6 [10]. Tapering the cantilever beam from the base to the tip will improve and distribute evenly the stress along the length of the beam as shown on Figure 2.21. A beam can be tapered along its thickness and/or also along its width. By tapering the thickness, a better stress distribution and more flexibility will be achieved.

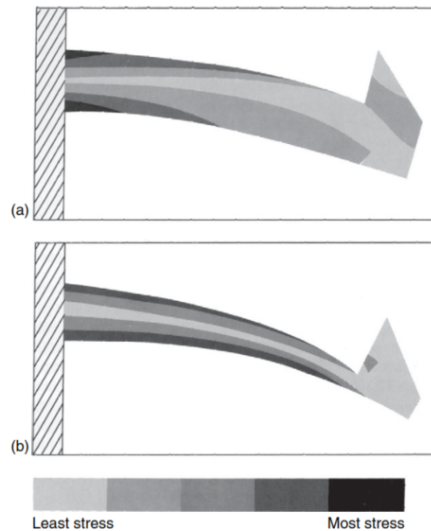


Figure 2.21: Stress concentration of a snap-fit cantilever beam with a constant and tapered cross section [10].



### 2.5.6 Rules of thumb for cantilever snap-fit beam design

The handbook [9] gives some recommendations and rules of thumb for cantilever snap-fit beams design. This rules will be affected by the snap-fit application, material, shape variation and processing variation.

Beam thickness at the base ( $T_b$ ): if the beam protrudes from a wall,  $T_b$  should be at least 50 to 60% of the wall thickness. If the beam is an extension of the wall,  $T_b$  should be equal to the thickness of the wall.

Beam length ( $L_b$ ): The total cantilever hook beam ( $L_t$ ) is divided into the length of the beam ( $L_b$ ) and the retention part length ( $L_r$ ). Beam length should be taken between 5 to 10 times the thickness of the beam ( $[5-10] \times T_b$ ). Shorter beams are much less flexible and create higher stresses at the base. Larger beams are more flexible but become weaker for retention.

Insertion face angle ( $\alpha$ ): the shallower the angle, the lesser the force required to deflect the hook. A commonly used angle is  $25^\circ$  -  $35^\circ$ .

Retention face depth ( $Y$ ): the undercut ( $Y$ ) determines the total required deflection during engagement. For a beam length/thickness ratio  $L_b/T_b$  of 5:1, the undercut depth ( $Y$ ) should be less than  $T_b$ . For  $L_b/T_b$  ratio close to 10:1, the initial undercut depth can be equal to  $T_b$ .

Retention face angle ( $\beta$ ): the steeper the angle, the higher the retention strength. For a non-releasing or permanent lock the retention angle  $\beta$  should be between  $80^\circ$  -  $90^\circ$ . Due to frictional effects, any angle above a threshold angle will behave like a  $90^\circ$  angle.

Beam thickness at the tip ( $T_r$ ): at the retention face the thickness is usually equal to the base thickness ( $T_r = T_b$ ). However, as explained before the beam thickness of the beam could be tapered in order to improve the stress distribution along its length. A common  $T_b:T_r$  ratio for tapered beams range from 1.25:1 to 2:1. By applying tapering on a beam the deflection of the beam could increase and so strains could be reduced as much as 60%.

Beam width ( $W_b$ ): for beam theory to be applicable, the width should be less or equal to the length. For widths larger than  $\frac{1}{2}$  of the length, the snap-fit will behave more as a plate than a beam.

## 2.6 CASE STUDY

### 2.6.1 Introduction

Structural optimisation can modify and improve different characteristics of the design of a structure as explained before in Section 2.4. Sizes of cross sections can be optimized, the shape of the element or structure can be modified and also an optimal design could be obtained by optimising the topology. Structures and structural elements have witnessed an increasing design-improvement over the years. New structural designs have to be cost-performance efficient in order to be competitive and appealing for the clients in a tough engineering market.

Is it possible to improve even more an already weight-efficient and aesthetically pleasant truss design? An existing truss structure will be taken as case study to demonstrate a possible weight-reduction optimisation based on the

structural layout optimisation approach proposed by [1] and mentioned on Section 2.4. The structure that has been chosen for this research project is Wimbledon No.1 Court retractable roof trusses.



Figure 2.22: Wimbledon No. 1 Court roof.

### 2.6.2 Wimbledon Court No.1 roof

The image of the Wimbledon Court No.1 has been renewed after the re-development of some steel work elements and the additions of seat levels. Probably the most striking modification is the demolition and replacement of the existing roof built in 1997. The old roof was replaced with a  $83 \times 75m$  retractable roof made of a waterproof and translucent material that will guarantee uninterrupted tennis regardless the weather conditions.  $7500m^2$  of fabric covers the court and it weighs four tonnes. A picture of the new retractable roof can be observed on Figure 2.22. The retractable roof is made of translucent Gore Tenara, which is a type of Gore-Tex fabric. The designing and manufacturing company MOOG designed and developed the motion system for the retractable roof using hydraulic power units. The covered area is around  $5500m^2$  and it takes to open/close the entire roof safely and accurately only 8 minutes [31]. The design and planning of the roof took two years and the construction of it lasted 3 years. The installation was completed on April 2019.



Figure 2.23: Wimbledon Court No.1 retractable roof.



### 2.6.3 Structure

The roof structure includes 11 movable steel prismatic trusses that support a translucent, weather-resistant fabric canopy. Each truss is approximately 75m long and has an average lift weight of 93 tonnes [32]. Sheffield-based engineering specialist SCX have been at the heart of the design, planning and construction of the No.1 Court roof. A secondary structure provides support to the rails that carry the moving roof. The engineering firm Advanced Computational Analysis (ACA) verified design of the steel trusses by conducting both static and dynamic 3-D analyses using ANSYS software. Real world load and stresses were considered and studied [33]. All the structural members are conformed by steel circular hollow sections.

It makes sense that additional elements which will be added on top of an existing structure must be as light-weight as possible since the extra weight will be carried out by the existing structure and transfer ed to its existing foundations. Any extra weight than the structurally allowed could lead to the need of reinforce the structure which imply additional and probably unnecessary costs. It makes even more sense the use of available optimisation tools on cases when besides adding a supplementary structure, this structure is required to be retractable or movable. Any variation on the weight the structure will affect the capacity-requirements of the motion system which again will be reflected on the final cost of the project.

All structurally, aesthetically and functional requirements have been fulfilled in the design of the retractable roof of the Wimbledon Court No.1 by the design team. For this reasons this retractable roof is a perfect example of a structure that must be as weight-efficient as possible. On this research project a steel truss from the retractable roof will taken and will be optimised searching for an even more weight-efficient truss structure using the optimisation approach presented by [1].

Unfortunately, essential information about the structural design of these trusses is not available for the public since the design information is governed by a confidentiality agreement. It means that information related to structural plans, details, loads considerations and assumptions, full geometry and the used cross-section could not be found. For this reason all the lacking information will be based on codes, pictures, reports and engineering judgement. This will not affect the product of the research project since, as explained before, one of the main objectives is to perform an structural optimisation procedure in a case study in order to compare the optimised structure with the original one. Then, a joint of the optimised structure will be design and analysed.

### 2.6.4 Geometry and design considerations

Considering the lack of necessary information, a structural analysis and design with real information and conditions will not be feasible. For this reason the following assumptions will be used:

### 2.6.4.1 Geometry

It is known that the trusses spans  $75m$  between supports and that each truss weight approximately  $93tons$  [32]. Looking at some pictures and drawings it can be observed that the truss is divided into 11 bays. The bays are equally-long except for the first and the last. The bottom chord of the truss is straight element and the top chord has a curvature.

For this research the truss structure was re-drawn using CAD software based on pictures and drawings found online. It was found that the total height at mid-span is  $6.50m$  and the height at the supports is  $3.30m$ . As mentioned before, the span is divided into 11 segments or bays and each one of those have  $6.50m$  of length. Figure 2.24 presents the geometry of a steel roof truss from the case study. The bottom chord has a length of  $71.50m$  and the curved top chord is  $75.36m$  long (arc length). The top chord curvature is formed by a  $20^\circ$  angle and a radius of  $221m$ .

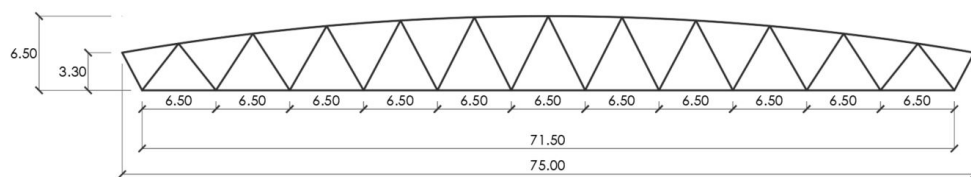


Figure 2.24: Geometry of Wimbledon Court No.1 roof truss (distances in meters).

### 2.6.4.2 Steel members and joints

All structural members from the top chord, bottom chord and diagonals are formed by steel circular hollow section (CHS). As shown on Figure 2.25 the diagonal steel members are connected to the bottom and top chord with bolted connections. A steel fin plate is welded into position to the top and bottom chord where the diagonals are bolted.



Figure 2.25: Wimbledon roof truss bolted joint.

### 2.6.4.3 Support conditions

The truss is simply-supported at its ends as shown on Figure 2.26. The supports do not allow movement along the truss axis. Since it is a retractable

roof, the trusses are supported on wheeled trolleys that run along a rail which allow movement perpendicular to the truss axis. As it is possible to observe on the figure the truss is supported at the ends of the top chord.

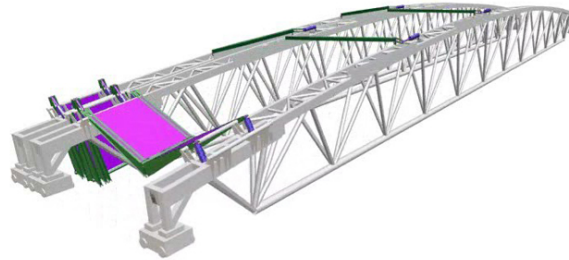


Figure 2.26: Support conditions of truss [11].

## 2.7 CONCLUSION

A truss is a lightweight structure which consist of triangulated system composed of straight interconnected members into joints. Usually a truss is composed of wooden members or cold or hot-rolled steel structural members. Only axial in-plane tension and compression forces are taken by the members and transferred to the supports. The members are usually connected to the top and bottom main chord. Welded and bolted are the most conventional connections.

Structural joints have a major impact on different aspects of a structure. Costs related to joints of a steel structure can reach the 50% of the final cost of the structure. Similarly, the assembly of joints have a direct impact on the assembly time of the structure.

More efficient designs can be achieved by implementing optimization procedures from the design phase to the construction phase of a structure. By implementing such tools, a balance between rationalization and material consumption can be achieved. Despite optimization techniques and optimization packages are becoming increasingly available for engineers and designers, optimized structures are not commonly used in real engineering practice due to the complex configuration an optimized structure might have, specially when using topological or layout optimization. Layout optimization can be used for optimizing a truss structure. The recently developed two-step optimization approach proposed by [1] looks promising and will be implemented and analysed on the case-study truss.

Snap-fit connections seems an efficient way to connect two elements that stand the action of tensile and compressive forces. They are usually composed of thermoplastic material which allows multiple assemblies and dis assemblies. This connecting concept will be further studied and developed since is a fundamental part of the research.

The chosen case-study truss will be used to show how an already weight efficient and aesthetically pleasant truss can be further optimized without compromising its functionality.

## Part II

### STRUCTURAL DESIGN AND OPTIMISATION

# 3

## STRUCTURAL DESIGN OF STEEL TRUSSES

### 3.1 INTRODUCTION

This chapter describes the structural design procedure applied on the case-study truss. As it was mentioned on the previous chapter, information regarding to the original structural design was not available. For this reason, assumptions based on the location of the case-study truss and based on engineering judgment were made. The following research sub-question is answered:

*Which are the design assumptions for the structural design of the case-study truss?*

This emphasis on this chapter is on the load assumptions using the Eurocode as guidance based the location of the case-study truss, and on the structural design of the truss. The results obtained on this chapter are used in Part [iii](#), where the comparison between the case-study truss and the optimized truss is discussed.

### 3.2 ASSUMED LOADS

Using a correct load distribution and load pattern when designing a structure is of great importance. The acting of a load may vary between different structures. For this reason a study of the possible loads on a structure must be investigated prior the structural design.

The Eurocode EN 1990 identifies 3 different loads on structures:

- Variable load ( $Q$ ): Imposed loads on building floors, beams and roofs, wind action or snow loads.
- Permanent load ( $G$ ): Self-weight of structures, fixed equipment.
- Accidental load ( $A$ ): Explosions or impact from vehicles.

At locations where earthquakes could occur, seismic loads must be considered. A seismic load ( $A_E$ ) is an action that arises due to earthquake ground motion and it can be either considered as variable or accidental action, depending on the available information (see Eurocode EN 1991 and EN 1998). Normally a fire risk assessment should be also part of a design and it is also considered as an accidental action (see Eurocode EN 1991-1-2). Accidental loads have a very small probability to occur. For this reasons they will not be taken into account in this research project.

## Load cases

Structures are usually design under the most critical load case. A load case is determined by making load combinations of loads that act on the structure at the same time. A load combinations is composed of permanent, variable and accidental loads. Since in this thesis accidental loads are assumed that will not be governing, a load combination will be composed only by permanent (G) and variable (Q) loads.

The Eurocode distinguishes two types of limit states: the Ultimate Limit State (ULS) and the Serviceability Limit State (SLS). The ULS is applied when safety of people and/or safety of structures is concerned. The SLS takes into consideration the comfort of the people and occupants of the building under normal circumstances.

### Ultimate Limit State

According to the Eurocode EN 1990-2002, a structure which is design for ULS needs to be verified for different sates. The ultimate limit states that will be considered in this research project are the following:

- EQU: Loss of static equilibrium of the structure or any part considered as a rigid body. Safety factors shown on Figure 3.1.
- STR: Internal failure or excessive deformation of the structure or structural members. Safety factors shown on Figure 3.2.

Permanent actions		Leading variable action	Accompanying variable actions	
Unfavourable	Favourable		Main (if any)	Others
$\gamma_{gj,sup} G_{kj,sup}$	$\gamma_{gj,inf} G_{kj,inf}$	$\gamma_{q,1} Q_{k,1}$		$\gamma_{q,i} \Psi_{0,i} Q_{k,i}$

Figure 3.1: Load factor for ULS EQU. Reproduced from BS-EN 1990:2002.

Where the partial safety factors for EQU limit state are:

$$\gamma_{gj,sup} = 1.10$$

$$\gamma_{gj,inf} = 0.90$$

$$\gamma_{q,1} = 1.50$$

$$\gamma_{q,i} = 1.50$$

And the partial safety factors for STR limit state are:

$$\gamma_{gj,sup} = 1.35$$

$$\gamma_{gj,inf} = 1.00$$

$$\gamma_{q,1} = 1.50$$

$$\gamma_{q,i} = 1.50$$

Permanent actions		Leading variable action	Accompanying variable actions	
Unfavourable	Favourable		Main (if any)	Others
$\gamma_{gj,sup} G_{kj,sup}$	$\gamma_{gj,inf} G_{kj,inf}$			$\gamma_{q,i} \Psi_{0,i} Q_{k,i}$
$\psi \gamma_{gj,sup} G_{kj,sup}$	$\gamma_{gj,inf} G_{kj,inf}$	$\gamma_{q,1} Q_{k,1}$		$\gamma_{q,i} \Psi_{0,i} Q_{k,i}$

Figure 3.2: Load factor for ULS STR. Reproduced from Bs-EN 1990:2002.

Since the accidental loading ( $A$ ) is not considered, the frequent ( $\Psi_1$ ) and quasi static value ( $\Psi_2$ ) will not be taken into account. According to Table A1.1 from the BS-EN 1990:2002 Annex A, for roof structures the value of  $\Psi_0$  is equal to zero.

Taking into consideration the above mentioned, the load to consider at the ULS is:

$$F_d = \gamma_g G_{k,j} + \gamma_q Q_{k,1} \quad (3.1)$$

Failure of the roof structure has major implications regarding to the loss of life of people and a very large economic and social impact. Therefore, the roof structure is considered as consequence class 3 (CC3) which implies the highest reliability class (RC3). An additional reliability factor  $K_{FI}$  must be included into the load combination for ULS. This means the partial factors can be multiplied by  $K_{FI} = 1, 1$ .

The following combination of actions for persisting design situation must be considered.

$$F_d = 1.35 G_{k,j} (BS - EN1990 : 2002, clause 6.10a) \quad (3.2)$$

$$F_d = 1.2 G_{k,j} + 1.5 Q_{k,1} (BS - EN1990 : 2002, clause 6.10b) \quad (3.3)$$

### **Serviceability Limit State**

As mentioned before, the SLS guaranties comfort and the proper functioning of the structure under normal circumstances. The load equation for SLS is the following:

$$F_d = \gamma_m G_{k,j} + \gamma_m Q_{k,1} \quad (3.4)$$

Where  $\gamma_m$  is the partial factor for material characteristics and it is equal to 1.0.

#### **3.2.1 Variable load ( $Q$ )**

##### **3.2.1.1 Wind load**

Eurocode EN 1991-1-4:2005 [34] presents the standards methods to calculate the structural resistance required to withstand the load cause by wind actions on buildings. Wind is classified as variable since wind varies over time and space and wind actions are not always present. The Eurocode classifies the wind action into two categories:

- Quasi-static response
- Dynamic and aeroelastic response



Dynamic wind load on stadiums or sport courts roofs can only be calculated accurately with the help of wind tunnel testing. As mentioned before there is a lack of information from the structural design and design considerations of the case study truss. For this research on project only quasi-static wind response will be considered.

### ***Wind velocity and wind pressure***

The basic wind velocity  $v_b$  in a region in Europe can be determined using the following formula, which considers a 10 minutes wind velocity at 10m above ground of a terrain with low vegetation for a return period of 50 years:

$$v_b = c_{dir} \cdot c_{season} \cdot v_{b,0} \quad (3.5)$$

where:

$v_b$  = basic wind speed [m/s]

$c_{dir}$  = wind direction factor

$c_{season}$  = season factor

$v_{b,0}$  = fundamental value of basic wind velocity [m/s]

Since the Wimbledon Court No.1 is located close to London, the national annexes from the United Kingdom were used (BS NA EN 1991-1-4:2005). They subscribe a value of 1.0 for the wind direction factor  $c_{dir}$  and the season factor  $c_{season}$ . On its location the wind basic wind speed is  $v_b = 23.1 \text{ m/s}$ .

The characteristic peak velocity pressure  $q_p$  one of the main parameter in the determination of the wind actions on a structure and it is the pressure caused by the wind velocity and can be determined using the following relationship:

$$q_p = \frac{\rho}{2} \cdot v_b^2 \quad (3.6)$$

Where  $\rho$  is the density of air and can be taken as  $1.25 \text{ kg/m}^3$ . Then, the characteristic peak velocity will be  $q_p = 0.33 \text{ kN/m}^2$ .

The value of the basic wind speed has to be transformed into the corresponding value at the reference height of the structure. This velocity is known as the mean velocity ( $v_{mean}$ ) and depends on the roughness and the orography of the site where the building is located:

$$v_{mean} = c_r(z) \cdot c_o(z) \cdot v_b \quad (3.7)$$

Where:

$v_{mean}$  = mean velocity [m/s]

$c_r(z)$  = roughness factor

$c_o(z)$  = orography factor (usually taken as 1.0)

### ***Terrain roughness***

According to the Eurocode EN 1991-1-4:2005 the roughness factor  $C_r(z)$  depends on the height of the structure above ground level and the ground roughness of the terrain upwind of the structure. The highest point of the roof structure of the Wimbledon Court No.1 is 25m above ground level.

The roughness factor is related to a minimum height  $z_{min}$ :

$$c_r(z) = k_r \cdot \ln(z/z_0), \text{ but } z \geq z_{min} \quad (3.8)$$

$$k_r = 0.19 \cdot (z_0/0.5)^{0.07} \quad (3.9)$$

Where:

$k_r$  = terrain factor

$z_0$  = roughness length

$z_{min}$  = minimum height

Table 3.1 shows the roughness length and the minimum height for the Wimbledon Court No.1 roof.

Terrain category	$z_0$ , [m]	$z_{min}$ , [m]
III Area with regular cover of vegetation, suburbs	0.3	5

Table 3.1: Terrain categories. Reproduced from Table 4.1 EN 1991-1-4:2005.

Then:

$$k_r = 0.19 \cdot (z_0/0.5)^{0.07} = 0.19 \cdot (0.3/0.5)^{0.07} = 0.183 \quad (3.10)$$

$$c_r(z) = k_r \cdot \ln(z/z_0) = 0.183 \cdot \ln(25/0.3) = 0.81 \quad (3.11)$$

Resulting in an average wind speed of 18.7 m/s at 25 meters height:

$$v_{mean} = c_r(z) \cdot c_o(z) \cdot v_b = 0.81 \cdot 1.0 \cdot 23.1 \text{ m/s} = 18.7 \text{ m/s} \quad (3.12)$$

The peak velocity pressure depends on the basic pressure, the wind profile and the gust factor:

$$q_p(z) = q_b \cdot [c_r(z)]^2 \cdot \left[1 + \frac{7}{\ln(z/z_0)}\right] = 0.56 \text{ kN/m}^2 \quad (3.13)$$

#### Wind pressure for Quasi-Static response

Eurocode EN 1991-1-4:2005 accounts for the external ( $w_e$ ) and internal  $w_i$  wind pressure of a building. The wind pressure depends on the geometry of the structure.

$$w_e = q_p(z_e) \cdot c_{pe} \quad (3.14)$$

$$w_i = q_p(z_i) \cdot c_{pi} \quad (3.15)$$

Where:

$w_e$  = external wind pressure [kN/m<sup>2</sup>]

$w_i$  = external wind pressure [ $kN/m^2$ ]

$c_{pe}$  = external pressure coefficient

$c_{pi}$  = internal pressure coefficient

$z_e, z_i$  = reference height of the structure

Owing to the fact that there is no clear information about the number and size of the openings on the facade, it is assumed that the facade will not influence the roof behaviour under the action of wind. On this research project wind action will be analysed only on the roof and not the facades. Since the chosen case study is a retractable roof, different scenarios in which wind load act will vary. When the roof is completely closed the roof structure behaves as an flat roof and when it is for example, half way open, the structure behaves as a canopy roof.

### *Pressure coefficients*

As mentioned before there is no information about the assumptions that have been used for the structural design of the Wimbledon Court No.1 roof. It is possible that the engineering firm performed a wind tunnel test for different scenarios in order to obtain more accurate pressure coefficients. For this reason, some assumptions and simplifications will be made in this research project.

The wind loads are calculated using a division in pressure coefficients: external and internal coefficients. According to the Eurocode EN 1991-1-4:2005 the external pressure coefficient is subdivided into local ( $c_{pe,1}$ ) and global ( $c_{pe,10}$ ) effects. Global effects are used for areas larger than  $10 m^2$ .



Figure 3.3: Top view of the Wimbledon Court No.1 roof.

The court will be simplified as an simple rectangular building with flat roof. As shown on Figure 2.22 the roof is slightly curved. The angle with respect to the start of the roof is less than  $5^\circ$  and for this reason when the roof is closed (see Figure 3.3) it will be considered as a flat roof. Table 3.2 shows the assumed pressure coefficients for the roof when considered as a flat roof taken from BS EN 1991-1-4.

Wind Coefficients	
Zone	$C_{pe}$
F	-2.0
G	-1.4
H	-0.7
I	-0.2 / +0.2

Table 3.2: External pressure coefficients for flat roofs (assumed with sharp edges).  
Table NA.5 BS-EN 1991-1-4:2005.

Two wind situation must be considered. Wind load parallel to the in-plane axis of the trusses (see Figure 3.4) and wind load acting perpendicular to the trusses axis (see Figure 3.5). The assumed pressure coefficients are presented on both figures within its respective zone. Figure 3.4b shows the zone distribution for a truss which is located on the middle of the roof while Figure 3.5b shows 3 truss positions: at the beginning (case (i)), close to the beginning (case (i)) and a truss located at the middle of the roof (case (iii)). For this research project, an internal truss located on the middle of the roof will be considered (case (iii)) from Figure 3.5b and the presented case from Figure 3.4b)

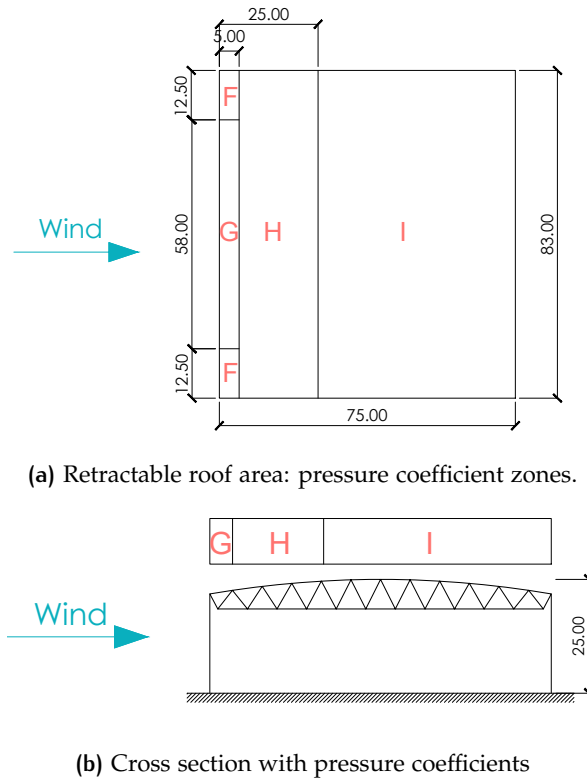
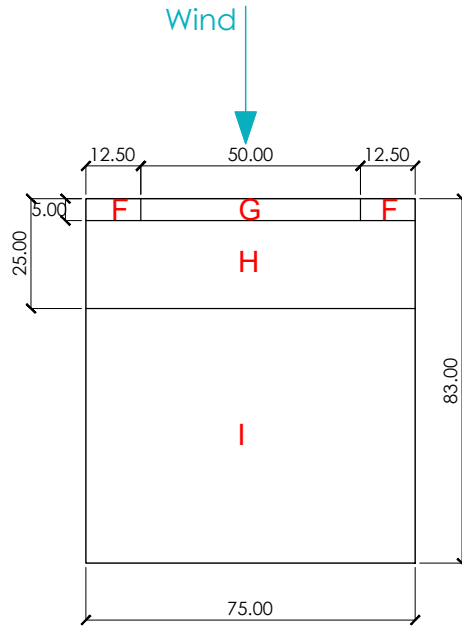
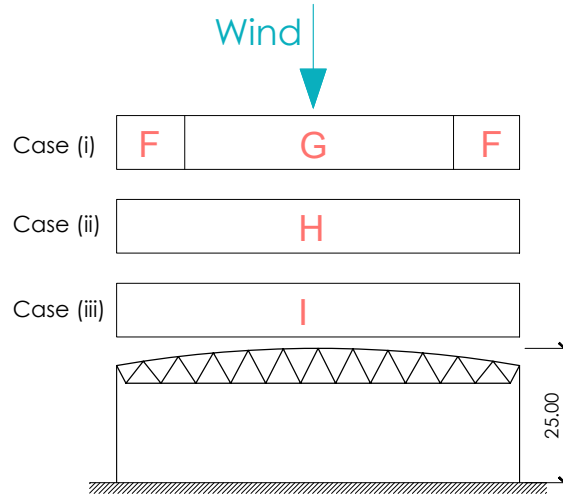


Figure 3.4: Pressure coefficient for case study roof for wind situation 1.

The wind forces ( $F_w$ ) on the building's main structure in case of quasi-static response must be calculated according to section 5.3 of the Eurocode



(a) Retractable roof area: pressure coefficient zones.



(b) Cross section with pressure coefficients

Figure 3.5: Pressure coefficient for case study roof for wind situation 2.

EN 1991-1-4:2005. The force is determined by the vectorial summation of the external, internal and the friction forces. The friction forces will be neglected.

$$\text{External forces : } F_{w,e} = C_s C_d \cdot \sum_{\text{surfaces}} W_e \cdot A_{ref} \quad (3.16)$$

$$\text{Internal forces : } F_{w,i} = \sum_{\text{surfaces}} W_i \cdot A_{ref} \quad (3.17)$$

Where:

$C_s, C_d$  = structural factor

$A_{ref}$  = Reference area of the individual surfaces

The coefficients  $C_s, C_d$  will be taken as 1.0, assuming that the roof structure has a natural frequency greater than 5Hz (section 6.2 Eurocode EN 1991-1-4:2005). Since there amount of openings is unknown, the opening ratio is not possible to estimate. For this reason the internal pressure coefficients  $c_{pi}$  will be taken as the more onerous of +0.2 and -0.3. For roof structures the wind force becomes equal to the difference between the external and internal resulting force.

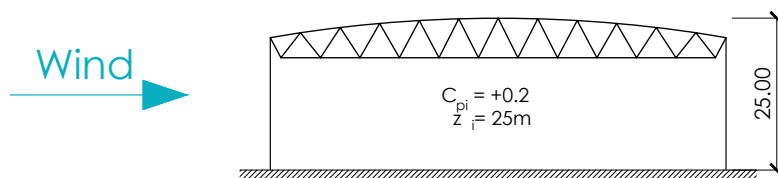


Figure 3.6: Internal pressure coefficient.

Assuming that the distances between trusses is equal 9.50m, the distributed forces on a internal truss are according to Figure 3.7. This figure shows the most onerous case of all possible combinations for an internal truss. The complete table with the calculated wind load with all determined coefficients is presented on the Appendix A in Figure A.1.

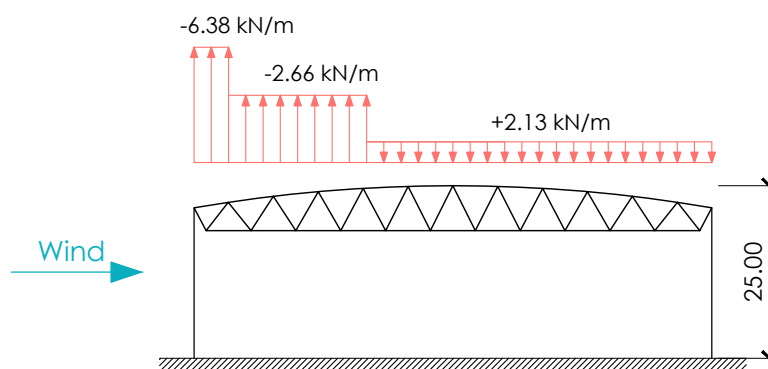


Figure 3.7: Wind force on the central trusses of the roof for wind situation 1 (not influence by roof zone F).

### 3.2.1.2 Snow load

Eurocode EN 1991-1-3:2003 [35] presents the standards methods to calculate the structural resistance required to withstand the load cause by snow actions on buildings. The snow load on roofs is obtained by multiplying the ground load by a factor. The roof load depends on different factors, such as the shape of the roof, the thermal properties of the roof, the surface roughness, the height under the roof, the surrounding area, the presence of surrounding buildings and the local climate.

The snow load  $s$  on roofs can be calculated following the equation presented on EN 1991-1-3:2003 clause 5.2 :

$$s = \mu_i \cdot C_e \cdot C_t \cdot s_k \quad (3.18)$$

Where:

$\mu_i$  = roof shape coefficient

$C_e$  = exposure coefficient

$C_t$  = thermal coefficient

$s_k$  = characteristic value of the ground snow load for the relevant altitude

According to the snow-maps provided by the Eurocode EN 1991-1-3:2003, at the altitude and location of the Wimbledon Court No.1 (Zone 3) the characteristic value of the ground snow load  $s_k$  could be taken as  $0.50 \text{ kN/m}^2$  (see Figure NA.1 from BS EN 1991-1-3:2003). The exposure coefficient  $C_e$  will be taken as 1.0 since it is considered that the location has a normal topography (Table 5.1 EN 1991-1-3:2003). Similarly, the thermal coefficient  $C_t$  will be taken as 1.0, since the thermal transmittance of the roof is not known.

### Roof shape coefficient

The roof shape coefficient  $\mu_i$  coefficient takes into account the possibility of the movement of snow accumulation due to wind. This coefficient adjusts the ground snow load to a snow on the roof considering this effects. For roofs that have a slope close to  $0^\circ$  the roof shape coefficient can be taken as 1.0. As mentioned before, the angle of the case study roof is  $5^\circ$ . Then the snow load will be calculated as following:

$$s = \mu_i \cdot C_e \cdot C_t \cdot s_k = 1.0 \cdot 1.0 \cdot 1.0 \cdot 0.50 \text{ kN/m}^2 = 0.50 \text{ kN/m}^2 \quad (3.19)$$

Due to the prismatic shape of the trusses, for snow actions the roof could be considered as a pitched roof. Eurocode En 1991-1-3 accounts for the undrifted and drifted load arrangements for different types of roofs. Figure 3.8 shows the snow load shape coefficients for pitched roofs, where case (i) shows the undrifted load arrangement while case (ii) and (iii) shows the drifted situation.

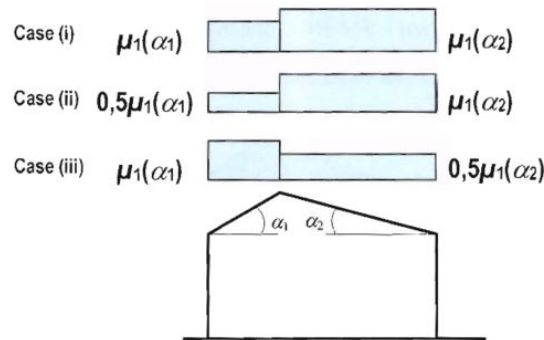


Figure 3.8: Snow load shape coefficients - pitched roofs. EN 1991-1-3.

Assuming that the distances between trusses is equal  $9.50\text{m}$ , the distributed forces due to snow load on a internal truss are according to Figure 3.9.

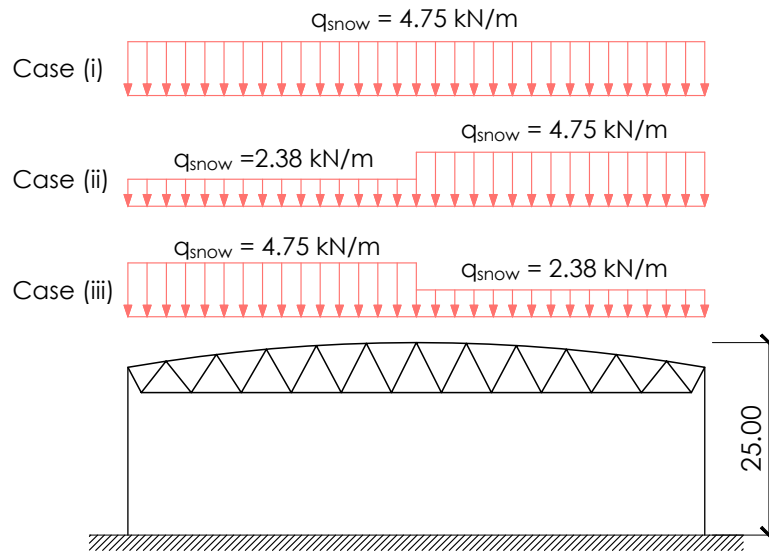


Figure 3.9: Snow load distribution on a internal truss for undrifted and drifted load arrangement.

Due to the geometry and symmetry of the analyzed roof, the less favorable situation is when there is not drift of snow, which is Case (i) from the Figure 3.9.

#### 3.2.1.3 Superimposed load

Load caused by people while repairing the roof must also taken into account. According to the Eurocode EN 1991-1-1, the imposed load for a roof that is not accessible except for normal maintenance and repair will have a load  $q_k$  in between 0 and  $0.4 \text{ kN/m}^2$ . Due to the nature and use of the retractable roof it is expected that high maintenance will be required and additional tools and machines will be needed to repair and/or maintain the roof. An imposed load of  $q_k = 0.7 \text{ kN/m}^2$  will be used in this research.

#### 3.2.2 Permanent load (G)

Other loads than wind and snow loads must be taken also into account. Loads such as installed equipment and loads due to the cladding of the roof. Knowing that is a retractable roof, permanent equipment to open and close the roof is needed. That equipment is placed on top of the trusses, as shown on Figure 3.10. Additional to that, each truss has a catwalk to facilitate repair and maintenance of the trusses. Taking into account this, plus the fabric covering weight ([36]) and possible lighting permanent installations on the trusses, a total permanent load of  $q_k = 1.0 \text{ kN/m}^2$  will be considered on this research.





Figure 3.10: Permanent equipment on steel trusses.

### 3.2.3 Load combinations

The load cases, both for ULS and SLS, obtained in Section 3.2 will be the ones applied on this research study (see Equations 3.1, 3.2 and 3.3). Table 3.3 shows an overview of the loads that will act on a central truss (Center-to-center distance taken as  $9.5m$ ), as explained on the previous section. All loads were calculated and analyzed on the same zones divisions of the truss as shown on Figure 3.4 based on the wind action.

Load (kN/m)	Zones		
	G	H	I
Wind	-6.38	-2.66	2.13
Snow	4.75	4.75	4.75
Imposed on roofs	6.65	6.65	6.65
Permanent	9.50	9.50	9.50

Table 3.3: Permanent and variable loads acting on a central truss (including wind situation 1).

Load (kN/m)	Zones
	I
Wind	2.13
Snow	4.75
Imposed on roofs	6.65
Permanent	9.50

Table 3.4: Permanent and variable loads acting on a central truss (including wind situation 2).

For the calculations five load combinations (LC) for ULS have been taken into account and are composed of the following loads:

- LC1: Permanent load
- LC2: Permanent load + Wind situation 1

- LC<sub>3</sub>: Permanent load + Wind situation 2
- LC<sub>4</sub>: Permanent load + Imposed load
- LC<sub>5</sub>: Permanent load + Snow load

The load combinations and its coefficient factors are summarized in the tables below:

<b>LC1: Permanent load</b>		
	<b>SLS</b>	<b>ULS</b>
<b>Permanent load</b>	1.0	1.35

Table 3.5: Coefficients for LC1.

<b>LC2: Permanent load + Wind situation 1</b>		
	<b>SLS</b>	<b>ULS</b>
<b>Permanent load</b>	1.0	1.2
<b>Wind 1</b>	1.0	1.5

Table 3.6: Coefficients for LC2.

<b>LC3: Permanent load + Wind situation 2</b>		
	<b>SLS</b>	<b>ULS</b>
<b>Permanent load</b>	1.0	1.2
<b>Wind 2</b>	1.0	1.5

Table 3.7: Coefficients for LC3.

<b>LC4: Permanent load + Imposed load</b>		
	<b>SLS</b>	<b>ULS</b>
<b>Permanent load</b>	1.0	1.2
<b>Imposed load on roof</b>	1.0	1.5

Table 3.8: Coefficients for LC4.

<b>LC5: Permanent load + Snow load</b>		
	<b>SLS</b>	<b>ULS</b>
<b>Permanent load</b>	1.0	1.2
<b>Wind 2</b>	1.0	1.5

Table 3.9: Coefficients for LC5.

All load combinations with the final load  $F_d$  in  $kN/m$  are presented from Table A.1 to Table A.5. These tables can be found on the Annex A. LC<sub>4</sub> is the less favorable load combination and will be the one considered for further designs and optimization procedures in this research project. LC<sub>4</sub> is presented below:

LC 4: Permanent + Imposed load						
	ULS			SLS		
	Zones			Zones		
Load (kN/m)	G	H	I	G	H	I
<b>Permanent</b>	11.40	11.40	11.40	9.50	9.50	9.50
<b>Imposed</b>	9.98	9.98	9.98	6.65	6.65	6.65
<b>F<sub>d</sub></b>	<b>21.38</b>	<b>21.38</b>	<b>21.38</b>	<b>16.15</b>	<b>16.15</b>	<b>16.15</b>

Table 3.10: Loads for load combination 4.

### 3.2.4 Maximum deflection

Deflection on the structure has to be controlled. Limits on the deformation need to be specified in order to limit the rotation at the supports of the member. Excessive deformation could result on damage on the cladding of the roof and could generate a feeling of insecurity to the occupants of the building. Eurocode does not specify deformation limits. Therefore, the UK national annexes need to be consulted.

According to the national annex BS-NA-EN 1993 the maximum vertical deflection for roofs that are sensitive to damages on the cladding and is calculated from the load combination that includes dead + imposed load can be takes as:

$$w_{max} \leq \frac{L}{500} \quad (3.20)$$

Although, using Equation 3.20 and knowing that the span ( $L$ ) of the truss is 75 m the obtained maximum allowable deflection is 15 cm, it is assumed that the permanent equipment which allows the roof to be a retractable roof and lays on top of the steel trusses are very sensitive to vertical deflection. Consequently, the vertical deflection of the truss structure will be limited to only 5 cm.

## 3.3 ASSUMPTIONS FOR STRUCTURAL ANALYSIS

### 3.3.1 Assumed loading scheme

As presented before on this research, five load combinations were considered. ULS and SLS load were obtained for each load combination. It is presented on Section 3.2.3 that load combination 4 (LC<sub>4</sub>), which is composed of permanent and imposed load, is the less favorable for the structure and will be the one used for all structural analysis and optimization procedures. The load is normally applied in multiple point loads that coincide with every joint on the top chord. This is a more realistic assumptions as the secondary beams rest usually on those nodes. However, assuming a distributed load is more practical for comparing both, the case study truss with the optimized truss. Therefore, the obtained load will be applied as a distributed load acting along the top chord of the truss.

Assuming a distributed load instead of an equivalent multiple point load does not change the internal load distribution. However, an an additional

bending moment is generated on the top chord members. This bending moment could cause the need for bigger cross sections.

### 3.3.2 Assumed mechanical scheme

A mechanical scheme could be explained as a simplified representation of reality in which connections can be assumed either hinged, semi-rigid or rigid. Connections of trusses are assumed to act as hinges, permitting free rotation of the bars around the joint. Assuming hinged connections prevents considerable bending moments to develop on the members. Therefore, bar elements can only support an axial force [37]. However, connections in reality have always a certain degree of rotational stiffness. For this reason deformation capacity in the joint is required to allow a plastic hinge to form. On this report, all connections will be assumed as hinged-connections. Figure 3.11 shows the assumed mechanical scheme.

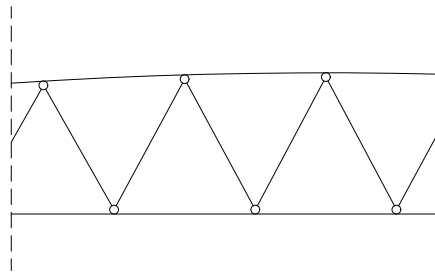


Figure 3.11: Assumed mechanical scheme.

## 3.4 STRUCTURAL ANALYSIS WITH KARAMBA3D

The structural analysis of the case study truss presented on Section 2.6 is performed using Karamba3D. Karamba3D is an Finite Element structural engineering tool plug-in for Grasshopper. Grasshopper is a visual programming language and environment within the CAD software Rhinoceros3D.



Figure 3.12: Structural design workflow.

Karamba3D uses three different analysis algorithms to analyse a structure: First Order analysis, Second Order analysis and Large Deformation analysis. For First order analyses neglect the change of length in axial or in-plane direction. It is assumed that axial force does not have influence on the stiffness of the member. Analysis performed based on Second Order analysis

take that into consideration. Compression forces decrease the structure's stiffness while tensile forces increase it [38]. The large deformation analysis can be used to simulate the behaviour of hanging models such as cables. On this research first order analysis will be used to analyse the steel truss structure. It is expected that deformations due to axial forces will not influence the load distribution of the truss.



Figure 3.13: 3D model of analyzed truss with Karamba3D

#### 3.4.1 Size optimisation

Within Karamba3D there is an "Optimize cross section" component which optimize the structure following the size optimization strategy. Each cross section of the structure is optimized and the most appropriate cross sections is chosen. It takes into account the load bearing capacity of the beam element while fulfilling deflection limits specifications [38]. Cross sections are optimized within a certain family per element e.g. HEA, HEB, HEM, etc. First, the forces on each member are determined. Then, the first cross section that fulfil the load bearing capacity and utilization checks within the chosen family of cross sections is selected. Finally, the load the distribution of forces is checked. If it has changed, then step two is repeated. As mentioned before on Section 2.6.4.2, the case study truss is composed of steel circular hollow section members. Therefore, Circular Hollow Sections (CHS) will be the used family for the analysis of the case study truss.

It is important to mention that the input order of the cross section list where the beam elements are selected from, influences the final output. The component checks one cross section and if this one does not satisfies the requirements checks goes to the next one on the list until it does. These list are ordered by height of the cross section in Karamba3D. For hollow cross sections this order may not be the optimal since properties such as cross-sectional area or moment or inertia are not properly order. This means that the final output might not be the optimal. For this research, a list of steel CHS cross section ordered by height will be used as data base.

The "Optimize Cross Section" component takes also into consideration the buckling length of the members while analysing the structure. By default local buckling of individual elements is assumed [38]. On this research a buckling length equal to the length of the member is assumed.

### 3.4.2 Model definition

A 2D parametric model based on geometry, support conditions and material of the case study truss presented in Section 2.6 is created withing the Grasshopper environment. Steel S355 is used as material for all members of the structure (see Table 3.11) and Circular Hollow Sections (CHS) are used for all members. Once the final geometry is created, the model was structurally-analysed using the structural-design plug-in Karamba3D, as mentioned before. The less favorable load combination for ULS presented in Section 3.2.3 is used as load input for the structural analysis.

Once the geometry, loads, support conditions, material and cross sections information is set and introduced, the model is assembled and the structure is analysed. As mentioned on the previous section, a cross section optimization process was performed on the analysed structure.

#### Assumptions

On this research it is desired to find a truss structure that is as similar as possible in weight and in geometry to the case-study truss. For this reason, for architectural and constructability matters the structural members were divided in three groups: top chord, bottom chord and diagonal members. Every member that belongs to each group are forced to have the same cross section. This means that e.g., every member belonging to the diagonals group will have the same cross section. As mentioned on 3.2.4, the deflection limit of 5 *cm* is established.

It is also assumed that that the truss structure is simply supported on its ends. The truss structures are part of the retractable/movable roof and therefore are not part of a moment resistance frame. Figure B.1 from the Appendix B shows the Grasshopper script of the structural analysis from the case study truss.

Steel S355 Material properties	
E-modulus	2.1E5 $N/mm^2$
Poisson ratio	0.3
Yield strength	355 $N/mm^2$

Table 3.11: Steel S355 material properties.

### 3.4.3 Results

After the structure is analysed and the cross sections are optimized within a deflection limit of 5 *cm* at mid-span the results are obtained. The final truss is composed of 3 different cross sections as presented on Table 3.12 and in Figure 3.14. The steel truss has a final weight of 84.96 *tons* and under the action of the analysed ULS load case, a displacement of 5.15 *cm* is found.

#### 3.4.3.1 Forces diagrams

The resulting normal force, shear force and bending moment diagrams can be seen in Figure 3.15. As expected, mainly normal forces (N) are resisted

Cross Sections	
Group	CHS Cross section
Top Chord	CHS 406.4 x 25.0
Diagonals	CHS 219.1 x 20.0
Bottom Chord	CHS 406.4 x 40.0

Table 3.12: Cross section names for the structural members.

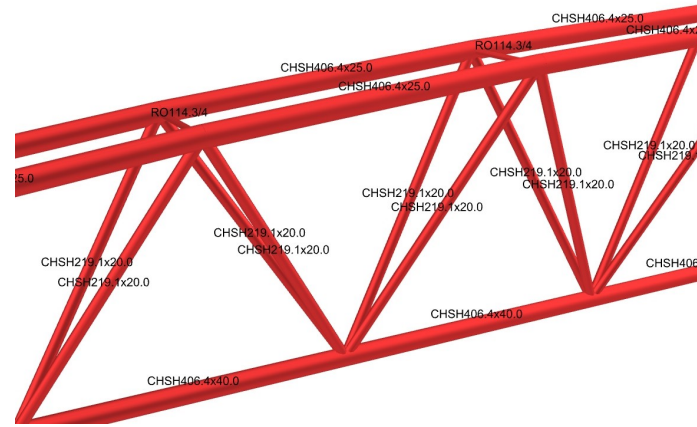


Figure 3.14: Conventional truss: structural design

and transferred by the structural members. The bending moments that can be observed on Figure 3.15c are caused by the distributed load which is applied on the top chord of the truss, as explained before. Owing to the applied arrangement or rationalization of structural members in groups, the utilization factor of those members decreases significantly. A table with the bending moment, shear and normal forces from every element of the truss are presented on Annex B at the Section B.1.1.



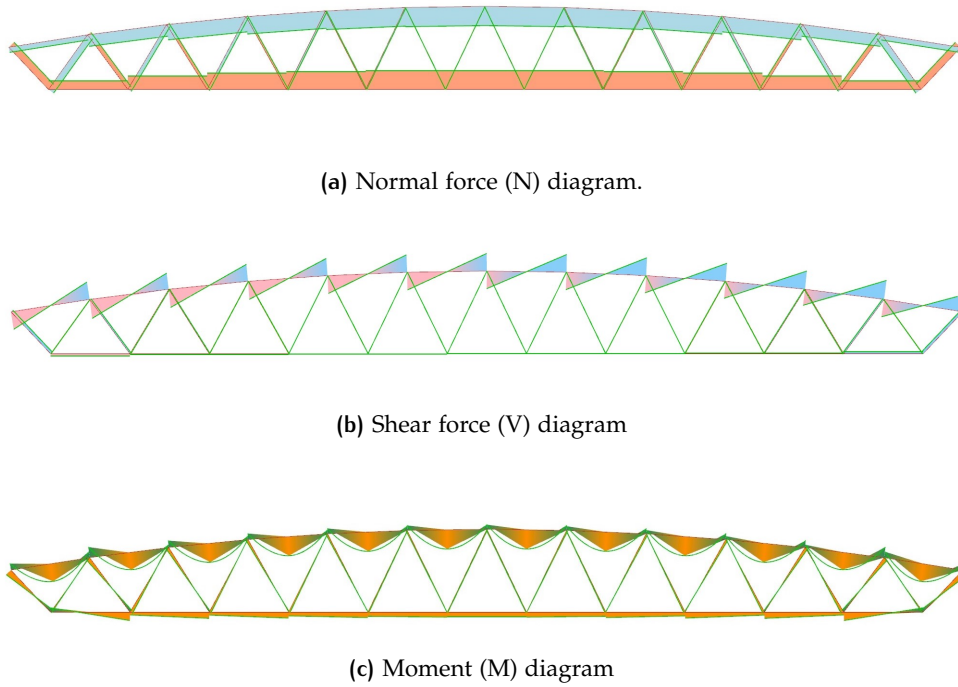


Figure 3.15: Forces diagrams from the design case study truss

### 3.5 CONCLUSION

This chapter provides the assumptions considered to perform the structural design of the case-study truss and the structural design itself, both based on the regulations presented on the Eurocode.

Different load configurations and load cases were analysed and it was found that less favorable load combination is composed of permanent load and imposed load on the top chord of the steel truss.

The structural design was performed employing the less favorable load combination using the design-tool Karamba3D. After the design of the case-study truss, a final weight of 85 tons was obtained. This weight is comparable and significantly close to the 93 tons the original truss weights, based on the literature review.



# 4

## OPTIMIZATION OF STEEL TRUSS FROM CASE STUDY

### 4.1 INTRODUCTION

It is known that reducing the material consumption of structures is a complex but necessary challenge in nowadays construction industry. Therefore, different optimization procedures and methods have been developed in order to achieve the intended purpose of developing a cost-efficient structure that requires as minimum weight as possible. As mentioned in Section 2.4.4 there are several methods that are being used for structural optimization. The application of these methods is based on the requirements from each different project. The different available methods for optimizing frame structures are size Optimization, shape optimization and topology optimization.

As mentioned before, one of the main goal of this research project is to open up new solutions by creating an innovative joint for optimized truss structures that enables an economically competitive erection of the structure. Therefore, an existing truss structure is optimized using topology optimization, which will be called on this research as layout optimization. On this chapter the following research sub-questions are answered:

- *How is the structural optimization-approach applied on the case-study truss?*
- *What are the main differences between the convectional and the optimized truss?*

### 4.2 LAYOUT OPTIMIZATION

Once the structural design of the case-study truss is performed and deformations of the structure and stresses on the members are checked, the truss structure layout is further optimized. As mentioned in Section 2.4 a layout optimization process is performed on the case-study truss. The optimization process based on the two-step approach procedure proposed by [1] and explained in Section 2.4.5 is followed.

Different structural tools that allow to optimize a structure using topological-optimization have been explored. However, Peregrine is the tool which will be used on this research due to the fact that is a complete and ready-to-go user friendly tool. Peregrine is a powerful structural layout optimization plug-in for Grasshopper, the algorithmic modelling environment build into the Rhino 3D CAD software. Within Peregrine a minimum volume frame topology can be found, for a given set of loads, support and material properties. Figure 4.1 shows the software used for the optimization process.

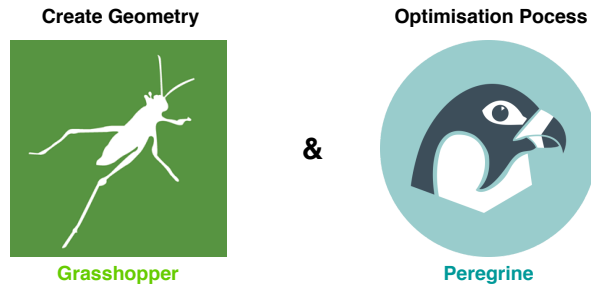


Figure 4.1: Optimization software.

### 4.3 STRUCTURAL OPTIMIZATION WITH PEREGRINE

As mentioned in Section 2.4, conventional layout optimization is based on the ground structure method, first proposed and discussed by [26]. Using this method an optimized structure can be obtained in which unnecessary members from a highly interconnected truss can be removed while keeping the nodal location fixed on its initial position. This could lead to an approximation to an optimal Michell truss or structure [39]. However, according to [28], employing this method will generate layouts that are too complex to fabricate in practice. The methodology presented in [28] seeks to extend the scale of truss layout optimization problem including buildability constraints using mixed integer linear programming (MILP). As result, a useful and possible feasible conceptual design will be obtained with a significant decrease of time compared to other methods.

After the MILP formulation finds the globally optimal solution for a given ground structure, an second non-linear geometry optimization is implemented for in a refinement stage [28]. This method is applied in Peregrine, the optimization software used to optimize the case-study truss.

#### 4.3.1 Peregrine workflow

By following a simple workflow, minimum volume layouts of elements forming a truss can be obtained. In order to perform an optimization process within Peregrine four features need to exist [40]:

1. A design domain
2. Material properties
3. Support conditions
4. One or more loads

Initially, the starting topology, the externally applied loads, the support conditions of the problem, the geometric and material properties needs to be define. These features are used as basis of the optimization process. Further refinement, post-processing and editing of the output will lead to an optimal and potentially more practical output. Figure 4.2 shows the Peregrine workflow in a left-to-right manner.

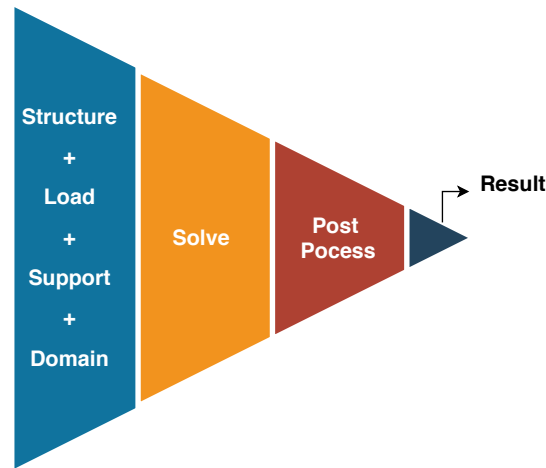


Figure 4.2: Optimization process workflow.

#### 4.3.2 Peregrine validation

As mention in Section 2.4, using Michell theory [30] a minimum volume structure can be found. It was established that, although using this theory a optimal benchmark can be obtained (see Figure 2.14), the resulting truss-like layout is challenging or impossible to realize in real engineering practice. Therefore, in order to show how Peregrine works and how optimization process workflow is performed a Michell-like cantilever truss is recreated within this structural optimization tool.

##### 4.3.2.1 Michel cantilever truss example

The classical Michell cantilever problem uses a three-force problem approach. In which two of them are the support load and there is one external point load on at the end of the truss. A Michell truss could be composed of almost infinite amount of members. Therefore, for practical purpose the possible positions and numbers of nodes are restricted within the design domain. The design domain used on this example containing the support conditions and the point load is presented on Figure 4.3. An external point load is used and applied at the end of the cantilever design domain. Since this example is used only as an explanatory example the applied loads values and design domain dimensions are not shown on this report.

As explained before, once the four basic components are defined and set, the optimization process begins. Peregrine finds the optimal layout which is the benchmark. The benchmark is directly linked to the chosen ground structure. Figure 4.4b shows the Michell-like truss benchmark for the defined design domain. This benchmark is the optimized layout resulting from the chosen ground structure, presented on Figure 4.3.

Figure 4.4 shows the original Michell truss and the one obtained using the Peregrine tool. It can be concluded that within Peregrine a layout which assembles a Michell truss can be simply generated.

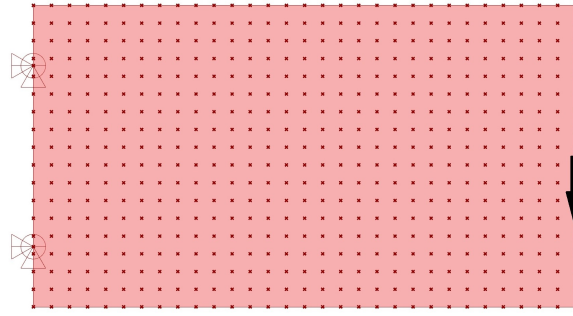


Figure 4.3: Michell-like truss design domain.

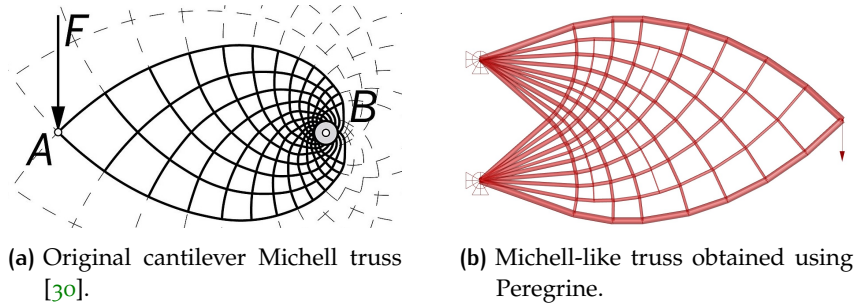


Figure 4.4: Original Michell truss vs Michell-like truss obtained using Peregrine.

#### 4.3.2.2 Michell truss rationalization post-process

Once the benchmark is obtained, different less complex layouts can be generated applying a rationalization post-process. For this example, the benchmark is first rationalized, where some joints positions are moved to more favorable positions. The rationalized layout is presented on Figure 4.5c. Then the solution is simplified, where the number of elements is reduced while still possessing a volume below a permissible value. Figure 4.5d shows the most basic possible layout for the specified problem.

With this simple Michell-like truss example shown on Figure 4.5 it is possible to observe how the two-step approach proposed by [1] and presented in Section 2.4.5 can be implemented and applied on a simple layout problem. Additional to that, it is remarkable how much the weight of a structure can be reduced by implementing optimization processes on the design phase. It also comes into sight that despite the increase of the numbers of nodes and elements, comparing layout on Figure 4.5c with the simple-shaped layout on Figure 4.5d the volume remains low and similar to the benchmark layout on Figure 4.5b.

Figure 4.6 shows the difference in volume from the different layouts after the optimization and the post-processes versus the total number of nodes each layout has. Sub-figures 4.5a, 4.5b, 4.5c and 4.5d represented with dots on Figure 4.6. There is a significant required volume to withstand the applied load between the simple layout structure, which is composed of 2 members, and the benchmark and the rationalized layout. This can be clearly observed on Figures 4.5 and 4.6. Similar examples can be found in [28] [41].

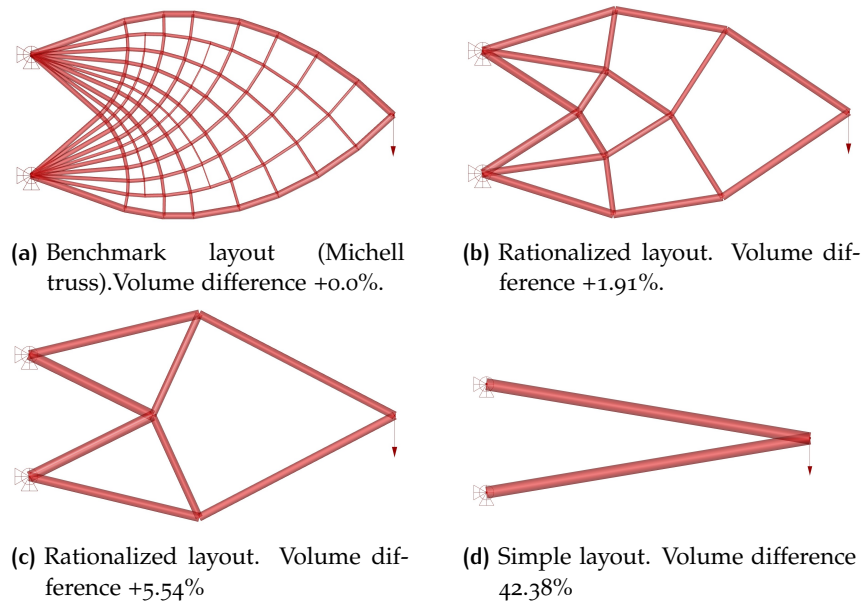


Figure 4.5: Michell-like truss benchmark and post-process

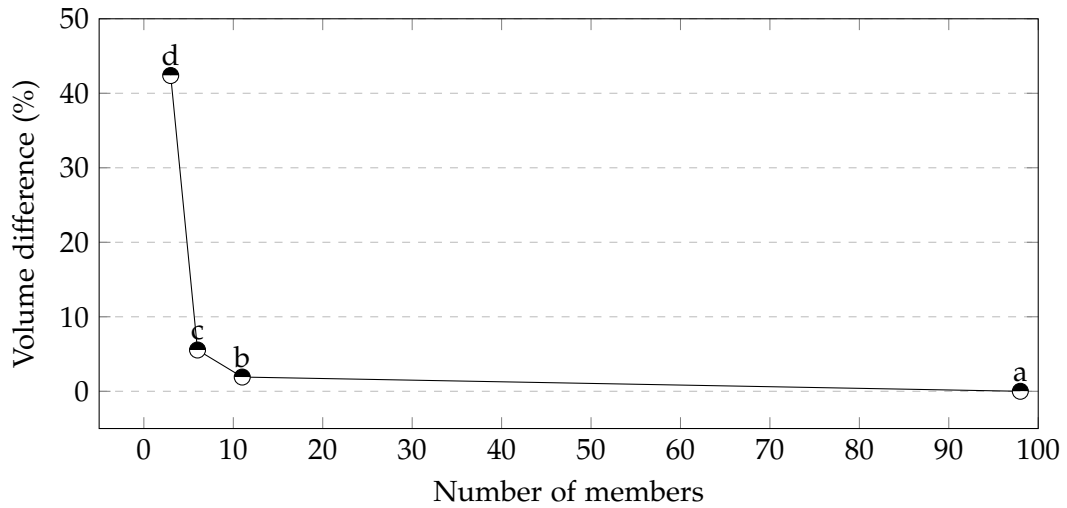


Figure 4.6: Different layouts volume vs number of nodes: results after limiting the numbers of nodes per layout.

#### 4.3.2.3 Conclusion

Within this example the optimization procedure that will be performed on the case-study truss is briefly introduced and demonstrated. It also shows how an optimization problem is assembled and defined on Peregrine. Similarly, the two-step approach can clearly be understood, where the global optimal layout (the benchmark) is found followed by a rationalization post-process. Finally, after all the required post-processes are completed the complexity of the topology is reduced resulting in a simplified, but optimized layout that is more feasible to realize in real engineering practice.

## 4.4 SHAPE DEVELOPMENT

### 4.4.1 Introduction

Similar to the previous example, the two-step approach method explained in Section 2.4.5 is used to optimize the case-study truss presented in Section 2.6. As mentioned on that section, the structure is composed of 11 bays forming a simple warren-like truss structure. The truss spans a distance equal to 75m and is composed of the top and bottom chord and the diagonals members.

Figure 4.7 shows the required steps in order to achieve an optimal truss. First, the layout from the conventional truss is optimized resulting in the benchmark layout. Then, the benchmark is manually rationalized until the optimal layout is found. All the steps are further explained and developed on this section.

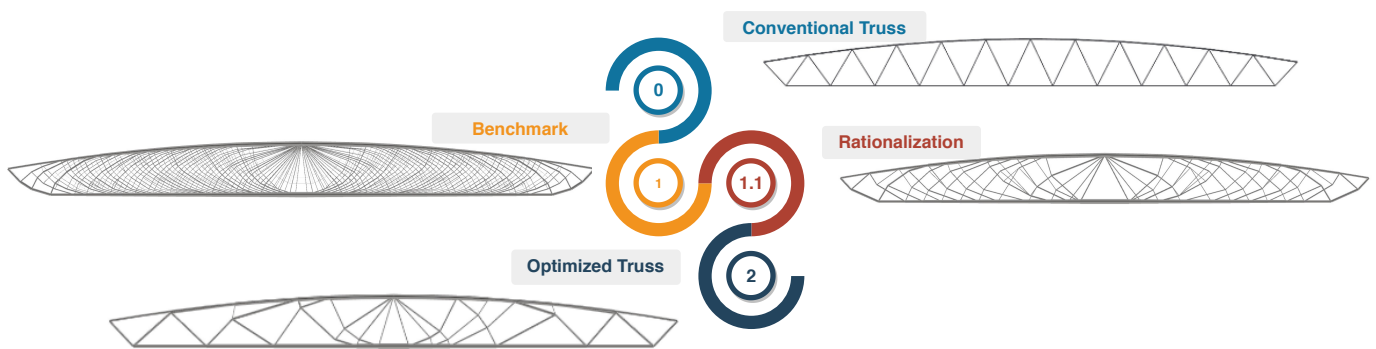


Figure 4.7: Optimization methodology steps.

### 4.4.2 Step 1: Benchmark

The global optimum, or the benchmark, is the resulting layout after an layout-optimization process is performed on a design domain. As explained before, benchmark is generated without taking into consideration any buildable considerations. This means that no restrictions on the number of nodes and elements are set nor the numbers of connecting elements per node. The result would assemble a Michell truss for and specified load condition.

In order to generate the the global optimum layout the four features mentioned in Section 4.3.1 have to be prescribed: a design domain, material properties, support conditions and external loads.

#### *Prescribed loads*

The resulting load presented in Section 3.2.3 is applied along the top chord as uniformly distributed load in  $kN/m$ . Only the ULS load case is considered on this optimization process.

#### *Support conditions*

As it is presented on the assumptions in Section 3.4.2 and as is its usually in real engineering-design practice, the truss structure is considered as a

simply-supported structure. Vertical translation is restricted at the two support points and horizontal movements are restricted at one support point.

### *Material properties*

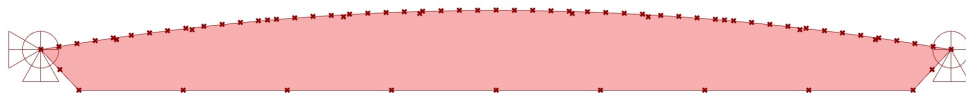
The same material properties used for the members on the structural design of the conventional truss are also used on the optimization process, being this steel S355 (see Table 3.11).

### *Design Domain*

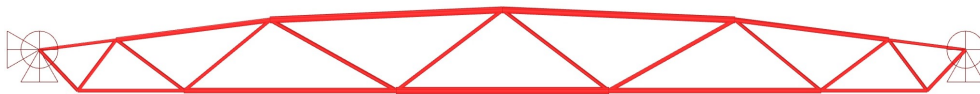
The geometric area within the optimized structure must exist has to be set in Peregrine. The used surface has the same shape and geometry as the case-study truss outer border. The output from the optimization process is highly influenced by the chosen design domain. Within Peregrine is possible to customize the nodal division within the design domain.

On this research three different design domain have been studied with different nodal divisions:

1. **Design domain 1:** a low node-populated domain without internal possible nodes (see Figure 4.8a). Only nodes on the outer members can be connected with members.
2. **Design domain 2:** a intermediate node-populated domain with two internal rows of nodes (see Figure 4.9a). Internal nodes can be connected with members.
3. **Design domain 3:** a dense node-populated domain with six internal rows of nodes (see Figure 4.10a). Internal nodes can be connected with members.



(a) Design domain 1.



(b) Benchmark for design domain 1.

**Figure 4.8:** Optimized benchmark layout for design domain 1.



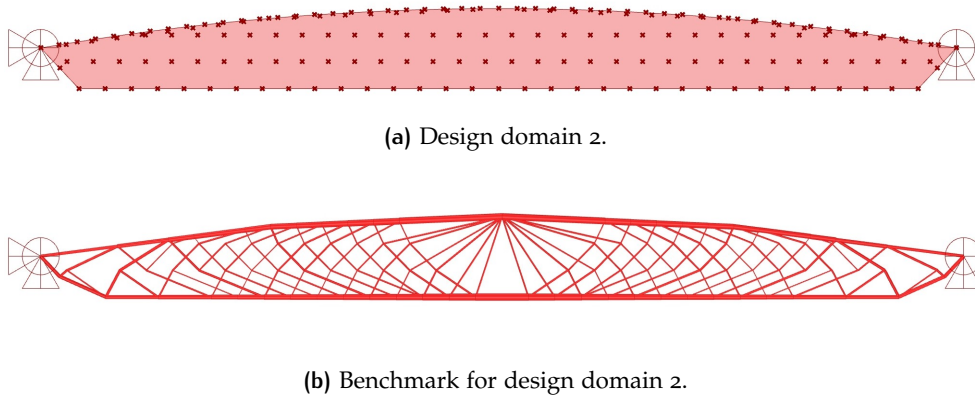


Figure 4.9: Optimized benchmark layout for design domain 2.

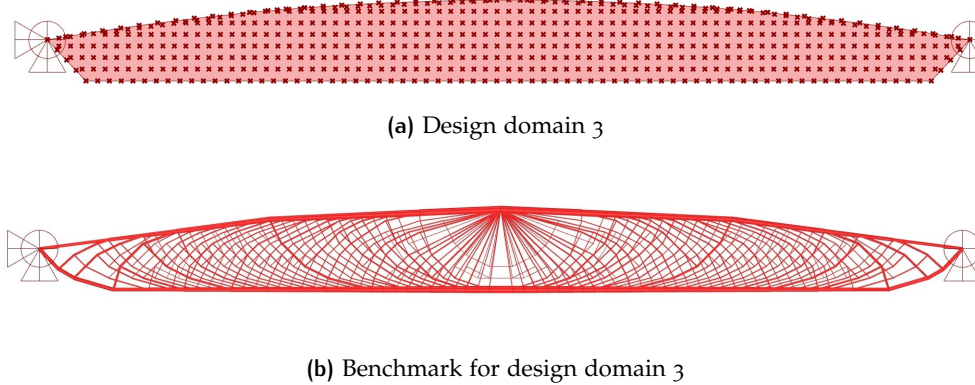


Figure 4.10: Optimized benchmark layout for design domain 3.

For each design domain a benchmark layout is found. Figures 4.8b, 4.9b and 4.10b show the global optimum layout (benchmark) for the analyzed three design domains.

It can be clearly observed how the nodal division within the design domain influences and modifies the layout geometry complexity. For a low populated nodal division, such as Design domain 1, the resulting benchmark is similar to a conventional shaped-truss such as a Warren truss. This layout will not transfer loads as efficient as layouts resulting from a more node-populated domain. This could be represented on the final weight of the structure. On the other hand, this benchmark layout is composed of less members and less nodes, which could be beneficial for the assembly and construction process.

With the increment of internal nodal division the number of members and joints increases, thus the complexity increases too. This is the case for Design domain 2 and 3. Despite the increase of members and nodes, the load is distributed more efficiently and the members need to withstand lesser loads. Therefore, the members cross sectional area is reduced. This was demonstrated with the example presented in Section 4.3.2.



#### 4.4.2.1 *Final benchmark*

The resulting benchmark from the optimization process of design domain 3 (see Figure 4.10) presents a very complex node configuration. The resulting layouts resembles a Michell truss and it is very unlikely that, after the rationalization post-process a practical solution could be found. On the other hand, the global optimum resulting from design domain 2 looks promising and will allow simpler structures to be produced. For this reason, the benchmark obtained from design domain 2 (see Figure 4.9) will be taken as the starting point for the rationalization process.

#### 4.4.3 Step 2: Post-processing

Once Step 1 is completed a minimum volume layout-output is generated. As mentioned before, this result is based on the numerical ground structure-based layout optimization method considering only stress and equilibrium constraints, presented on [1] [28] and used in Peregrine. The second step consist on rationalize the global optimum taking into account complexity and buildability considerations. The main objective of Step 2 is to move from the resulting solution from Step 1 to a simplified problem that is a feasible solution for real engineering practice.

The rationalization process could be seen as a secondary manual optimization which on every step is included a linear size optimization and non-linear geometry optimization steps, which allows the adjustment of the nodes position [1].

##### 4.4.3.1 *Peregrine post-processes*

There are six different post-process components within Peregrine. Each component has a different function and can be used after an optimization or post-process step. Each post-process can be used individually or in combination with others post-process components. Figure 4.11 shows the six post-process components that are available in Peregrine. Similarly, a short description of each post-process function can be found on the list below [40]:

- **Rationalization:** moves the position joints from an optimized geometry to more favorable position. A maximum numbers of nodes and a maximum number of iterations are allowed as input.
- **Simplification:** reduces the number of elements that are connected at a joint. The user can specify a permissible percentage of volume increase after the complexity is simplified.
- **Crossover:** introduces nodes where members are crossing each other and overlapping. A permissible volume increase and the proximity ratio below crossovers will be created can be specified by the user.
- **Filter:** removes members with a cross-sectional area below a specified threshold. The user can specify a permissible percentage of volume increase.

- **Merge:** combines nodes within the structure domain that lie within a prescribed merge radius. The user can specify a permissible percentage of volume increase and the value of the radius.
- **Reduce complexity:** attempts to reduce the number of elements after the maximum number of members at joint and the volume increase limit are specified by the user.



Figure 4.11: Types of post-processes within Peregrine

#### 4.4.4 Applied post-processes

Different post-process configurations were studied before the final optimized truss was obtained. After that every post-process is performed a different layout is obtained. As mentioned before, as many post-processes as required can act together in the same optimization problem as sort of a chain model. It is recommended by the authors [40] that a rationalization process should be carried out after an optimization post-process in order to generate a less complex layout after every iteration.

The final post-processes chain used on this research that generates the final optimized layout is presented on Figure 4.12. An image of the Grasshopper canvas showing the final post-process configuration including the user-input parameters can be found on Figure B.9.

#### 4.4.5 Final optimized layout

The following list shows the performed post-processes before the finally optimized layout is obtained. The volume difference that is presented on every figure presented below represents the difference in volume compared to the chosen benchmark.

- **Benchmark:** the resulting layout from design domain 2 (see Figure 4.9) is taken as the benchmark and starting point.

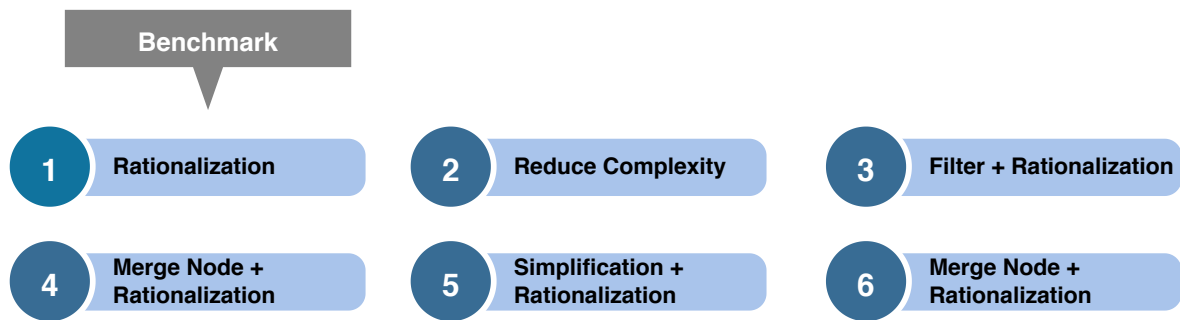


Figure 4.12: Post-process workflow.



vol diff: +0.0%

- **Post-process 1:** the benchmark is rationalized and joints are moved to more favorable positions leading to a layout with lower structural volume.

vol diff: -0.3%  
Rationalization

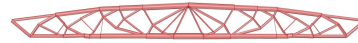
- **Post-process 2:** the number of elements is shortened by reducing the complexity while setting a maximum number of members at one node to 10. Later the layout is rationalized.

vol diff: +12.1%  
Reduce complexity M:150 N:10  
Rationalization

- **Post-process 3:** elements with a cross-sectional area below a specified filter threshold are removed. The threshold was specified to 3% of the cross-sectional area of the largest element in the solution.

vol diff: +0.2%  
Rationalization  
Filter 3

- **Post-process 4:** nodes that lie within a prescribed ratio of 1  $m$  are merged together. Later the layout is rationalized.



vol diff: +0.4%  
Rationalization  
Merge Node 1

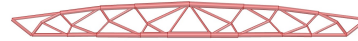
- **Post-process 5:** the layout is simplified and the number of elements that connect at the nodes is reduced. For this step, a maximum number of elements per node is set to 5. The the layout is rationalized.



vol diff: +10.1%  
Simplification Mod:2  
Rationalization

vol diff: +0.8%  
Rationalization  
Simplification Mod:2

- **Post-process 6:** finally, nodes that lie close to each other within a radius of 2  $m$  are merged together. Later the layout is rationalized.



vol diff: +0.9%  
Merge Node 2  
Rationalization

The final layout was created taking into account buildable considerations and accounting complexity constrains. Engineering judgement played a big role in the in achieving the final result while setting the post-process chain. As mentioned before, the different post-processes can be applied in any desired order. Therefore, a huge amount of solutions can be obtained. For the objectives of this research project a layout with a favorable node-member configuration was desired to achieve.

The layout chosen as the final optimized truss which is presented on Figure 4.13 has a promising node-configuration and it shows a very small increase of volume (+0.9%) compared to the benchmark. The numbers of elements per node is a important factor that influences the final output which was also considered and controlled during the optimized process. Furthermore, the internal nodes are distributed in a favorable way for the truss assembly, which will be discussed further on the following chapters.

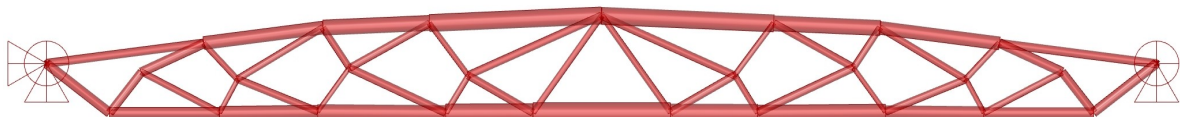


Figure 4.13: Final layout.

## 4.5 STRUCTURAL DESIGN OF THE OPTIMIZED TRUSS

In order to compare both, the conventional-shaped case study truss (see Figure 3.13) with the optimized layout truss (see Figure 4.13), a structural analysis on both truss must be preformed. Chapter 3 and more specifically Section 3.3 show the assumed loads and structural assumptions for the structural analysis of the case-study truss. The optimized truss is design following the same guidance and considerations.



Figure 4.14: Structural design workflow.

### 4.5.1 Assumed loading scheme

The same applied loads for the case study truss (see Section 3.3.1) are used for the structural design of the optimized truss. The most unfavorable load combination presented on Section 3.2.3 is applied as equally distributed load along the top chord of the truss.

### 4.5.2 Assumed mechanical scheme

The same mechanical scheme assumed for the case-study truss (see Section 3.3.2 and used for its design is used for the design of the optimized truss. All joints are assumed as hinges. Therefore, bar elements will only withstand axial forces.

### 4.5.3 Structural analysis with Karamba3D

The optimized truss is designed using Karamba3D in the same matter as the conventional case-study truss explained in Section 3.4.

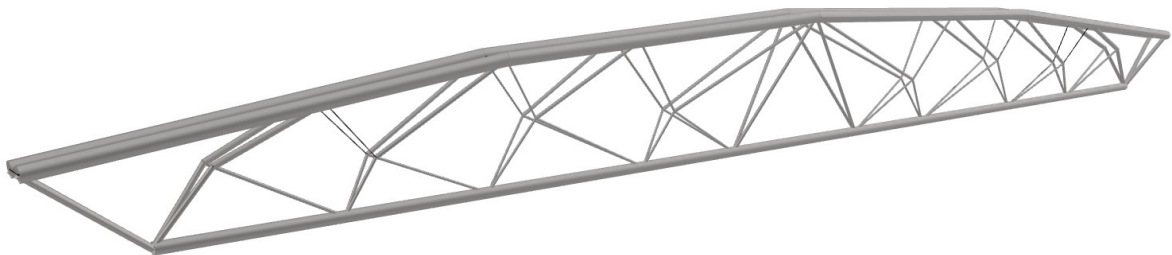


Figure 4.15: 3D model of analyzed truss with Karamba3D.

### Size optimization

After the optimized steel truss structure is design using Karamba3d the cross sections are optimized employing the karamba3d size optimization component "optimize cross section" in the same way as performed for the case-study truss. As explained in Section 3.4.1, cross sections can be optimized within a certain family of sections. Similarly to the case-study truss design, Circular Hollow Sections (CHS) are the used family for this analysis.

### Model definition

As mentioned before, the optimized truss structure is design under the same parameters and considerations than the case-study truss design presented in Section 3.3. Steel S355 is used for the structural members and its properties are shown on Table 3.11.

Once the geometry, loads, support conditions, material and cross section information is prescribed, the model in Karmba3D is assembled and the structure is analysed. A 5 cm displacement limit at mid-span is established. Figure B.11 on the Appendix B shows the Grasshopper script of the structural design from the optimized truss structure.

#### 4.5.4 Results and comparison

After the structure is analysed and the cross sections are optimized within a deflection limit of 5 cm at mid-span the results are obtained. Different solutions can be found from the optimized truss depending on the various cross sections that are being used.

The layout-optimization process generates a structure in which every single elements is optimized separately, which means that every element could have a different cross section. Within Karamba3D is possible to group different members to a certain cross section in order to rationalize the structure and make it less challenging to build. Although grouping members will ease the construction of the structure, could probably result in a significant increase of the total volume of the structure. Three different solutions of the optimized truss are presented and analysed on this research:

- **Solution 1:** no members are grouped. This is the first result generated from the size-optimization process within Karamba3D (see Figure 4.16).



Figure 4.16: Solution 1: no members grouped.

- **Solution 2:** members belonging to the top and bottom chord are grouped in separate groups. The internal members are not grouped (see Figure 4.17).

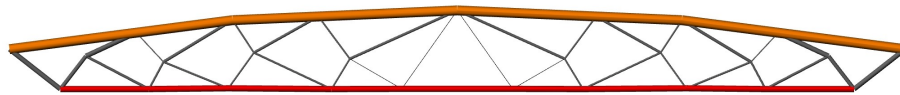


Figure 4.17: Solution 2: Top chord and bottom chord grouped into 2 different groups.

- **Solution 3:** members belonging to the top and bottom chord are grouped in separate groups. Some internal members are grouped (see Figure 4.18).

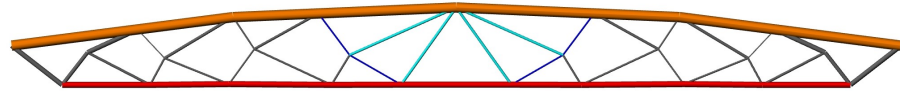


Figure 4.18: Solution 3: Top chord, bottom chord and some diagonal members grouped into different groups.

Every truss from each solution will be composed of different cross sections which will the building and assembly process more tedious.

As mentioned in Section 3.4 the buckling of the elements are also checked within Karamba3D. A table with the bending moments, shear and normal forces from every element of the truss is presented on Annex B at the Section B.1.1.

#### 4.5.5 Chosen internal node

Once the final shape of the optimized truss is known and the structural analysis of it has been performed, the next step in this research is to develop a design concept of a innovative joint for the internal nodes of the optimized truss. The following chapter will be dedicated to completely to the design concept and its structural analysis. In order to have an starting point, a representative internal node must be chosen. Based on the geometrical configuration and on the high nodal forces the internal node presented in Figure 4.19 is the chosen node for future analyses.

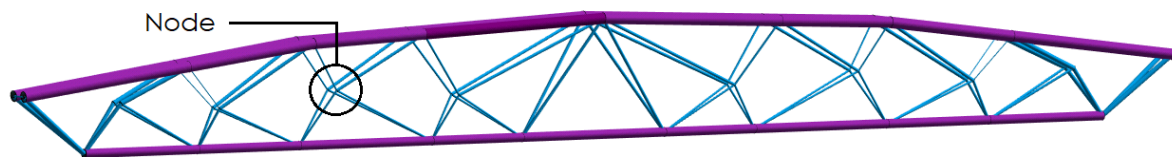


Figure 4.19: Internal node.

Figure 4.20 shows the nodal axial forces on the elected node. It can be observed that the maximum axial tensile force and the maximum compressive force are similar in magnitude but with opposite sign (close to  $\pm 130 \text{ kN}$ ). For this reason, and in order to have a small margin of error, the design of the design concepts will be based on the following criterion:

- Required resistance for tensile force:  $140 \text{ kN}$
- Required resistance for compressive force:  $140 \text{ kN}$







The main comparison parameters are the weight, deflection and number of different cross sections. Therefore, the resulting values from all of these parameters are obtained for each solution.

Table 4.3 presents the number of different cross sections for which each truss structure is composed of. A complete comparison between the conventional-shaped case-study truss and the optimized truss is presented in Table 4.2. Similar results can be found on [42], where an optimized and later rationalized truss structure is compared against other truss geometries. On this paper the volume ratio and deflection for constant stresses are also compared.



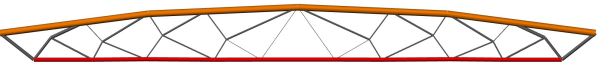
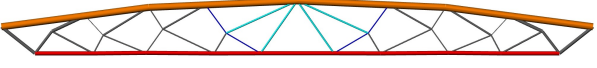
Type of truss	Deflection (cm)	Weight (tons)	Weight difference (tons)	Weight difference (%)
 Case-study truss	5.15	84.96	0	0%
 Optimized truss: Solution 1	4.98	71.63	-13.33	-15.69%
 Optimized truss: Solution 2	5.11	78.29	-6.67	-7.85%
 Optimized truss: Solution 3	5.05	80.28	-4.68	-5.51%

Table 4.2: Relative efficiency of the various analysed types of trusses compared to the case-study truss

Type of truss	Number of different cross sections
Case-study truss	3
Solution 1	19
Solution 2	16
Solution 3	15

Table 4.3: Number of different cross sections.

## 4.7 CONCLUSION

The two-step approach proved to be an efficient optimization methodology to find an optimized layout with a similar weight than the less-weight possible layout (the benchmark). It was demonstrated that an optimized layout with a non-complex members and node configuration can be obtained with the help of the optimization-tool Peregrine. It demonstrated to be intuitive and in combination with the required post-processes good results can be achieved if a correct initial design configuration is inputted.

The obtained final layout on this research has a promising geometrical node-member combination. This final shape configuration is used as input for Part [iii](#). Finally, the structural design of the optimized truss, which was performed under the same circumstances and based on the same assumptions as the case-study truss, a considerable reduction in weight when both trusses are compared. Despite the load distribution is improved and considerable weight reduction was obtained, the optimized truss is composed of at least eight times more different cross sections than the case-study truss.

## Part III

### INNOVATIVE JOINTS

# 5 | CONCEPTUAL JOINT DESIGN BASED ON SNAP-FIT CONNECTIONS

## 5.1 INTRODUCTION

As explained in Section 2.4, after a topological optimization process (or layout optimization for frame structures) is applied on a structure, the resulting optimized structure could have a non-conventional geometrical configuration of elements and nodes. This could be challenging both for designers and manufacturers. Additionally, trying to realise such structures with conventional joints might increase the cost the structure or might be not possible at all.

It was demonstrated in Section 4.4 that a truss structure can be layout-optimized and that a considerable reduction in weight can be achieved. It was also proven using the two-step optimization approach proposed by [1] that an optimized and buildable layout configuration can be obtained. The final optimized truss can be observed in Figure 4.13 and Figure 5.1. At the same Figure it is possible to notice the non-conventional configuration of internal member and nodes.

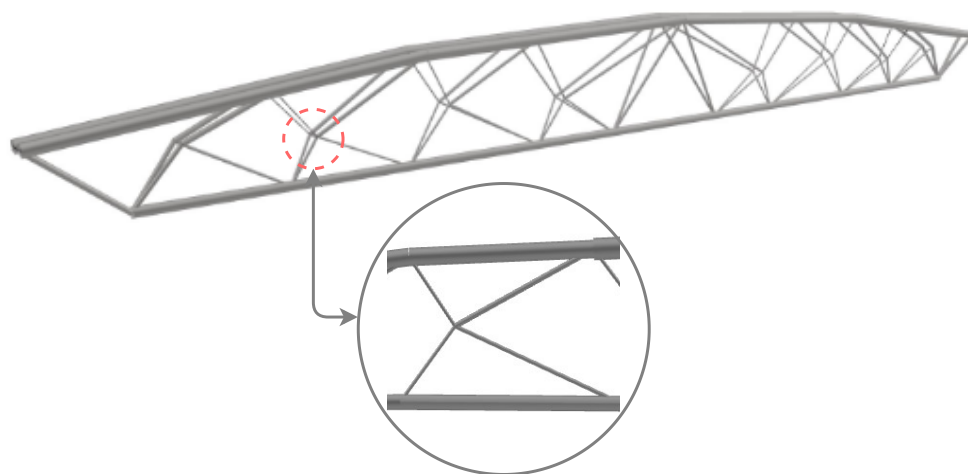


Figure 5.1: Internal node

Once the final shape of the optimized structure is known the next logical step is to develop a concept for the internal joints.

A different approach to connect steel members to each other on optimized truss structures creating a structural connection is investigated on this research project. The design of the connection is based on the snap-fit connecting principles, its behaviour and based on the fact that different members can be connected to one node with different arrival angles, as shown in Figure 5.1. This joining technology reduces the need for specialized tools and eliminates the use of mechanical fasteners such as bolts and welds, two of the most used connecting methods for steel structures. A snap-fit connec-

tion can be defined as an easy and quick method of joining and locking two or more elements together. Important aspects of snap-fit connections such as the main characteristics, composition, its advantages and disadvantages have been discussed in Section 2.5.

On this section an innovative design joining concept of the most loaded internal node of the optimized truss presented on the previous section (see Section 4.5.5) based a cantilever snap-fit connection is developed.

Snap-fit connections are usually designed with thermoplastic materials due to its high flexibility, its high elongation and low coefficient of friction [8]. Such material have enough strength and stiffness for small scale applications. For larger scale applications where larger forces are required to be carried, materials with different mechanical properties may be required. This research project is an exploratory feasibility study of the use of steel snap-fit joints as internal nodes for the optimized steel truss presented on the previous chapter 4.

On this chapter the following research sub-questions are answered:

- *How does the innovative joint looks like and how is its structural detailing?*
- *How does the snap-fit connecting mechanism structurally behave during the installation and disassembly phase?*
- *How does the innovative joint behaves structurally during its usage phase?*

## 5.2 METHODOLOGY

Developing an innovative concept of a structural connection is not an easy task. Before a final design is obtained different design steps are required. This section presents the used methodology to achieve a final and functional design concept.

- As a first step, the connecting principles behind snap-fitting will be studied. At this step the different components a snap-fit connection is composed of will be presented. Furthermore, the three main phases to which the snap-fit connection will be exposed are introduced. This phases will clarify how a snap-fit connection resists tensile and compressive forces.
- On the next step, a general idea of how the snap-fit principles will be used and scaled to a structural connections will be presented. Based on the these principles a general concept will be developed.
- Based on the general concept, two design concepts will presented. Each concept will be tested using FE models in order to understand its behavior under specific circumstances such as the deflective behavior of the cantilever snap-beam and the influence of the numbers of tips while resisting tensile forces.
- Finally, based on the results obtained from the previous concepts, a final design concept will be presented. Extensive FE analyses will be

performed for each phase and the structural behaviour of the innovative connection will be studied.

### 5.3 SNAP-FIT PRINCIPLES

As it was mentioned before, connections play an important role at every stage of a structure; from the planning and design to the construction and use of the structure. The assembly and installation of conventional connections, such as welded or bolted connections, is nowadays standardized and the procedure is well known. Experienced and authorized workers can perform such connections with relative ease. For this reason, how conventional connections behave under the action of the designed loads is more critical than the assembly or disassembly of the joint.

For a concept of an innovative joint which is based on snap-fit connection every phase represents a challenge. Knowing that the functionality of such connections is based on the principles behind a regular cantilever snap-fit connection. A correct assembly of the connection is essential in order to achieve a successful performance during the entire life of the joint. This could mean for both the usage phase of the joint and also to a possible reuse of it. If the joint is properly design circularity could be achieved. Snap-fits can be designed to be assembled and disassembled multiple times or to create a "permanent" connection.

The joint based on a snap-fit connection needs to be design to fulfil three main phases: the assembly phase, the phase during the use of the joint and the final disassembly. Contact between the inserting element and the locking element plays a key role on the behaviour of the joint during all three phases. For this reason, it is important to study the required mechanical stresses and strains on the snap beam during assembly, disassembly and also after assembly [43].

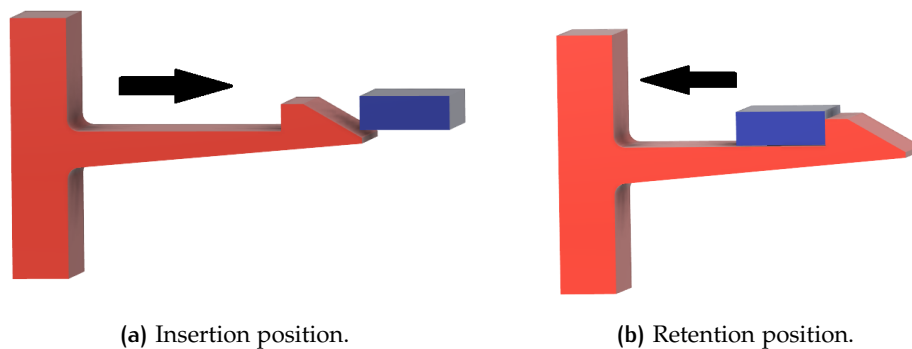


Figure 5.2: Inserting part (red) and retaining part (blue) at different positions.

#### 5.3.1 Components

A snap-fit connection is usually composed of two different components, as shown on Figure 5.2:

- **Inserting part:** is the moving element that is introduced or inserted into its final retention position. It behaves structurally as a cantilever beam which while being inserted deflects before returning to its original position. The inserting part is represented in red color on Figure 5.2.
- **Retaining part:** is the element that allows the interlocking of the inserting part. This is usually a fixed part and due to its geometry, deflection or change of shape of the part is not allowed during the assembly or the use of the connection. This part will be capable of taking tensile and compressive forces that come from the steel members. It is represented in blue on Figure 5.2.

### 5.3.2 Phases

#### Assembly phase

This phase consists on pushing the inserting unit towards the retaining unit into its final position. The cantilever structural behaviour of the inserting units is used for the assembly of it. In order to have a proper assembly some design criterion are required to be met:

- During assembly the inserting part is elastically deflected under the contact between both the inserting and retaining part. This can be observed in Figure 5.3.
- Larger stresses than the yielding stress and higher strains than allowable strain of the material may cause permanent deformation at the base of the beam which can cause a non-perfect mating between the two parts. This will decrease significantly the resistance under the action of loads of the connection.
- Stress concentration at the base of the beam can be controlled and reduced by tapering the height of the beam starting from a defined height at the base of the beam and reducing it constantly until the end the beam. Another method is introducing a round filled radius at the edge that connects the cantilever beam and the base. These methods were presented in Section 2.5 and can be observed in Figure 2.21 and in Figure 5.3.

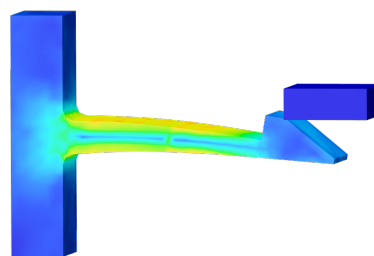


Figure 5.3: Von Mises stresses on a snap-fit assembly procedure.

### Usage phase

Once the snap beam is correctly assembled and tip is at its final position, which will be called retention position (see Figure 5.2b), the joint is held together by the interfaces created by the contacting surfaces. For the innovative joints a few design considerations are required:

- The necessary resistance between the two surfaces will depend on the design requirements.
- As mentioned before, a snap-fit connection can be designed either to be assembled and disassembled multiple times or to be a permanent connection, which makes disassembly very difficult using the snap-fit principle (see Section 2.5). The innovative design concept on this research project requires a permanent connection in order to be able to resist the design axial forces.
- The usage phase will be divided into two sub-phases since the connection needs to resist both tensile and compressive force:
  - Retention for tensile forces
  - Retention for compressive forces
- The elasto-plastic properties of steel play an important role in the behaviour of the connection during the use of the joint. This will be further studied and discussed on this section.

### Disassembly phase

For a snap-fit joint the disassembly difficulty will greatly depend on the angle  $\beta$  of the retraction side of the tip or "hook", as shown on Figures 2.19 and 2.20 (see Section 2.5). For a joint that is fabricated out of thermoplastic material this difficulty will be represented on the amount of force needed to unhook the tip. Due to the elongation properties of such material and if the tensile yielding strength is not exceeded the beam will return to its initial position after the deflection produced by the disassembly. However, steel has a elasto-plastic behaviour which makes disassembly challenging. Once the yielding point of a steel member is reached plastic deformations will occur. When a "pulling-out" force is applied to a snap-fit, the tip is in contact with the retaining unit creating a shear force at the tip (or hook). If the tip and the snap-beam are not properly design, a bending moment will be generated at the tip due to the eccentricity of the contact-force. Stress concentration will be developed at the base of the tip causing rotation and irreversible damages. This can be observed on Figure 5.4.

As it was mentioned before, in order to being capable of resting the required nodal forces, a permanent connection is required. Although this will hinder the disassembly possibility, others disassembly methods will be discussed on this chapter.



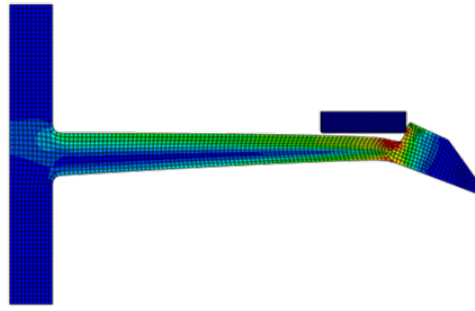


Figure 5.4: Von Mises tresses on a steel snap fit after disassembly.

## 5.4 INNOVATIVE JOINT: GENERAL CONCEPT

The innovative joint concept is developed based on the snap-fit principles presented in Section 5.3 and based on the fact that different members can be connected to one node with different arrival angles, as shown in Figure 5.1.

Additional to that, in order to ease the assembly and improve the assembly time of the whole structure it is desired that the innovative connection does not require the use of additional fasteners such as welds or bolts. In the same way a conventional snap-fit connection is composed of two components as explained in Section 5.3.1, based on the same principles, the innovative joint developed in this research project will also have two main components. In spite the components from the innovative joint are required to have similar functions than the conventional snap-fit components, these are modified to fulfil the structural en geometrical requirements. The general joint concept is presented in Figure 5.7.

- **Inserting Unit:** Presented in 5.5 and in Figure 5.7a, the inserting unit will be composed of different serrated tips or "hooks" which will allow the steel connecting beam to resist tensile forces coming from the member of the truss. The tips in charge of resisting tensile forces are colored in red on the following image. In order to being able to resist compressive forces the inserting unit requires an additional tip or block, which is represented in yellow color in Figure 5.5.

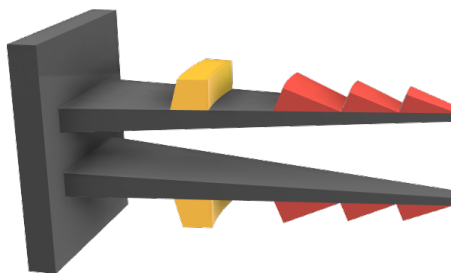


Figure 5.5: Parts of the inserting unit.

- **Retaining Unit:** Knowing that after the optimization process the internal members of the truss can be connected to each other non-symmetrically, as shown on Figure 5.1, the retaining unit must allow such configuration. Therefore, the retaining unit will be composed of two circular

steel plates connected by a steel cylinder as shown on Figure 5.6. The steel plates will have serrated indentations to allow proper connection between the inserting units tips and the retaining unit.

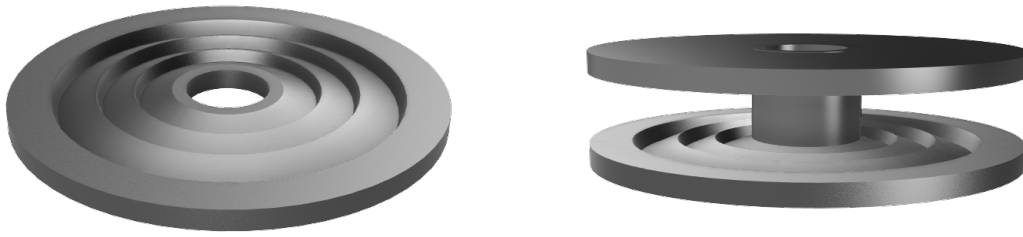
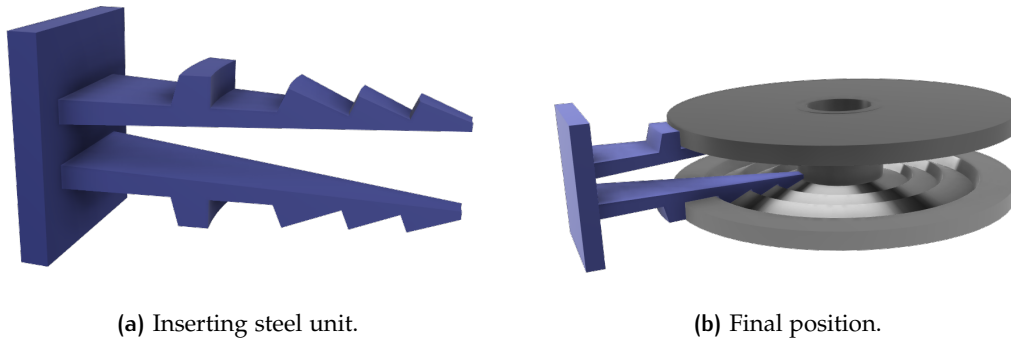


Figure 5.6: General concept of the innovative connection.

All along this section different design concepts based on the general concept shown on Figure 5.7 are discussed and analyzed until the final design is reached. The concept presented before is not the final concept, although the connecting idea and principles will be kept during this research project.



(a) Inserting steel unit.

(b) Final position.

Figure 5.7: Innovative general concept components.

The illustrations presented in Figure 5.6 and in Figure 5.7 do not represent the final design. They are used to demonstrate how the snap-fit principles will be used on the innovative joint.

## 5.5 NUMERICAL ANALYSES

Owing to no experimental works were conducted in this research, extensive finite element analyses (FEA) were executed. The FEA are used to study and describe the behaviour of the innovative joint under the action of axial tensile and compressive forces. Due to the lack of experimental works no calibrations models were used and assumptions based on previous studies and researches were made.

All finite element analyses were performed using ABAQUS/CAE 2019 software which has proven to a good and reliable software for various engineering problems.

Depending on analyzed phase (see Section 5.3.2) the FE model will require specific characteristics moving from general static analyses to explicit

dynamic analysis. General aspects of the FE analyses such as meshing, loading, contact between parts and boundary conditions are discussed under this section. Steel S355 is widely used as material for the construction of steel structure due to its mechanical properties its east accessibility. For this reasons, steel S355 is used as material for all FE analysis for both parts of the joint, the inserting and retaining part. The material model is presented on the following section.

### 5.5.1 Material models

Steel material properties such as stresses and strains can be measured from material testing. The resulting properties are often specified as Engineering stress-strain curves. In order to simulate a more realistic behaviour of a steel connection using Finite Element Analysis, the true stress and true plastic strain relationship is often used. The true stress ( $\sigma_{true}$ ) and the true plastic strain ( $\epsilon_{true}$ ) can be determined using the following equations [44]:

$$\sigma_{true} = \sigma_{eng}(1 + \epsilon_{eng}) \quad (5.1)$$

$$\epsilon_{true} = \ln(1 + \epsilon_{eng}) \quad (5.2)$$

However, since no material testing were performed for this research project the engineering stress - strain relationship is not available. For this reason an approximation of the material properties using bi-linear elastic with linear strain hardening is the appropriate, which follows the guidance specified in the Eurocode 1993-1-5 Appendix C6 for Finite Element methods of analysis. The hardening slope is the reduced stiffness ( $E/100$ ).

Steel S355 is used as material for the connecting elements which has a yield strength of 355 MPa and the ultimate strength is taken as 510 MPa. The elastic modulus is 210000 MPa and the density of the material is 7850 kg/m<sup>3</sup>. Poisson's ratio of steel is set to be 0.3.

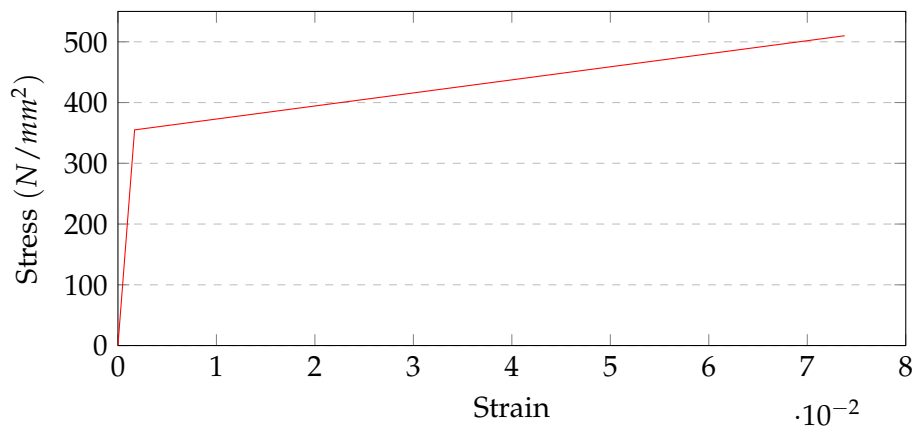


Figure 5.8: Steel s355 bi-linear stress-strain relationship.

Plasticity in Abaqus defines the post-yielding behaviour of the material. The plastic data define the true yield stress of the material as a function of the

Strain Stress relationship				
Eng Stress	Eng Strain	True Stress	True Strain	Plastic Strain
0	0	0	0	0
355	0.00169	355.60	0.00169	0.0
510	0.07381	547.64	0.07121	0.0686

Table 5.1: Stress and strain conversions.

true plastic strain [44]. Table 5.1 shows the conversion from Engineering to True material properties data. The plastic strain is obtained by subtracting the elastic strain from the value of the total true strain, as is expressed on the following equation.

$$\epsilon_{pl.true} = \epsilon_{true} - \epsilon_{elastic} = \epsilon_{true} - \frac{\sigma}{E} \quad (5.3)$$

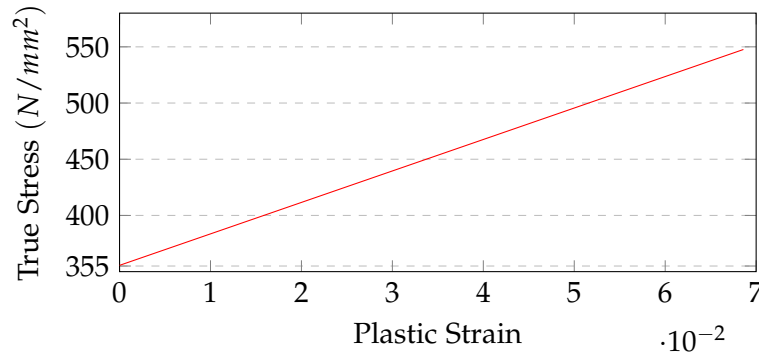


Figure 5.9: Steel S355 material curve used in Abaqus.

### 5.5.2 Geometry and boundary conditions

The two units presented in Section 5.4 are modelled as two different parts on every FE analyses. Fully-constraints conditions are applied on the retaining unit whereas the the constraints of the inserting unit will vary depending on problem's needs. In general, the inserting unit base will be fixed (horizontal displacement may not be restrained depending on the analysis) in order to achieve a cantilever behavior of the snap-beam. In order to save computational time, symmetry was used and half of the total inserting unit is modelled on all FE analyses. Similarly for the same reason, only a section of the retaining unit is modelled.

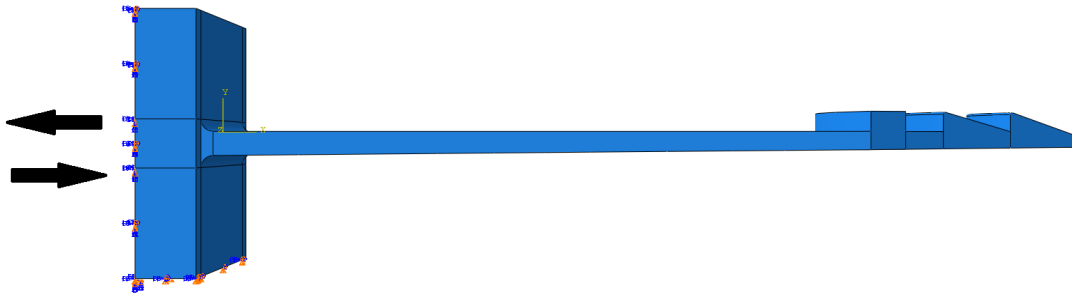


Figure 5.10: General boundary conditions for inserting unit.

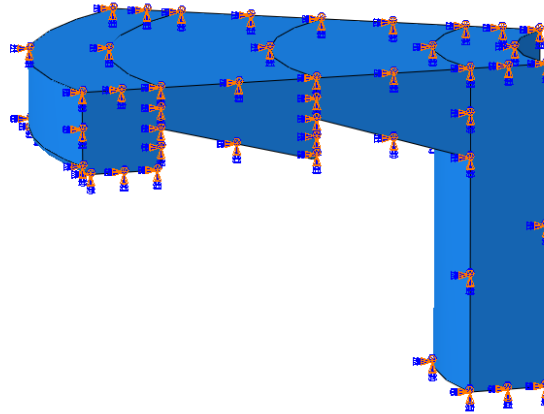


Figure 5.11: Boundary conditions for retaining unit (fully fixed).

### 5.5.3 Finite element mesh

In order to minimize the mesh distortion as much as possible a fine mesh of hexahedral continuum 8-node finite elements with reduced integration is an appropriate and recommended finite element mesh for solid [44] [45]. For this reason, both elements (inserting and retaining units) for all FE analyses are composed of 8-node linear brick with reduce integration elements (C3D8R).

Mesh size varies for different parts depending on their importance and size. Since the contact between the units is expected to happen at the inserting and retaining unit, a finer mesh with 1 *mm* elements was set. For the beam-plate of the inserting unit a courser mesh was used with 2 *mm* elements, as shown in Figure 5.12.

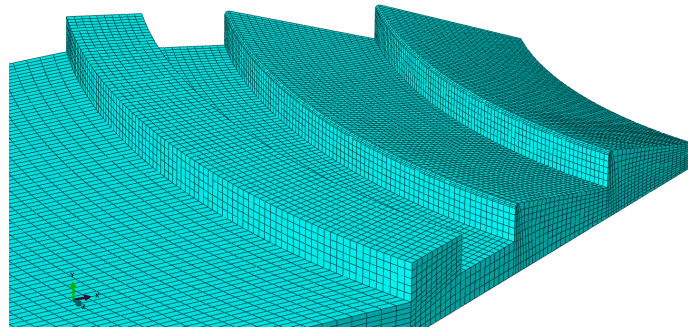


Figure 5.12: Inserting unit mesh

#### 5.5.4 Loading

Depending on the problem's requirements, either force controlled or displacement controlled analyses were used. The required design forces that the node needs to take is presented in Section 4.5.5. A displacement controlled analysis was used at the assembly phase since it was required the movement of the inserting unit through an specified dimension. Figure 5.13 shoes the custom amplitude function for the assembly phase. Since a correct interlocking between both units is important, time-displacement function required to be slow and accurate at the end of the analysis. For all other FE analyses a linear amplitude function was used.

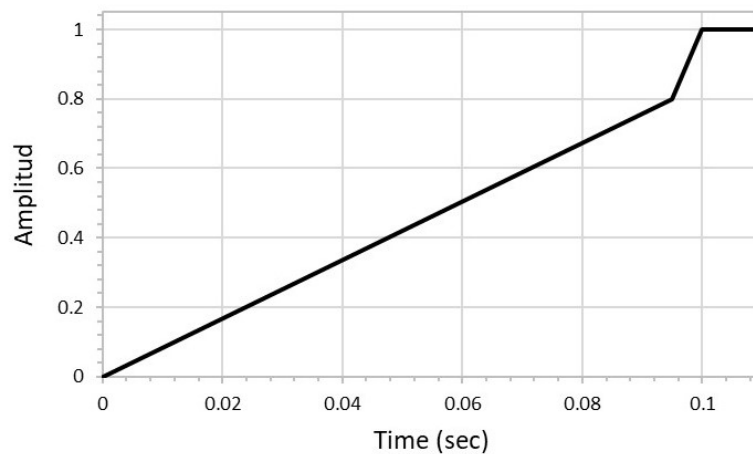


Figure 5.13: Custom loading amplitude function.

#### 5.5.5 Contact

Contact between both units play an important role an all FE analyses. Therefore, it has to be defined properly. For all analysis tangential behaviour with friction formulation penalty was used and a steel-to-steel friction coefficient of 0.4 was assumed. Additionally, normal behaviour contact as "Hard" contact was used. Depending on the analysis either general contact or surface-to-surface contact as defined.

## 5.6 DESIGN CONCEPTS

Three main design concepts (DC) are analyzed and discusses in this research project. All of them are developed and designed under the principles based on a snap-fit connection (see Section 5.3) and based on the general concept presented in Section 5.4. Every design concept will consist of the two components mentioned in Section 5.4. Different aspects such as ease of connection, use of material, disassembly procedure, concentration of stresses, permanent plastic deformation, among others, are taken into consideration before the final design is chosen.

### 5.6.1 Design concept 1

This design concept is a first attempt to develop a inserting unit capable of resisting the required nodal forces. In this design is desired to have as much sectional area as possible to resist tensile and compressive force and while still being able to deflect and behave as a snap-fit connection. Based on this principles design concept 1 (DC1) is developed. DC1 can be observed in Figure 5.14.

This concept consist of two cantilever beams composed of two cut "U" sections connected to each other at the base. Every beam has horizontal tapered plate with 3 tips at the end of it. The tips will be in charge of resisting the nodal forces. In order to take advantage of the retaining properties of a snap-fit connection the retaining angle  $\beta$  (see Figure 2.20) of all three tips is  $90^\circ$ . In addition, two tapered vertical plates are connected to each side of the horizontal flat beam. A circular perforation can be found at the connection of the two vertical plates which is expected to allow the inserting unit to deflect without damage. A similar composite snap joint technology was developed for a high voltage transmission tower [46].

For this concept is important to understand the deflecting behaviour of the inserting unit. Knowing that the cross-sectional area is more than enough to resist the required compressive and tensile nodal forces and that the geometrical shape of the "u" profile is beneficial against buckling behaviour, the insertion or assembly of the inserting unit becomes the critical phase to consider. Therefore, a FE static general analysis was performed. Only half of the inserting unit was modelled in order to reduce computational time. Table 5.2 shows the main characteristics of the FEA.

FEA characteristics	
<b>Analysis type</b>	Static, General
<b>Finite element type</b>	3D8R: 8-node linear brick
<b>Duration</b>	1.00 sec
<b>Material model</b>	See Section 5.5.1
<b>Material properties</b>	Non-linear
<b>Analysis</b>	Displacement controlled
<b>Applied displacement</b>	4 mm

Table 5.2: FEA characteristics for design concept 1.

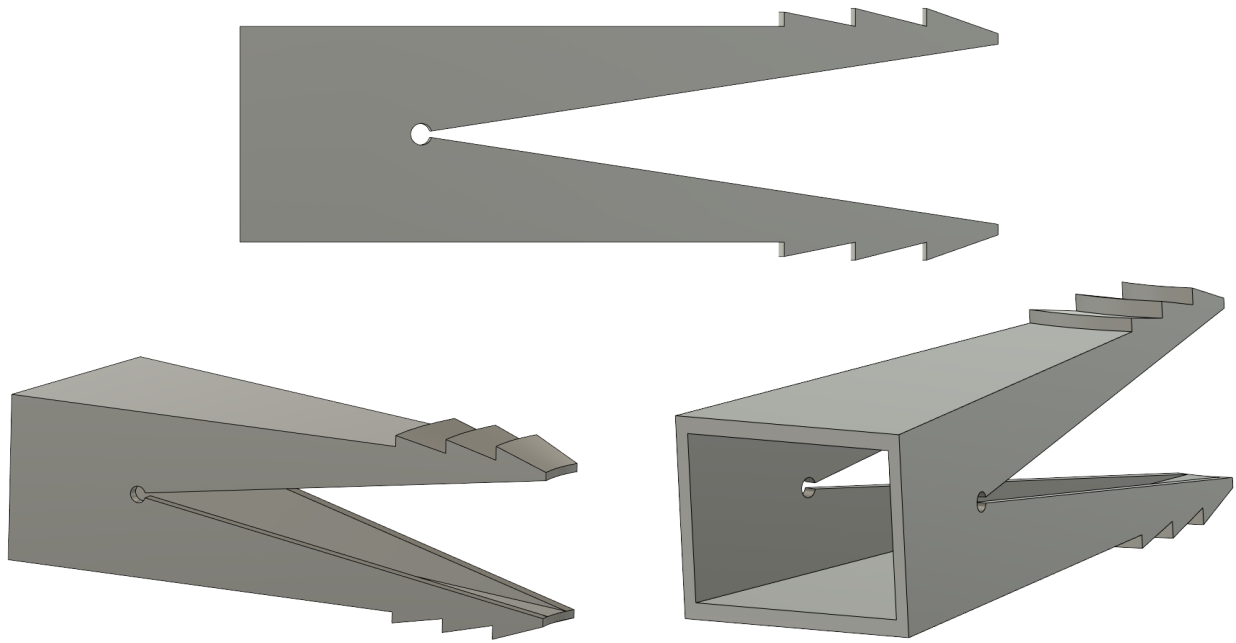


Figure 5.14: Design concept 1.

### Results

To study the structural behaviour of the inserting unit during the assembly phase a deflection of  $4\text{ mm}$  was applied at the first tip of the beam. Stresses, plastic strains and displacements were studied.

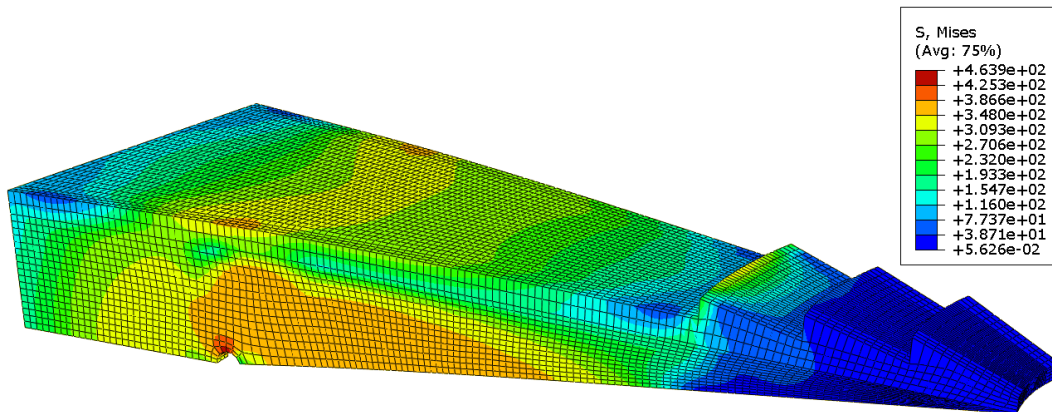
Figure 5.15: Von Mises stresses ( $\text{N/mm}^2$ ) of design concept 1.

Figure 5.15 shows stress distribution along the snap-beam when a vertical displacement of  $4\text{ mm}$  is applied at the first tip. As expected, deflection of the element is controlled by the vertical plates due to its higher second moment of area than the horizontal plate. At the same figure is possible to observe how stresses concentrate around the perforation. The opening acts as a fuse while taking the most amount of stresses.

Figure 5.16a shows the strain concentration around the circular perforation. It is possible to observe that around the top edge of the hole higher stresses than maximum allowable strain appear. This is reflected on the



stress-strain curve shown in Figure 5.16b where it can be clearly observed the elasto-plastic behaviour at the perforation. The displacement behaviour of the DC1 inserting unit can be found on the Annex C at Figure C.2. Similarly, the stress contour around the perforation and a cut-view of the inserting unit can be found at the same Annex at Figure C.1 and Figure C.4.

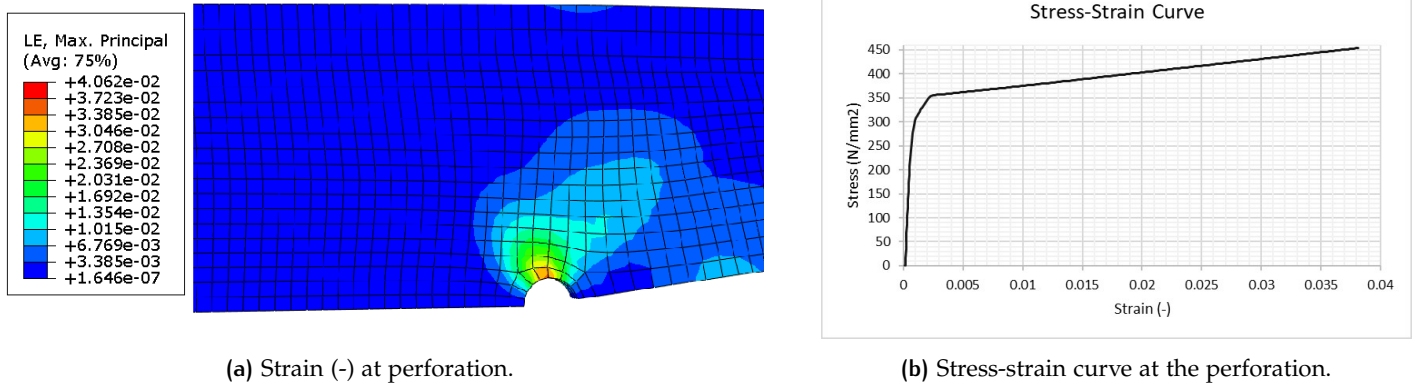


Figure 5.16: Stress-strain behaviour of design concept 1.

### Conclusions

This design concept has interesting strengths on its design such as the amount of cross-sectional area to resist nodal forces, the stress concentration at the perforation and the damage localization. This last aspect can be very helpful for designers since the damage of the element will not longer be at the base of the horizontal plate as it is usually for conventional snap-fit connections (compare Figure 5.3 with Figure C.4).

Although this fuse-behaviour could be beneficial, several factors make this concept not applicable for this case project:

- Due to the steel low-strain allowance it is not possible to achieve considerable deflection for the assembly phase of the inserting unit without the appearance of plastic strains at the perforation.
- The plastic deformation could lead to permanent damage and permanent deformation precluding a proper snap-fit functioning of the element.
- If the inserting unit faces permanent deformation after the assembly phase, the usage phase might be compromised.
- In addition, buckling of the vertical plate due to loads at the end of the tip must be considered in the design. This was not checked for this design concept.

The change in diameter of the opening requires to be studied in order to have a better understanding of this fuse-behaviour.

### 5.6.2 Design concept 2

Based on the previous results the second design concept (DC2) is developed. Knowing that adding vertical plates to a traditional snap-fit beam could prevent the beam to be inserted in the retaining unit, the second design concept consists of a flat horizontal plate inserting unit composed of three-tips and the retaining unit, similar to the general concept presented in Figures 5.7a and 5.5. In order to take advantage of the retaining properties of a snap-fit connection the retaining angle  $\beta$  (see Figure 2.20) of all three tips is  $90^\circ$ . Knowing that the inserting unit during assembly deflects as a cantilever beam, the last tip has the larger height being this reduced for the second and third tip as shown in Figure 5.17.

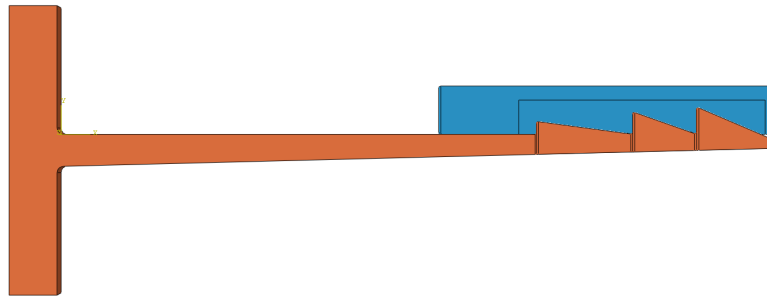


Figure 5.17: Design concept 2.

For this concept it is important to understand the contribution each tip has when resisting axial tensile forces. In order to prove this, a force controlled FE analysis was performed on the design concept 1 model. On this design concept only retention for tensile forces is tested. Table 5.3 shows the main characteristics from the FE analysis.

Although without a proper assembly of the inserting unit the retention for both compressive and tensile forces would be compromised, the insertion procedure is not checked on this design concept. This is because it is desired to obtain only the relationship between the number of tips and the resistance to tensile load.

FEA characteristics	
Analysis type	Dynamic, Explicit
Finite element type	3D8R: 8-node linear brick
Duration	1.00 sec
Contact type	General contact (Explicit)
Material model	See Section 5.5.1
Material properties	Non-linear
Analysis	Force controlled
Applied load	10 kN

Table 5.3: FEA characteristics for design concept 2.

## Results

As it was expected the load is not evenly distributed throughout the three tips. Figure 5.18 shows how the stress is concentrated along the contact edges between the inserting and the retaining unit. It can be clearly observed that the tip which is closes to the base of the beam carries the largest amount of load and that the end-tip has almost no influence on the load resistance. A chart showing the resistance to the load each tip has can be found on Annex C in Figure C.6. At the same section the reaction forces at every tip are plotted in Figure C.5.

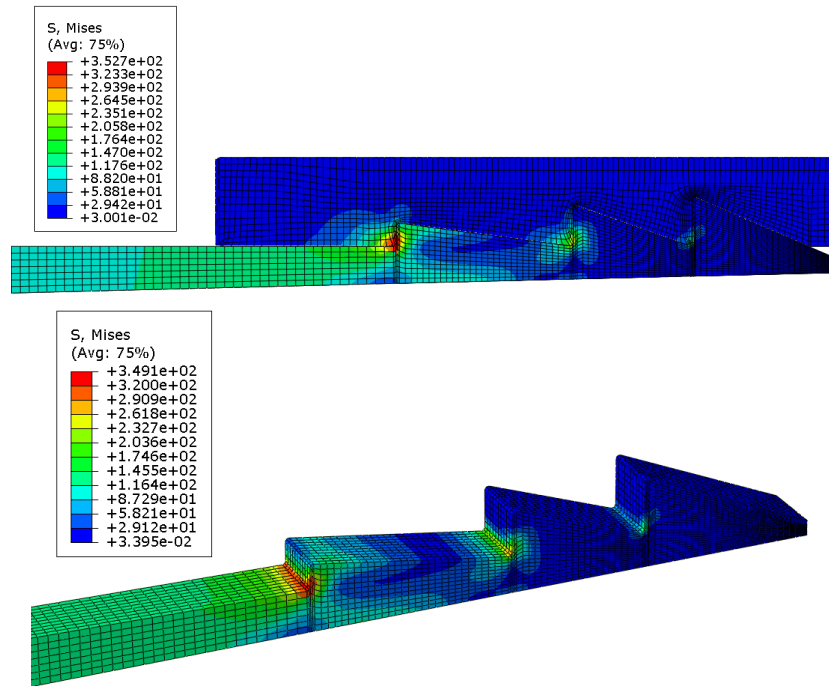


Figure 5.18: Von Mises stresses ( $N/mm^2$ ) for axial tensile loading condition for design concept 2.

Based on the results it was found that the load distribution goes as follows, being tip 1, tip 2 and tip 3 the first tip, middle tip and end tip respectively:

Load carrying contribution	
Tip 1	54%
Tip 2	38%
Tip 3	8%

Table 5.4: Tips load-carrying contribution.

## Conclusions

Taking into account that the load is not evenly distributed among all tips and that there is a significant difference of load carrying capacity between the first and the last tip it can be concluded that the tip at the end of the beam is not required.

Moreover, every additional tip increases the length of the beam and as consequence the diameter of the retaining unit will also increase. The incre-

ment of the numbers of tips will not improve the behaviour of the snap fit connection under tensile forces.

A concentration of stresses higher than the yielding stress at the contact between the first tip and the retaining unit might cause plastic deformation and permanent damage.

## 5.7 DESIGN CONCEPT 3: FINAL DESIGN

The previous design concepts contributed with very valuable results and outputs. The results obtained from DC1 are very helpful to understand the deflecting behaviour of a steel snap-fit beam and where plastic deformations are prone to appear. From DC2 was found that a third tip at the end of the cantilever snap-fit will not have a significant contribution to the load resistance of the unit and as consequence the diameter of the retaining unit will increase. By gathering all the knowledge and combining the strengths from the previous design concepts, the third and final design concept (DC3) is developed.

Similarly than the previous concepts, DC3 is composed of a inserting unit and a retaining unit:

### 5.7.1 Inserting Unit

Based on the previous information the inserting unit consist of a tapered horizontal steel plate. The inserting unit of DC3 is presented in Figure 5.19. It can be distinguished that the width of the plate is not constant until the end of it. The zone which will be inserted into the retaining unit has a variable width which will allow the member to be connected at any arrival angle to the circular plates.

The beam is composed of two triangular-shaped tips which will allow to resist tensile forces, as shown in blue at Figure 5.19, and a rectangular tip which is the one withstand compressive forces which is shown in red at the same Figure.

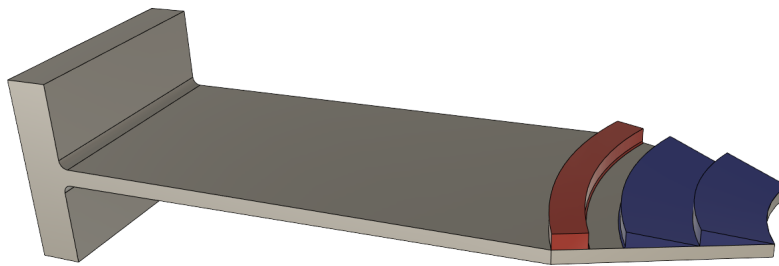


Figure 5.19: Design concept 3: inserting unit.

The total length of the inserting unit is 220 *mm* and the width at the base is 80 *mm*. It has a tapered height starting with 6 *mm* at the base and ending at 4 *mm*. A complete image with all dimensions can be found at Annex C in Section C.3.1 at the Figure C.7.

### 5.7.2 Retaining Unit

Similar to the general concept presented in Section 5.4 the DC3 retaining unit is composed of two steel serrated plates connected by a steel cylinder, as shown in Figure 5.20.

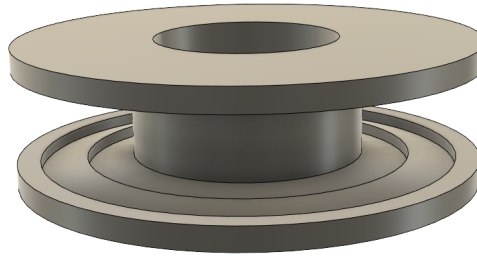


Figure 5.20: Design concept 3: retaining unit.

The diameter of the circular plates is 200 mm and the internal diameter of the internal cylinder is 80 mm. The thickness of the steel plates is 10 mm. A complete image with all dimensions can be found at Annex C in Section C.3.1 at the Figure C.8.

#### *Final position*

The use of tolerances are important for both the assembly and the usage of the node. Small gaps (1 mm gap) between the block use for resisting compressive forces on the inserting unit (see Figure 5.5) and the retaining unit are required to achieved a proper assembly. Once the inserting unit is introduced to the retaining unit, a perfect interlocking will occur. This interlocking will allow to resit the nodal axial forces. Figure 5.21 shows how the Circular Hollow Section (CHS) steel members from the truss will be connected to each other through the innovative joint.

At the following Figure it can be clearly observed how design principles defined at Section 5.3 are successfully achieved. On one hand the snap-fit connecting principle are used to assemble the element and to resit the nodal axial forces. On the other hand, the shape of the retaining unit allows any CHS steel member to be connected at any arrival angle to the node. This innovative joint will make internal nodes such as the one presented in 5.1 possible to realise in real engineering practice.

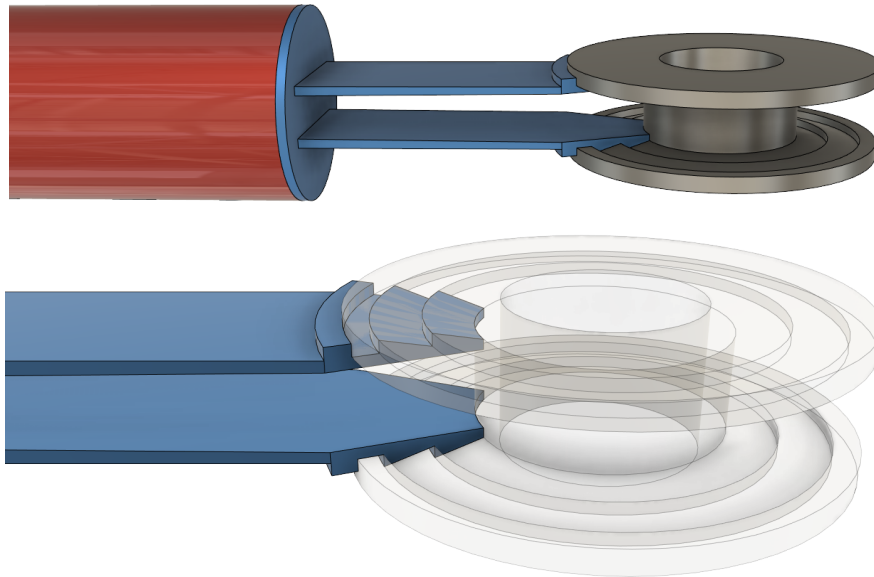


Figure 5.21: Final design: connection between inserting unit and retaining unit.

## 5.8 FINAL DESIGN CONCEPT: PHASES FEA

For the final innovative joint concept (Design Concept 3), FE analyses of all three phases presented in Section 5.3.2 will be performed and studied in depth.

### 5.8.1 Assembly phase

For a snap-fit connection it is of utmost importance to properly understand the material behaviour during the assembly of it. As it was mentioned before, snap-fit connections are usually made out of thermoplastic materials and for small scale connections. The mechanical properties of such material allows the cantilever beam of the snap-fit tip to deflect without permanent deformation. Similarly, due to the small scale of the application of such connections contact between the elements is not a critical.

For a steel connection based on the snap-fit principles it is desired that a snap-cantilever beam stays under the elastic range. Due to the elastoplastic mechanical properties of steel, once the beam reaches a deflection that produces stresses at the base beyond the yielding stress plastic strain may appear at the same location. This means that after deflection the beam will have permanent deformation and will not go back to its initial position. For the assembly of the final design concept (see figure 5.21) two inserting mechanisms are presented on this report. First a sliding insertion of the inserting unit and finally a manual insertion.

#### *Sliding insertion*

The sliding insertion consist on applying a force on the inserting unit and pushing it into its final position inside the retaining unit. In order to predict the behaviour of the inserting unit while being inserted into the retaining

unit a displacement-controlled FE analysis was performed. During a snap-fit the static problem becomes dynamic in nature due to the sudden lost of contact. Therefore, a dynamic implicit analysis was performed. Table 5.5 shows the main characteristics of the FE analysis.

FEA characteristics	
Analysis type	Dynamic, Implicit
Finite element type	3D8R: 8-node linear brick
Duration	0.11 sec
Contact type	Surface-to-surface contact
Material model	See Section 5.5.1
Material properties	Non-linear
Analysis	Displacement controlled
Applied displacement	50.02 mm

Table 5.5: FEA characteristics for the final design concept.

One complete inserting unit beam was modelled. However, in order to reduce the computational time of the FEA only a section of the retaining unit was modelled, as seen in Figure 5.22 in green and gray color respectively. It can be observed Figure 5.23 how the brick elements and the mesh is distributed along the unit. It is important to mention that a refinement of the mesh has been applied around round edges and at the surfaces of the tips.

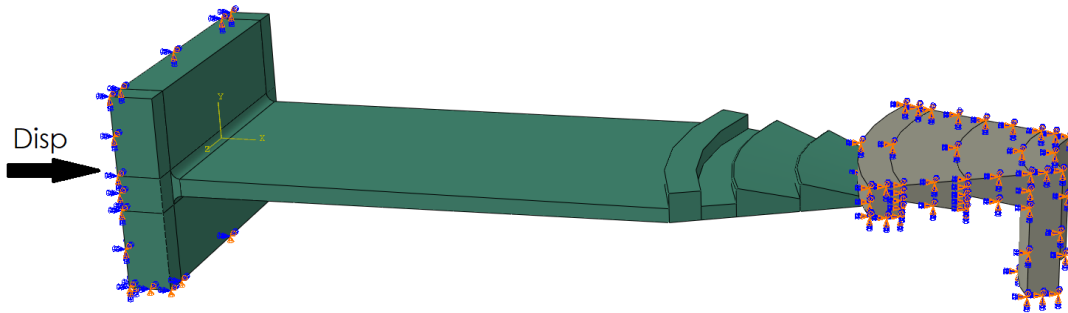


Figure 5.22: 3D models of the inserting and the retaining unit with boundary conditions.

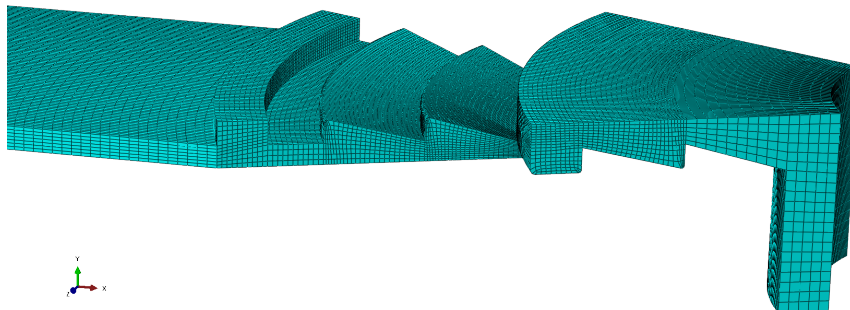


Figure 5.23: Meshing of the 3D model.

As starting points the following assumptions were made:



- Insertion of the beam was executed with a perfectly straight beam.
- The displacement is applied at the axis of the length of the beam.
- Both units are not in contact at the beginning of the analysis.
- The retaining unit is fully constraint as boundary condition.
- Edges that will be in contact between the two elements were filleted and rounded in order to obtain more accurate results and achieve a better stress distribution.

By applying a concentrated force or a pressure load at the base of the inserting unit the beam tends to move towards the direction of the applied force. In this case, the retaining unit is on the way of the movement which makes the inserting unit to deflect while being inserted. This will generate a bending moment at the base of the beam due to stress concentration as illustrated in Figure 5.25.

The stress-strain relationship at the base of the beam can be found at Figure 5.24. At that Figure it can be observed that the relationship is linear which means that the beam deflects elastically during the whole trajectory. This allows the beam to snap-back into its final position shown in Figure 5.7b without deformation at the base.

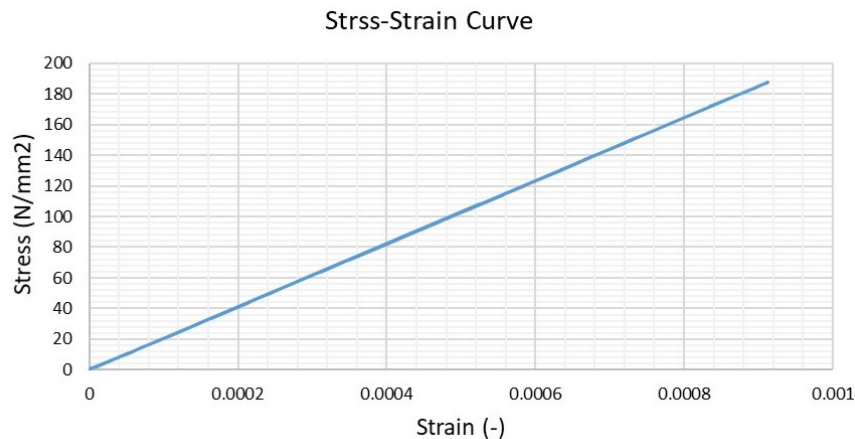


Figure 5.24: Stress strain relationship at the base of the beam.

Figure 5.26 presents the required force to insert the steel inserting unit into the retaining unit. At the graph two main peaks can be observed: a short peak at the time of 0.045 *sec* and a the largest one at 0.094 *sec* . Each peak represents the reaction force of each tip while being assembled. Once the cantilever snap-beam is finally inserted the reaction force goes back to 0. It can be spotted that the maximum force of 1508 *N* is required to slide the inserting unit into its final position. Figure C.11 shows the Von Mises stresses vs time of the analysis where the peaks correspond when higher stresses appear at the base of the beam. Deflection of each tip throughout the insertion phase is presented in Annex C at Figure C.12.

From Figure 5.25 is possible to realise that there is a concentration of stresses at the tips surfaces after the tip has being in contact with the retaining unit. Stresses and strains at specific nodes at the tip are analysed in



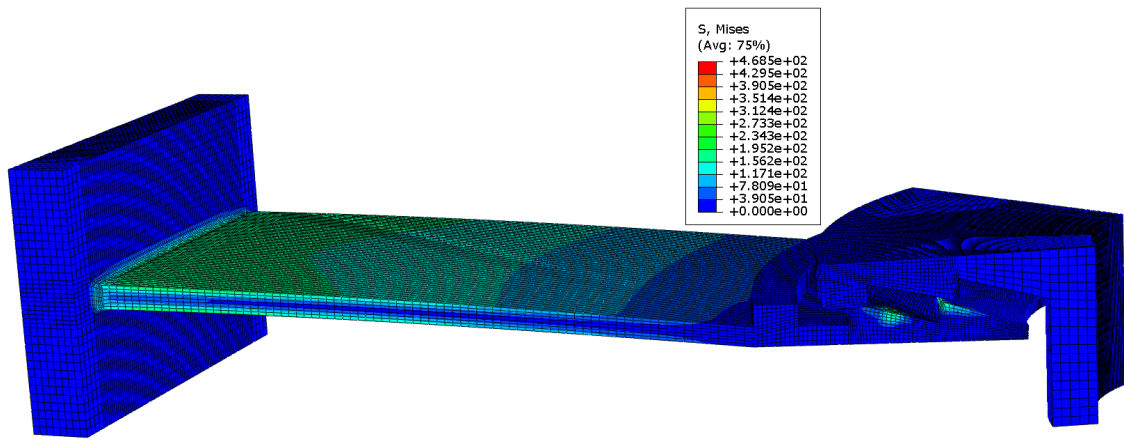


Figure 5.25: Von Mises stresses during the assembly of the joint.

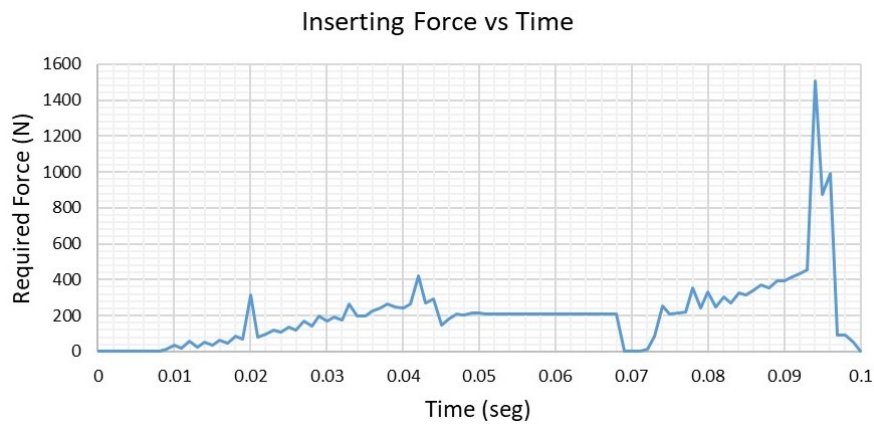


Figure 5.26: Assembly force.

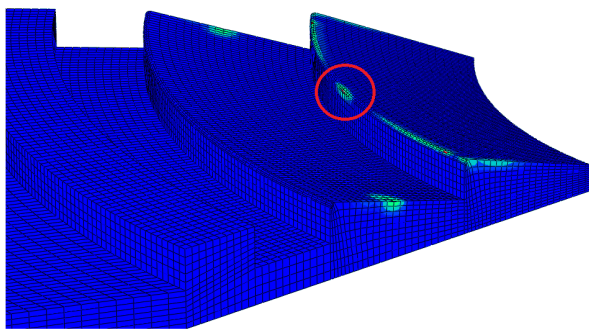
order to predict if the tip will present damages and deformations after the insertion of the beam. Figure 5.27a shows the stress concentration on the tips while the beam is being inserted. The red circle shows where the stress is the highest. Figure 5.27b illustrates the stress-strain relationship at that point. It can be observed that at that point stress beyond yielding stress occurs and steel reaches a plastic behaviour.

At Annex C the strain at the edge of the tip can be found in Figure C.9. Similarly, the stress vs time and strain vs time behaviour at the same node can be seen in Figure C.11 and Figure C.10.

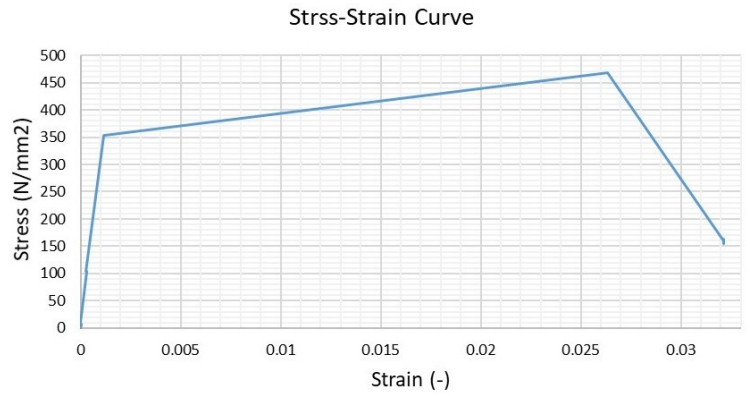
The appearance of plastic strains at the tips after the insertion of the beam could lead to localized permanent damage. The correct interlocking between the inserting unit and the retaining unit might be compromised if deformation of the material appears close to the edges of the tip. Therefore, a second inserting mechanism is presented on the following subsection.

### Manual insertion

The manual inserting mechanism consists of deflecting the cantilever beam with the external help of a pressing device, such as a U-frame press (see Figure 5.31). By applying a specified load at a certain position the beam will deflect and the snap-beam will be inserted into the retaining unit while



(a) Stress concentration at round edges.



(b) Stress-strain at round edge.

Figure 5.27: Stress-strain behaviour at the tips from the inserting unit.

deflected. Once the inserting unit is at its final position the load is gradually removed. Figure C.13 at Annex C illustrates how the manual insertion can be performed. Figure 5.28 shows where the load needs to be applied in order to allow the required deflection without exceeding yielding stresses at the base of the beam. Based on Euler-Bernoulli theory the deflection of the beam for certain load has been calculated. The calculation are presented in the Annex C at Section C.3.

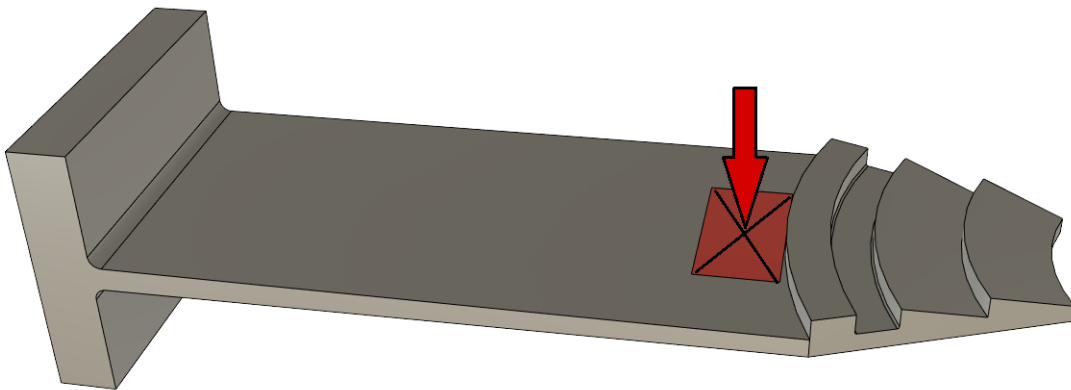


Figure 5.28: Manual Assembly

Different height and width configurations of the steel plate-beam have been analysed for in order to obtain the most favorable deflecting behaviour (see Figure 5.29). This will allow an easier and faster insertion of the beam under the action of the applied load shown in Figure 5.28. Table 5.6 shows a small study in which variations in height and in width of the beam are analysed and compared.

From the previous table can be deduced that the ratio between a beam with tapered height and a constant-height beam is 1.23 and the ratio between a width-variable beam and a constant-width beam is 1.1. It can be concluded that a tapered-height beam has larger deflection than a beam with variable width, for the same load at the same location while keeping the same stress at the base of the beam.

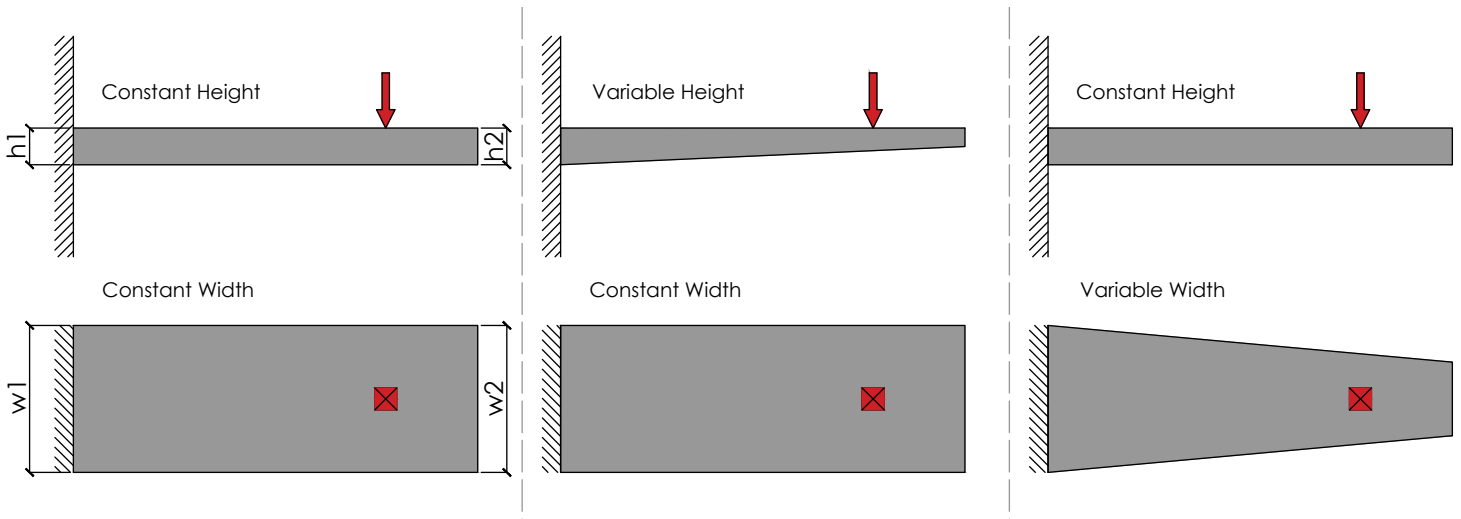


Figure 5.29: Different beams configurations

Beam with variable height and width			
Beam Type	Constant height and width	Variable Height	variable width
Length (mm)	220	220	220
Height base (mm)	6	6	6
Height tip (mm)	6	4	6
Width base (mm)	80	80	80
Width tip (mm)	80	80	40
Force (N)	1000	1000	1000
Position force (mm)	160	160	160
Deflection at force (mm)	4.51	5.54	4.99
Deflection at end (mm)	7.06	8.89	7.91
Stress at base (N/mm <sup>2</sup> )	333.3	333.3	333.3

Table 5.6: Height and beam configuration study.

Graph 5.30 shows the deflection shape of the tapered inserting unit after the load of 1000 N is applied at 160 mm from the base. It can be observed how the deflection shape is curved from the base until the point of application of the load (red line) and after this point the curvature becomes 0 (blue line).

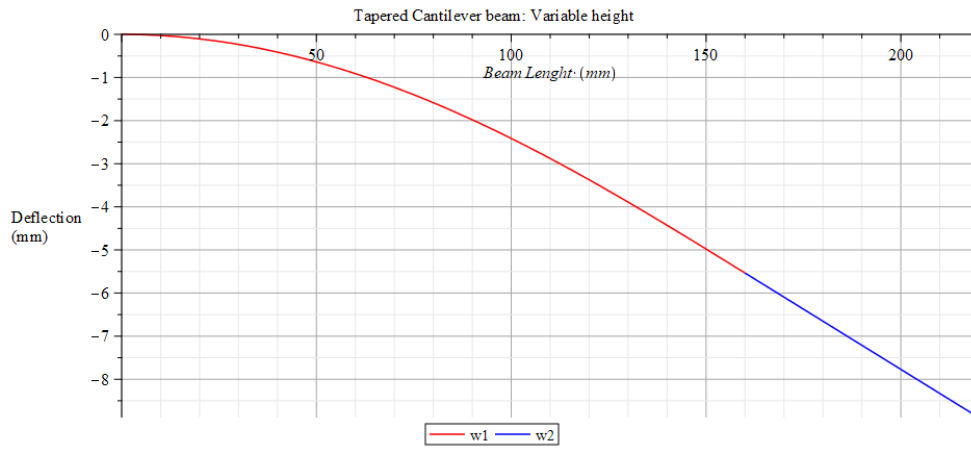


Figure 5.30: Snap-beam deflection shape.



Figure 5.31: Forged u-frame press.

This insertion method can be easily performed by a workman at site or at the workshop using a forged U-frame press (Figure 5.31) which its pressing maximum capacity can easily get over 40 kN. When applying this insertion method stresses at the tips of the beam disappear and the beam can be inserted easily into its final position. Moreover, the load appliance can be smooth and controlled. In order to prevent excessive bending of the steel plates and thus stresses beyond the yielding point at the base of the cantilever beam, additional safety measures can be taken. Figure C.14 shows how the deflection at the load application point can be controlled by adding simple control mechanism.

This manual assembly mechanism can be used effectively also to disassembly the innovative joint.

### 5.8.2 Usage phase

As mentioned in Section 5.3.2 the usage phase takes place when the assembly of the structure finalizes and it is operating normally. Once the assembly of the innovative joint is concluded it is ready to bear all nodal forces. As it was assumed on this research project only axial forces will be transmitted through the nodes. For this reason, the joint needs to resist only axial compressive and tensile forces.

Both, the inserting unit and the retaining unit, are composed of different elements (tips) that in charge of resisting and transferring all axial forces, as show in Figure 5.19 and Figure 5.20.

So as to predict the behaviour of the joint at its connected stage under axial tensile and compressive forces two FE analysis are performed:

#### Joint under tensile forces

In order to predict the behaviour of the connection under the action of a tensile load a FE analysis is required. A tensile load of 80 kN is applied on half of the inserting unit (only one snap-beam) when being connected to the retaining unit. It is assumed that the load is applied at the centroidal axis of the inserting unit. Similarly, it is assumed that the load is applied on a perfect structure (no imperfections). Table 5.7 shows the main characteristics used in the FE analysis.

FEA characteristics	
<b>Analysis type</b>	Dynamic, Implicit
<b>Finite element type</b>	3D8R: 8-node linear brick
<b>Duration</b>	1.00 sec
<b>Contact type</b>	Surface-to-surface contact
<b>Material model</b>	See Section 5.5.1
<b>Material properties</b>	Non-linear
<b>Analysis</b>	Force controlled
<b>Applied force</b>	80 kN

Table 5.7: FEA characteristics for axial tensile force.

Before analysing the FE model, it is necessary to check the yielding of the gross section of the inserting unit for a tensile load since it is expected that the cross section of it is capable of resisting such tensile loads. As it is shown on the following equation, the design strength of the cross section of one inserting unit is 116 kN. This is greater than the 80 kN required for the innovative joint.

$$\sigma_{dy} = \frac{A_g * f_y}{\gamma_1} = \frac{(360 \text{ mm}^2) * (355 \text{ N/mm}^2)}{1.10} = 116 \text{ kN} \quad (5.4)$$

Once the yielding of the gross section is checked, the quasi-static FE analysis is performed based on the information in Table 5.7. Figure 5.32 shows the distribution of Von Mises stresses along the connection at the time of 1.0 sec. This means that the totality of the load has been applied. As expected, stresses are concentrated around the contact surfaces between the inserting and the retaining unit.

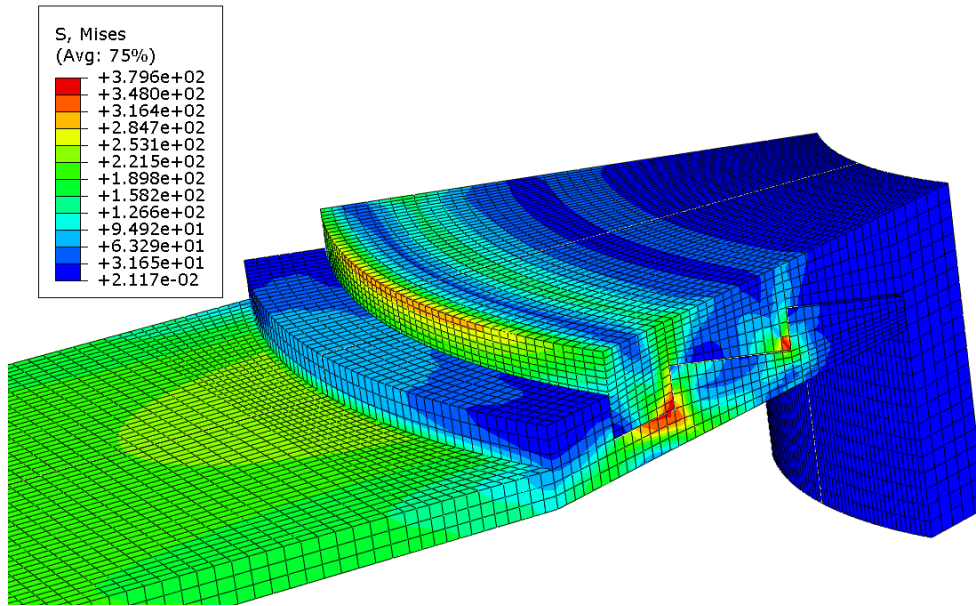


Figure 5.32: Von Mises stresses for 80 kN tensile load.

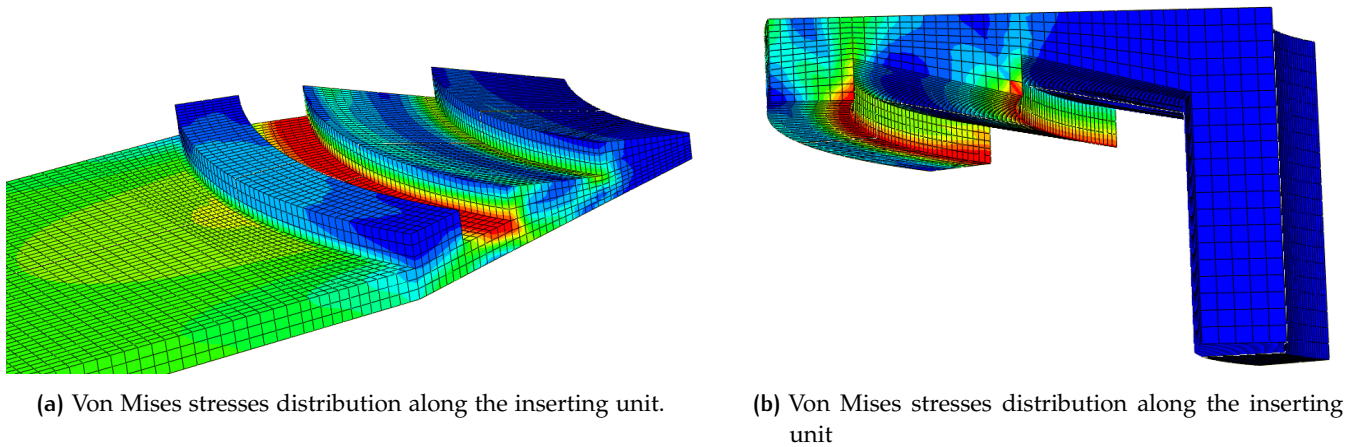


Figure 5.33: Stress-strain behaviour at the tips from the inserting unit.

The legend used in Figure 5.32 must be used to interpret both sub-figures in Figure 5.33. Figure 5.33a shows the stress concentration on the inserting unit. It can be seen in red color the stress localization around the edge which is in contact with the retaining unit. Figure 5.33b presents the stress distribution on the retaining unit.

The zone where the contour is plotted in red color in Figure 5.32 and in Figure 5.33 is where stresses concentrate the most therefore, becomes critical zone while resisting tensile forces. As consequence, the stress-strain behaviour at that zone is studied. More images where the plastic strains and stresses at both units can be appreciated are presented at Annex C from Figure C.15 to Figure C.17.

Figure 5.34 presents the strain-stress relationship of the red zones (see Figure 5.32 and Figure 5.33) from the inserting and retaining unit. The relationship between the stresses of the element and the applied force are presented in Annex C at Figure C.18. Based on both results it is possible to conclude



that the both units bear stresses higher than the yielding stress and that the edge from the retaining unit reaches plastic behaviour before the inserting unit. This could happen owing to the smaller area where the load is applied. This can be observed if Figures 5.33a and 5.33b are compared. From Figure C.18 is possible to observe that a load greater than 55 kN (110 kN for a complete inserting unit) the material at the edge starts to yield. Since the inserting unit is composed of two snap-beams, this value must be multiplied by two.

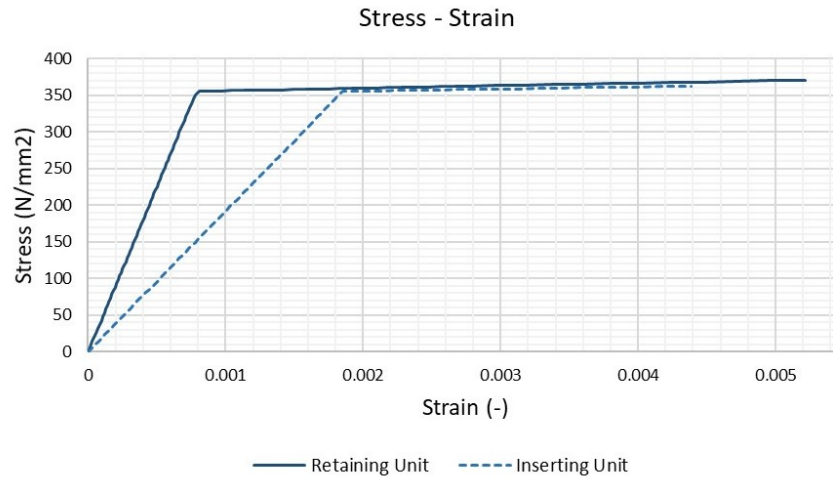


Figure 5.34: Stress-strain relationship at the inserting and retaining unit.

The appearance of plastic strains at the tip edges of both, the inserting and the retaining unit, could imply the presence of small permanent deformation at those edges. Although this might reduce the efficiency of the connection, specially if the load changes constantly from tensile to compressive forces repetitively, it is not as critical as the yielding and failure of the gross section of the inserting unit.

On the the other hand, since the contact between the two units dos not occur at the centroidal axis to either of the two units, eccentricities appear creating a bending moment at the tips of the snap-beam. This creates a rotation of the tip originating a small gap between the inserting tip and the retaining unit.

Figure 5.35 shows the gap by displaying the vertical displacement of the inserting unit. It can be clearly observed that after the interlocking elements the tip starts to rotate clockwise. Figure 5.36 present the relationship between the applied force and the vertical displacement for a node at the end of the beam. It clearly shows that until a force close to 55 kN the relationship is close to be linear and after this point the relationship presents a non-linear behaviour.

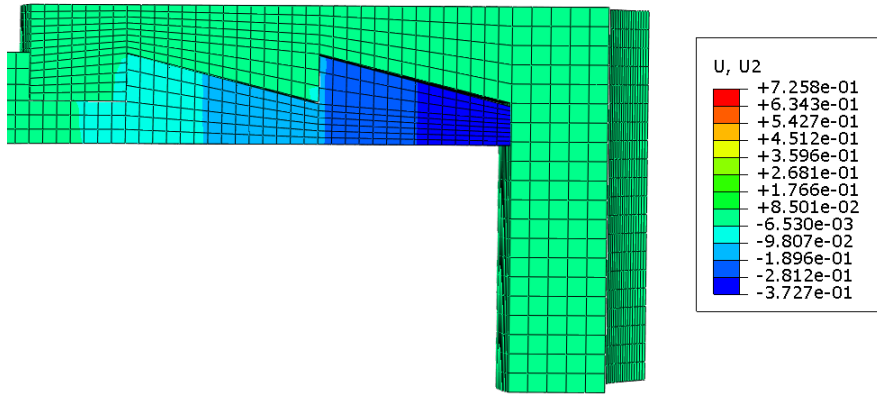


Figure 5.35: Vertical displacement of the end-tip of the inserting unit.

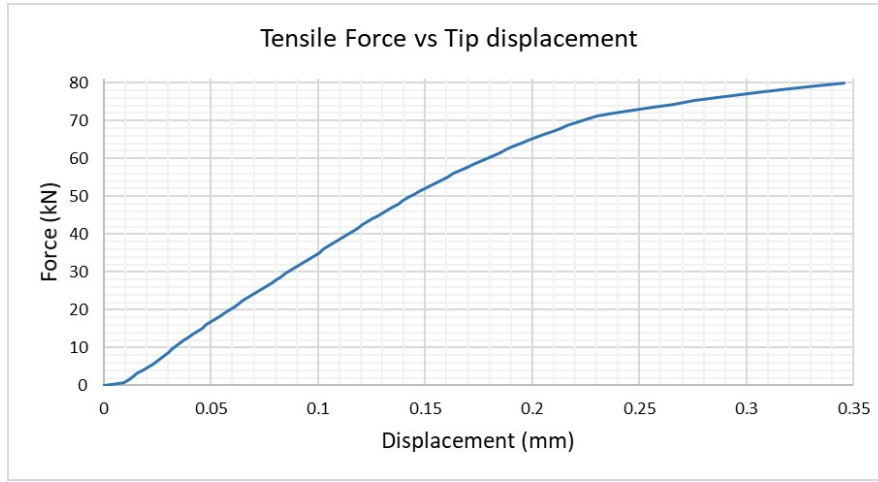


Figure 5.36: Applied force vs vertical displacement of the inserting unit tip.

### Joint under compressive forces

Initially, it is assumed that the snap-fit inserting unit under axial compression loading will behave as a fixed-free cantilever strut in which a compressive force  $P$  will act at its free-end similar as Figure 5.37. A first approximation of the compressive load resistance of the inserting unit can be calculated based on elastic buckling theory. The elastic buckling loads can be calculated assuming a constant flexural stiffness rigidity  $EI$  throughout its length, a perfectly elastic material and an axial compressive load applied along the centroidal axis of the member [12].

For a fixed-free cantilever strut the external bending moment at any cross-section can be expressed as the following:

$$EI\left(\frac{d^2y}{dx^2}\right) = -M = P(y_m - y) \quad (5.5)$$



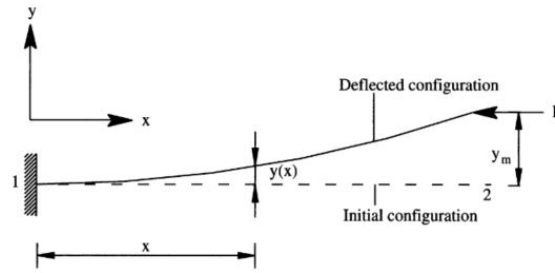


Figure 5.37: First buckling mode of a fixed-free strut [12].

The smallest Euler buckling load ( $P_{cr}$ ) corresponds to first buckling mode and it is expressed on the next equation:

$$P_{cr} = \frac{\pi^2 EI}{(2L)^2} \quad (5.6)$$

#### FEA buckling validation

In order to validate the results obtained from the finite element models (FEM) of the connecting tips under axial compression, the buckling behaviour and critical load ( $P_{cr}$ ) of a simple fixed-free cantilever steel plate is studied. For this validation a rectangular plate is 220 mm tall and the width and thickness are 40 mm and 6 mm respectively is used. The plate is modelled in Abaqus and then the results are compared with the ones calculated by hand.

An elastic eigenvalue buckling analysis is performed in Abaqus using only elastic properties of steel. This properties are shown in Section 5.5.1. For this analysis shell elements S4R are used with a thickness equal to 6 mm. A shell edge load of 1 N magnitude is applied on the top free-edge of the plate. At the bottom nodes all displacements and rotations are set to 0 which will resemble fixed conditions. Figure 5.8 shows the first buckling mode of the steel plate. The eigenvalue for Mode 1 is equal to 194.75 which means that the critical load for this mode is equal to  $P_{cr} = 7790$  N. The analytical calculation can be found on the following equation.

$$P_{cr} = \frac{\pi^2 EI}{(2L)^2} = \frac{\pi^2 (210000 \text{ N/mm}^2) (720 \text{ mm}^4)}{(2 * 220 \text{ mm})^2} = 7790 \text{ N} \quad (5.7)$$

Table 5.9 shows the comparison between the obtained results from the Finite Element Model and the analytical result obtained by calculating the load using equation 5.6.

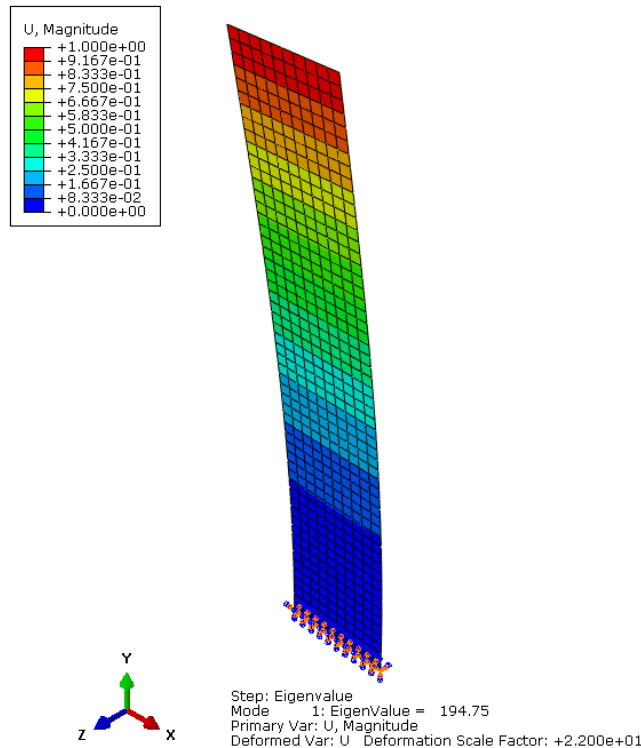


Table 5.8: Fixed-free edges steel plate buckling behaviour.

Euler buclinkg	
Type	Critical load $P_{cr}$ (kN)
FEM	7.79
Hand calculation	7.71

Table 5.9: Euler buckling load comparison.

Once the analytical and numerical results are in the same order of magnitude, the validation is concluded. As presented before, the inserting unit does not have a conventional shape. Therefore, analytical calculations can be difficult to obtain. In this cases the use of Finite Element Models is recommended in order to obtain more accurate results.

Eurocode NEN-EN 1993-1-6 Strength and stability of Shell Structures [47] present guidance to obtain the buckling limit state of steel shell structures. It also specifies the required steps in order to design the shell by global analysis using geometrically and material non-linear analysis with imperfections (GMNIA).

- As first step a linear buckling analysis (LBA) on the perfect structure should be perform to determine the elastic critical buckling load.
- A material non-linear analysis (MNA) should be perform to obtain the plastic buckling load.
- A geometrically and material non-linear analysis (GMNA) should be performed on the perfect structure to determine the elastic-plastic resistance.
- Finally, a geometrically and material non-linear analysis with imperfections (GMNIA) should be performed on the imperfect structure.

At the same section of the Eurocode NEN-EN 1993-1-6 ([47], section 8) it is specified that for a GMNIA an appropriate effect of imperfection could include geometric imperfections and material imperfections. It also mentions that generally, imperfections should be introduced by means of equivalent

imperfections in form of shape deviations of the shell, unless a better technique is used.

Although the inserting unit could be simplified as a shell structure and that a GMNIA analysis procedure could be used in order to obtain the buckling limit state, due to the non-conventional geometry and the mechanism the load is resisted this procedure is partially followed.

First, a linear buckling analysis (Eigenvalue buckling analysis) on the perfect inserting unit based on the design shown in Section 5.7 was performed to predict the buckling load. A distributed load was applied on the resisting surface of the retention block (see Figure 5.19) as shown in Figure 5.38. The buckling shape is presented in Figure 5.39. As expected for such analysis, for a fixed-free steel plate structure the buckling shape resembles Figure 5.37. It was obtained that the buckling load is equal to 40.1 kN.

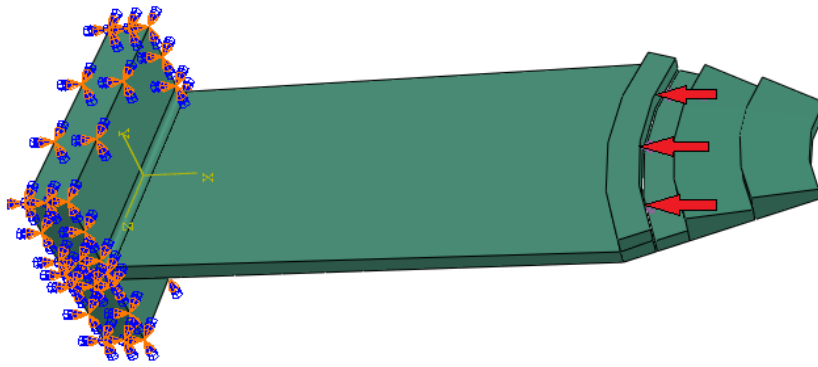


Figure 5.38: Load at the retention block.

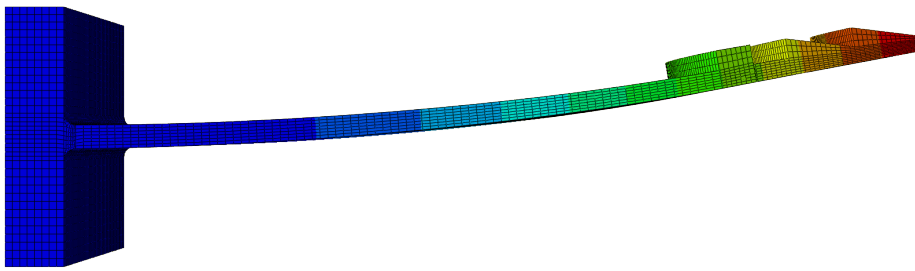


Figure 5.39: Buckling shape.

Once this result is known, the next step is to perform a GMNA FE analysis of the connection at its final connection position. Once the inserting unit is connected to the retaining unit, an axial compressive load of 80 kN is applied on half of the inserting unit. Material non-linearity is used on this analysis. Table 5.10 shows the characteristics used on the FEA.

Figure 5.40 shows connected position and the applied boundary conditions from the inserting and retaining unit. While connected, the contact between the retaining and the inserting unit provides to the joint an additional constraint. This contact in combination with the eccentric load the

fixed-free behaviour (Figure 5.39) of the snap-beam is modified. Figure 5.41 shows the vertical displacement of the inserting unit at the end of the analysis after the load is applied. From this figure is possible to observe that the snap-beam bows close to the tips. This gives an insight about how the new buckling shape will be and what constraints can be found at the end of the inserting unit. The retaining unit will not allow any vertical upwards movement of the inserting unit it due to the contact between the inserting unit tip and the retaining unit, as observed in Figure 5.40. Additionally, the horizontal movement of the tip will be also restricted.

Therefore, based on this description the end of the inserting unit will have similar constraints as a pinned support. Figure 5.41 shows the similarities between the obtained results and a buckling shape for a fixed-pinned strut. This will improve the behavior under compressive loads since the buckling critical load will increase due to the new boundary conditions.

FEA characteristics	
Analysis type	Dynamic, Implicit
Finite element type	3D8R: 8-node linear brick
Duration	1.00 sec
Contact type	Surface-to-surface contact
Material model	See Section 5.5.1
Material properties	Non-linear
Analysis	Force controlled
Applied force	80 kN

Table 5.10: FEA characteristics for axial tensile force.

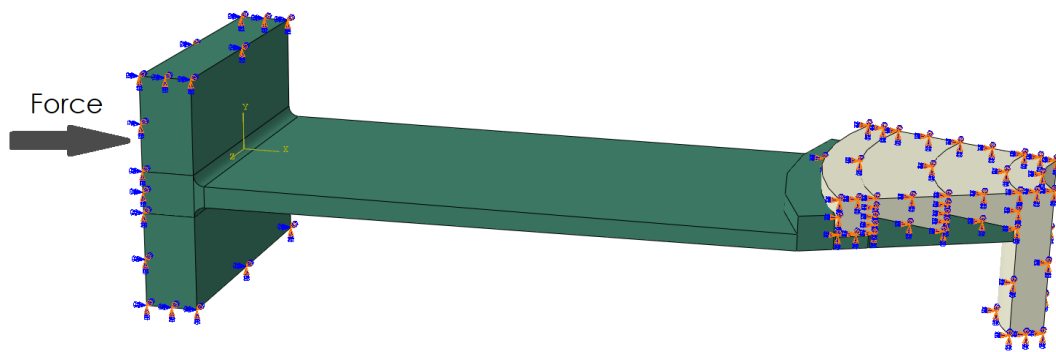
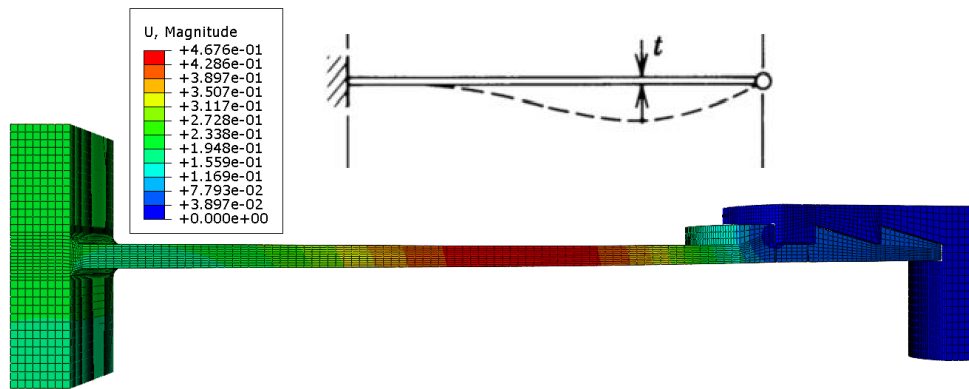


Figure 5.40: FE model of with boundary conditions.



**Figure 5.41:** Resulting vertical displacement after FEA (colored image) and first buckling mode of a fixed-pinned strut [13] (white and black top image).

Figure 5.42 shows the Von Mises stress distribution along the connection. The highest stresses are concentrated along the retaining block of the inserting unit due to the contact pressure between the two units. Two points from the inserting unit have been selected in order to show the mechanical behaviour at those spots. The two points are shown on Figure 5.43a. From that figure is possible to observe that stresses are concentrated both on the outer and inner side of the retaining block-tip.

Figure 5.43b shows the stress-strain relationship at both points. It can be seen that stresses at the inner edge of the block (Point 2) reach higher values than the yielding stress and that the inserting unit has a plastic behaviour at that zone. On the other hand, stresses at the outer zone of the block (Point 1) approximates the yielding strength of the material but does not exceed it.

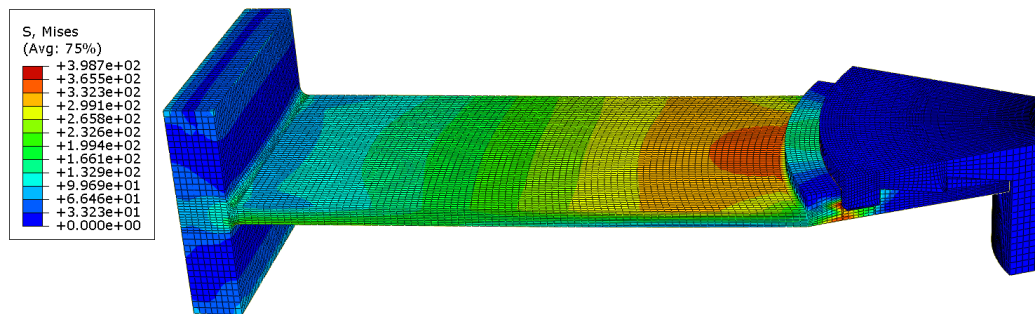


**Figure 5.42:** Von Mises stress distribution of the innovative connection under compressive loading.

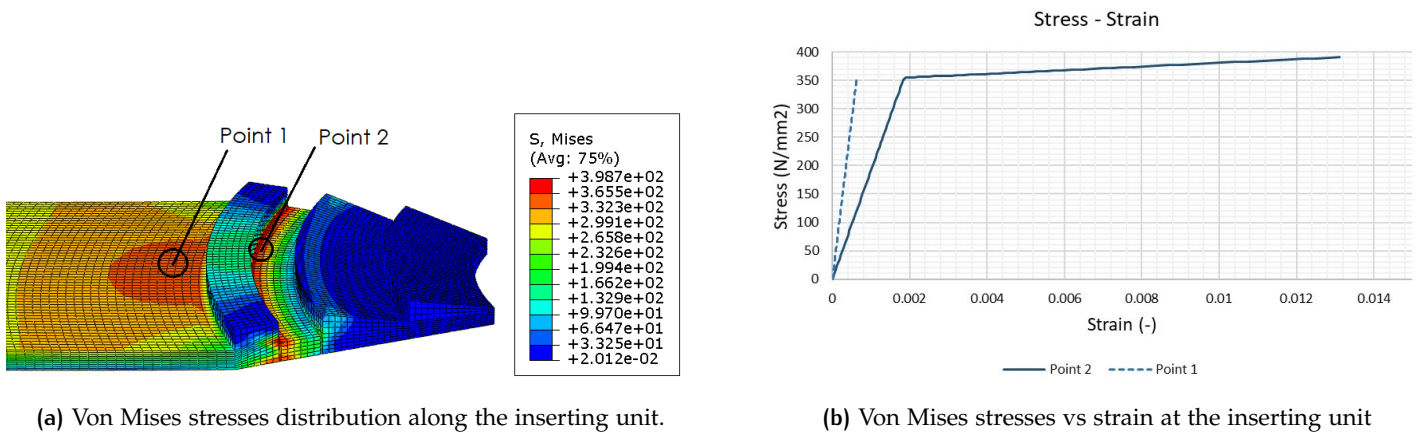


Figure 5.43: Stress-strain behaviour at the tips from the inserting unit.

The following Figure 5.44 presents the relationship between the Von Mises stresses and the applied compressive force of the inserting unit at points shown in Figure 5.43b, and at the retaining unit. It can be observed that yielding appears at Point 2 at a compressive force of 42 kN. Since the inserting unit is composed of two snap-beams, this value must be multiplied by two.

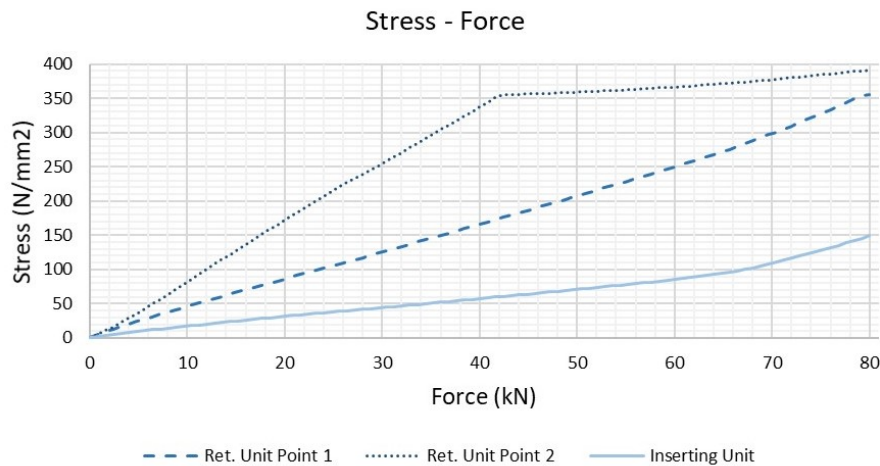
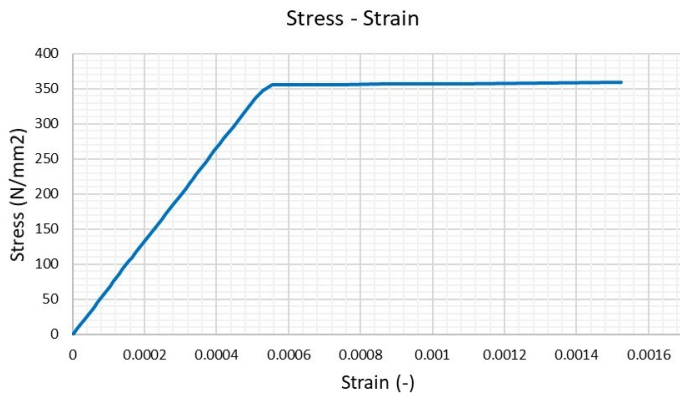


Figure 5.44: Von Mises stresses vs compressive force.

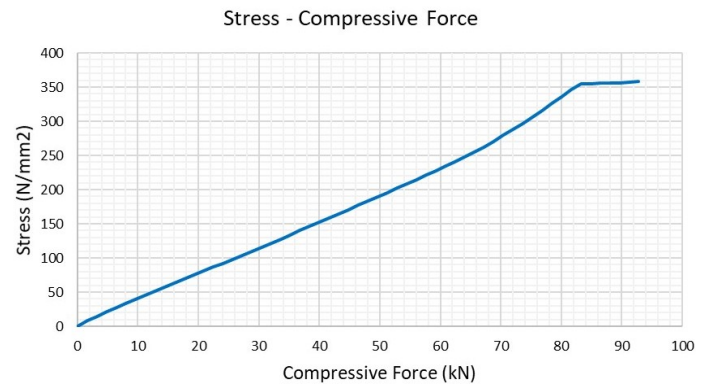
Figures from the strain and stress distribution along the inserting and retaining unit are presented at Annex C, from Figure C.19 to Figure C.21. The stress-strain relationship at a point on the retaining unit is presented on Figure C.22. The fore-displacement graph of a point at the bow of the plate (red zone in Figure 5.41) is presented in Figure 5.47.

Based on the previous information it is not possible to predict what would be the failure load of the joint under the action of compressive forces. Therefore, an additional FE analysis with similar characteristics than Table 5.40 was performed. In this analysis the applied compressive load was increased. Figure 5.45 shows the Von Mises stresses vs the strains at Point 1 (see Figure 5.43a) and the relationship between the stresses and the compressive force at the same point. It is possible to observe that, in comparison to Figure 5.43b,

after a load of around  $85\text{ kN}$  is applied, the steel plate presents a non-linear behavior



(a) Von Mises stresses vs strain at Point 1.



(b) Von Mises stresses vs compressive force.

Figure 5.45: Failure behavior under compressive loads.

Figure C.23 from Annex C represents the Von Mises stresses distribution along the inserting unit when a load of  $92\text{ kN}$  is applied. Figure 5.46 shows the vertical displacement of the unit at the same step. Here it is possible to observe how the inserting unit bows downwards while it buckles.

A point at the bowed side of the unit has been investigated and its behavior is presented in Figure 5.47. It can be seen that at a load of  $90\text{ kN}$  the curve becomes almost horizontal which means that even a small increment of load will generate a large displacement at the plate. At this point the plate starts to buckle and it can be concluded that  $90\text{ kN}$  per inserting plate beam ( $180\text{ kN}$  per tip) is the failure load of the connection.

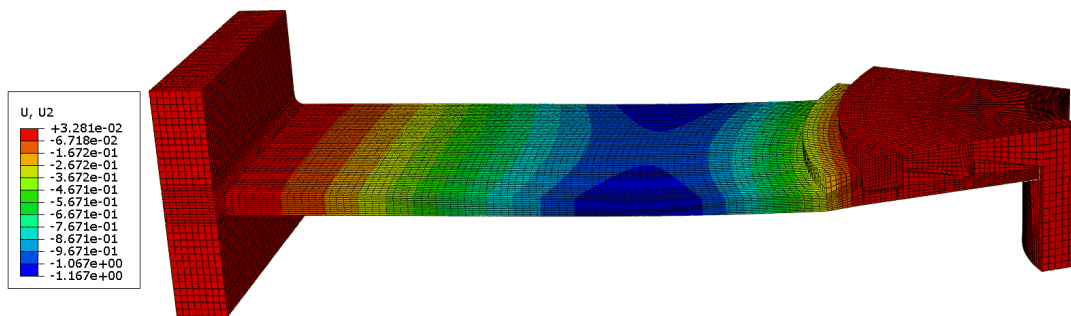


Figure 5.46: Vertical displacement (mm) at a compressive load of  $92\text{ kN}$ .



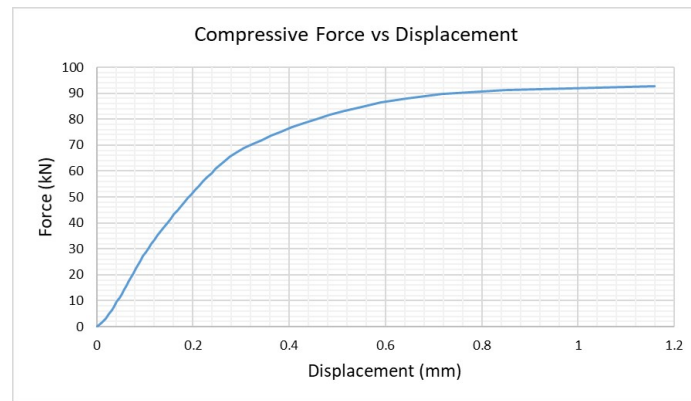


Figure 5.47: Force vs displacement at bowing zone of inserting unit.

## 5.9 CONCLUSION

Due to its high allowable flexibility and resilience, thermoplastics materials are ideal for snap-fit connections. On this research by cause of the large forces the internal forces must bear, steel is used as material for the innovative joint. It is challenging to scale a day-to-day small-scale connecting mechanism to use it as a structural connection on a large-scale application.

The design concept of a innovative connection for an internal node of the optimized truss on this research is developed based on the connectivity principles behind a snap-fit connection. The shape and the geometry of the innovative joint takes into consideration the internal member-configuration. Thanks to its features, it can be used for any internal node even if many members are connected to that node regardless the arrival angle of the members.

Based on the information collected from two preliminary design concepts, the final design concept was obtained. At the current state of art of steel-trusses assembly, it was found that a "manual" insertion mechanism is more suitable for the assembly of the joint. This method reduces any accidental over-loading at one tip of the inserting unit caused by non-fully-straight sliding insertion.

Under normal circumstances (usage phase) the unique shape of the final design concept allows to resist efficiently 110 kN (55 kN per snap-beam) of tensile force and 86 kN (43 kN per snap-beam) of compressive force, without the appearance of yielding stresses nor plastic strains. After this point, yielding starts to appear at the contact edges between the inserting and the retaining unit. Under the action of tensile load, the principal failure mode is yielding of the contact edge, generating a small rotation of the tip of the inserting unit. Whereas under compressive loads, buckling of the steel beam-plate is the main failure mode. It can be concluded that, under the action of compressive loads, 90 kN is the failure load and this is the point when the snap-beam will start to buckle.

The joint can be disassembled using a manual pressing device, based on the same principle of the "manual" insertion.



# 6 | REFLECTION

## 6.1 INTRODUCTION

To successfully achieved innovation it is required more than brainstorming and sketching some ideas. For many different fields, in order to create new product opportunities different steps need to be completed. To develop an innovative structural connection is not an exception. Unfortunately, on this research project not all steps have been fully developed and, before the design concept presented on this research can be used or applied in real engineering practice, additional research is required. On the previous chapters a problematic has been presented and studied, an idea has been developed and the structural behaviour of the innovative joint has been predicted based on FE analyses.

A recapitulation of these first steps are presented on the following section.

## 6.2 FIRST STEPS

### 6.2.1 The challenge

As presented in Chapter 2, connections of steel structures greatly influence the final cost of a structure, being its cost-percentage close to 50% of the final cost. On this cost are included factors such as the erection time needed to assemble a structure, the fabrication costs and design. Additionally, structures are usually design with spare capacity, which opens room for optimization procedures.

On this research project, as presented in Section 4.2, layout optimization was performed on a case-study truss structure. As a result from the optimization process a truss structure arranged with non-conventional members and node geometrical configuration was obtained. Realizing such connections using conventional joining technologies, such as bolted or welded connection, could represent a high cost for the constructor and the client.

The main challenge of this research was to develop a innovative design concept for an internal node of the optimized truss structure that improves the assembly time and allows any truss geometrical configuration to be built.

### 6.2.2 Idea generation

Once the problematic and the challenge are identified, an idea that fits the purposes needs to be developed. Based on this, snap-fit joining principle was found to be suitable for the required applications. This connecting mechanism is both, efficient resisting axial forces presented on truss structures and is a simple way of connecting elements together. Despite such connections

are commonly used for small applications to connect two plastic elements together, on this research an exploratory study to investigate the applicability of such connections as structural connections for the internal steel nodes of optimized steel trusses is presented.

### 6.2.3 Developing concepts

After a layout optimization is applied on a framed-structure the resulting optimized structure will probably have a non-conventional geometrical configuration of elements and nodes. This means that, as it was shown on Section 4.4, to one internal node different members can be connected at diverse arrival angles (see Figure 4.15). Based on this fact and knowing that the connecting principle is based on a cantilever snap-fit connection, a final design concept was developed (see Section 5.7). The final design was created by gathering information and strengths from two initial design concepts presented in Section 5.6.

### 6.2.4 Analyzing the concepts

Once the final design concept is developed, it is required to be tested. Different type of testing are required depending on the final goals of the project. On this research project extensive finite element (FE) analyses were carried out on the innovative joint in order to predict the structural behavior under the nodal forces obtained from the structural analysis of the optimized truss. The behavior of the joint under such forces was analysed for three phases: Assembly phase, usage phase and disassembly phase. This can be found in Section 5.8.

The most important assumptions for all FE analyses are presented below:

#### *Assumptions for the FE analyses*

- All analyses were done with a perfect structure.
- No imperfections were considered at the FE buckling analyses.
- The required load (as force or displacement) is applied at the centroidal axis of the inserting unit.
- On all FE analyses the retaining unit was modelled with all of its degrees of freedom constrained.

### 6.2.5 Final result

Figure 6.1 presents a part of the final optimized truss. It can be observed how the different steel members are connected to the internal node. It also shows the real dimension of the members compared to the innovative node.

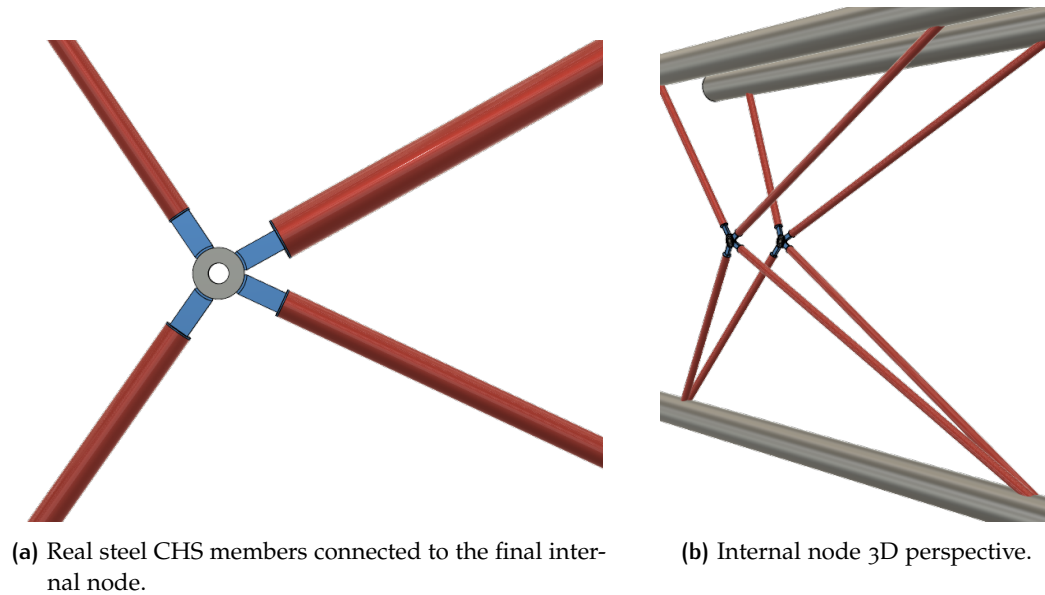


Figure 6.1: Optimized truss 3D assembly process.

## 6.3 NEXT STEPS

The steps developed on this project represent an important progress to the innovation process. Although a solid design concept was developed and the structural behaviour of the innovative joint under the action of real nodal forces was studied and predicted, further investigation must be carried out. Unfortunately due to time constraints, no laboratory testings were performed during this research project. Additionally, manufacturing of the steel units, connection between the joint and the members and finally, the total assembly of the truss are important steps to consider.

This last required steps, that have not been addressed yet on this report, are briefly discussed on this section:

### 6.3.1 Results validation

The results obtained from the FE analysis accomplished on this report are required to be validated. This can be done by manufacturing a real-scale innovative joint and setting up a laboratory test from which both results can be compared. Figure 6.2 shows the required steps in order to verify and validate a FE model. The computational model must be accompanied by the available codes and verified by analytical calculations. Eurocode must be used and followed on all stages of the validation procedure. Additional to this, the out-of-plane behaviour of the internal node must be studied and the rotational capacity of the whole joint must be examined.

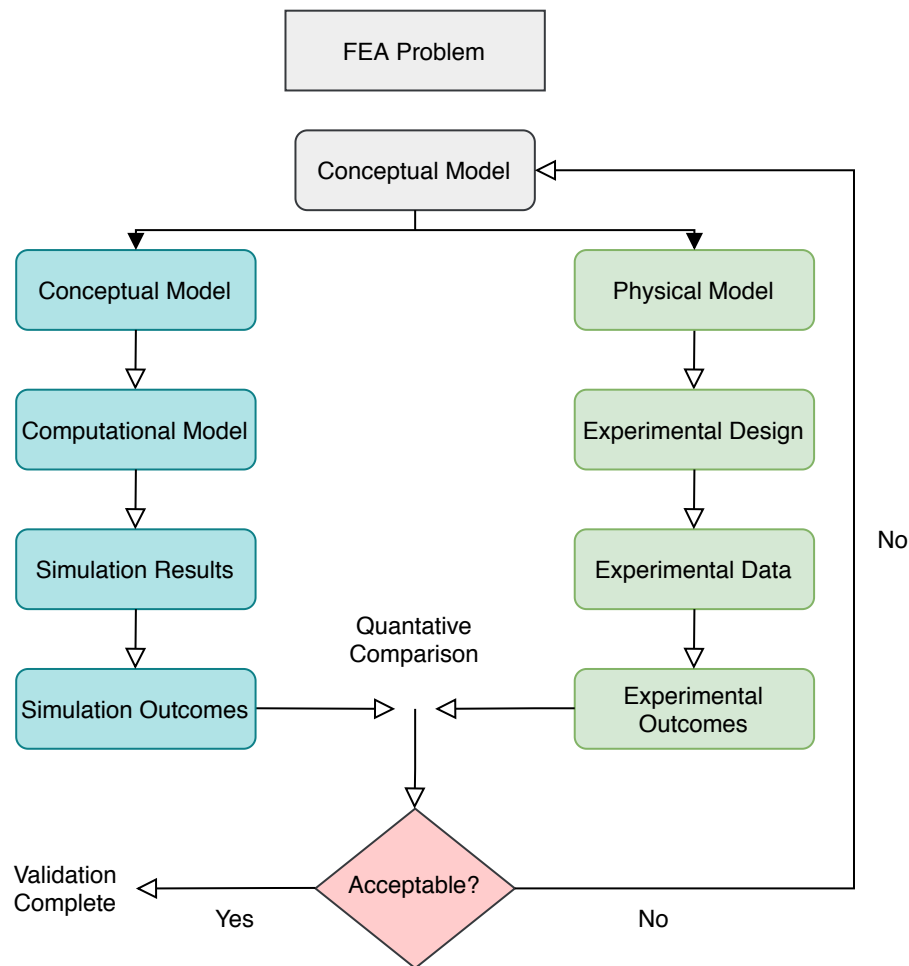


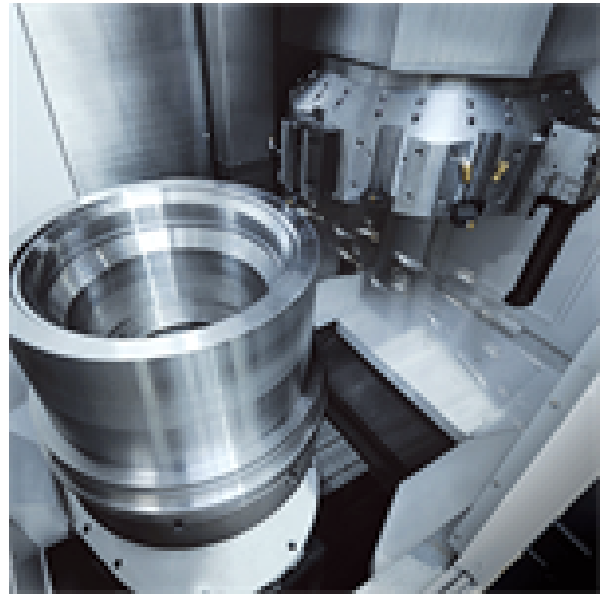
Figure 6.2: FEA validation procedure.

### 6.3.2 Manufacturing

The final design concept presented on the previous section does not have a conventional shape and the geometry of both, the inserting and retaining unit, is composed of lines with various angles and lengths. Manufacturing of this elements could be challenging and expensive when using conventional ways, such as casting. Furthermore, the designed connection will require high manufacturing precision in order to work properly. The interlocking between the two connecting units plays a crucial role in the correct load transferring at the node. A small deviation in dimensions during manufacturing could imply a significant decrease of the node efficiency. For this reasons, it is required to have accurate precision during the manufacturing process. Considering the precision that is required, the used material for the connection and the non-conventional shape of it, computer numerical control (CNC) milling is the most suitable manufacturing process for both units.



(a) CNC milling machine.



(b) CNC turning machine.

Figure 6.3: CNC milling machine during operation [14].

Computer numerical control (CNC) process automates the machine movements using a programmed code that gives instructions for precise movements. This accurate movements provide the ability to fabricate complex parts through the precise control of specialized tools. CNC machines can eliminate human error and achieve accuracy within  $0.0005\text{ in.}$  In combination with its versatility any imaginable shape can be created. Two different methods are usually used to transform raw material into a finished model. This methods work either by adding (additive) or removing (subtractive) material. 3D printing and CNC milling are examples of adding and removing material, respectively [48].

The milling process can be described as the cutting and drilling of a specific material such as wood or metal. A milling machine has the ability to cut in different angles and can move along different axes. The cutting capacity of the machine will depend on the degrees of freedom to which the movement is restricted. A milling machine could have 2-axis of movement to 5-axis of movement. This last one is the most complete and incorporates rotation in both x- and y- axes. Figure 6.3 presents a 5-axis CNC milling machine during functioning.

A CNC milling machine is machine that employs computerized controls and rotating multi-point cutting tools to remove material form a raw piece of material until the desired shape is obtained. The process can be defined broadly in four steps [49]:

- Designing a CAD model
- Converting CAD model into a CNC program
- Setting up the CNC machine
- Executing the milling operation

The inserting unit (see Figure 5.20) could successfully be manufactured using a CNC milling machine, shown in Figure 6.3a, and a CNC turning machine, presented in Figure 6.3b, can be used efficiently to manufacture the retaining unit (see figure 5.19).

### 6.3.3 Assembly

Until this point, important factors regarding to the design of the innovative joint have been studied in depth in Chapter 5, such as the final shape and its structural behaviour during the proposed three phases. By now it is clear that the assembly and disassembly of the node is achieved by introducing the inserting units of the steel members (steel circular hollow sections) into the retaining unit, and together form the connection. The complete assembly of the optimized truss presented on this report in Section 4.4 will be discussed on this section.

Steel trusses can be assembled in different ways. Depending on the size and complexity of the truss it can be assembled on site or at the workshop [16]. In most cases, the internal members of a truss are connected directly to the top and bottom chord of it. This facilitates the assembly since the joints will be located only at the top and bottom chord. As shown in Figure 4.15, the optimized steel truss developed in this research project has nodes both at top and bottom chord and has also internal nodes. From the same figure it is possible to observe that the internal configuration of members form a triangulated distribution. Although this configuration is not conventional, thanks to the concept behind the innovative joint proposed in this research, the assembly of this truss can take advantage of this triangulated structure. Optimized trusses could be assembled in parts and the circular shape of the retaining unit (Figure 5.6) makes possible to connect different members at different arrival angles.

On this research project an assembly procedure of the optimized steel truss is proposed based on the capabilities and principles of the innovative joint (see Section 5.3). Figure 6.4 shows the proposed assembly procedure for a planar truss (in 2D), which consists on dividing the optimized truss into smaller sections and then connecting them together. By dividing the truss into smaller sections, and then dividing them into a top and bottom section, as shown in Figure 6.4a, 6.4b and Figure 6.4c, a snap assemble can be achieved by connecting the upper and bottom part through the retaining unit, which is represented in red color in the figures. The round and serrated shape of the retaining unit plates will allow any inserting unit, that is attached to steel member, to be connected to each other using the snap-fit principle. This connecting procedure could decrease the truss assembly time since parts could be manufactured at workshops and they will be small enough in order to be transported by trucks to the construction site. Once at the construction site, the parts can be put together and the top and bottom chord can be connected, finalizing the assembly of the optimized truss.

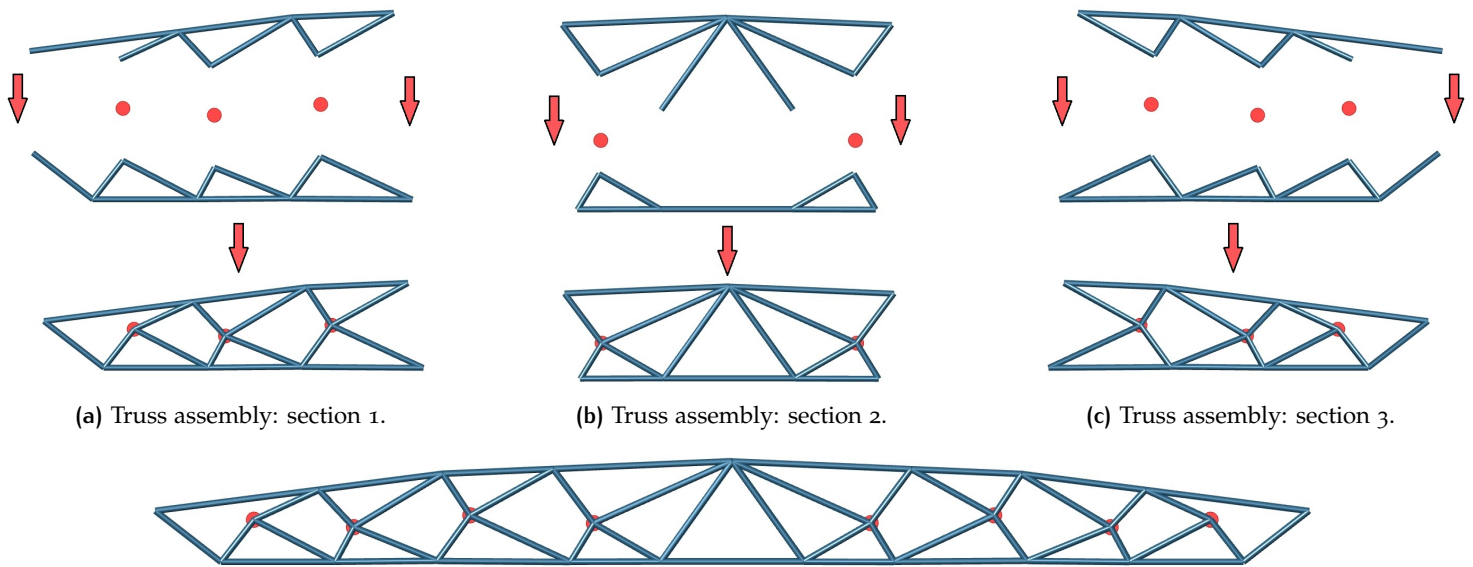


Figure 6.4: Optimized truss 2D assembly process.

Based on the proposed assembly procedure, on a 2D-truss all internal members will be connected vertically, in the same plane, to the innovative joint. Therefore, the snap-fit connecting principle will work efficiently and the inserting units can be inserted into the retaining unit. However, on non-planar trusses, such as 3D-trusses or V-shaped trusses, the employment of this principle might not be equally efficient.

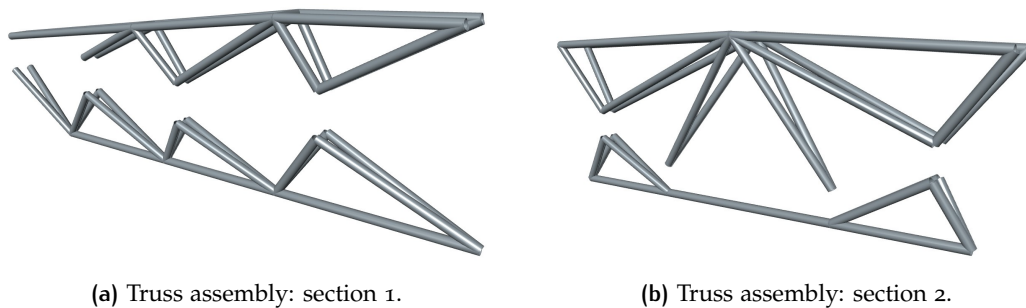


Figure 6.5: Optimized truss 3D assembly process.

Figure 6.5 shows how the sectioning of the whole truss can be applied on the V-shaped optimized truss for its further assembly. It is possible to observe that the internal members are tilted and have a small angle from the vertical plane. This will hinder the assembly of the truss using the snap-fit principle as connecting mechanism for the internal joints. Since the members-planes are slightly tilted, which forms the V-shape of the truss, in order to allow a correct assembly the retaining unit must be located at the same plane. This implies that an external aid must be used to keep the retaining unit into position while the truss is being assembled. This might be a difficult task to accomplish.

Considering that the V-shaped truss is symmetrical respect to a vertical longitudinal plane, the assembly of the V-shaped optimized truss can be



improved by connecting the retaining units from both planes. This will not only enhance the assembly procedure of the truss, but also improve the out-of-plane behaviour of the internal nodes. Figure 6.6 shows how this modification could improve the assembly of the optimized truss.

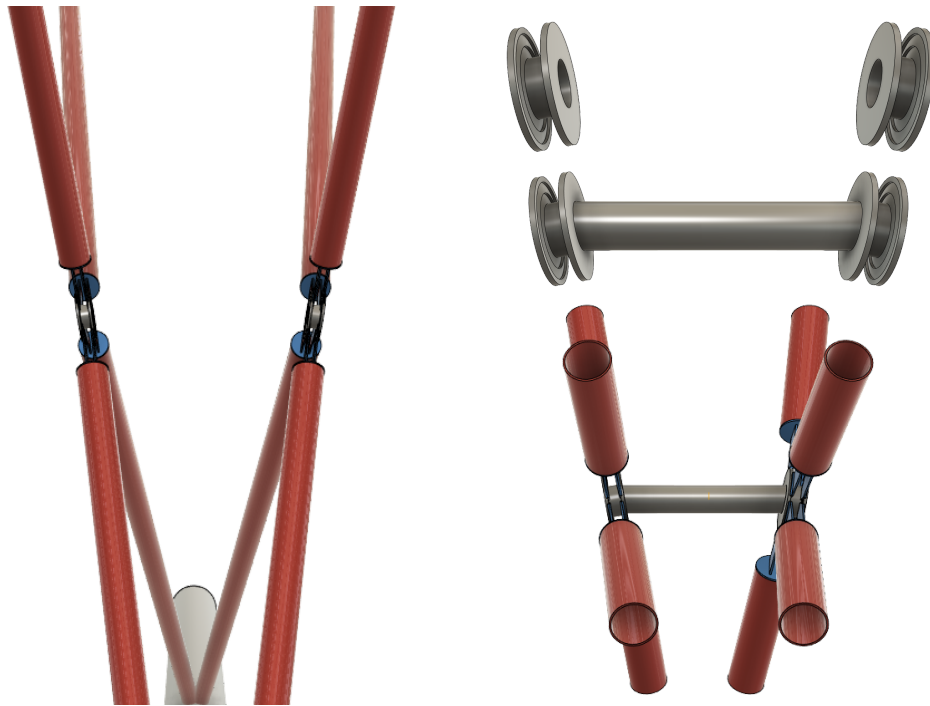


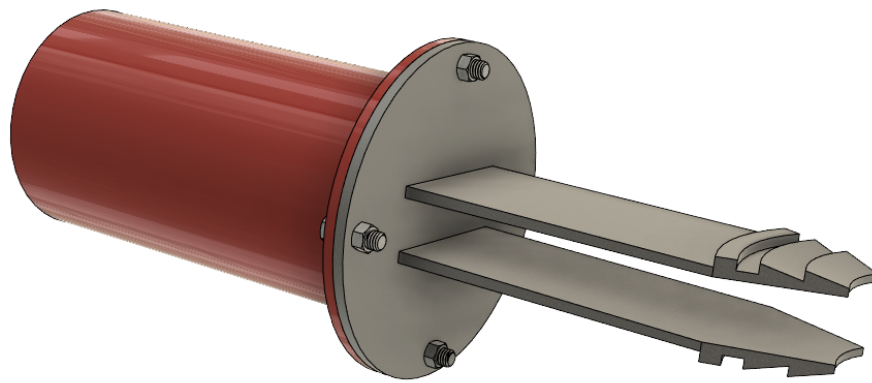
Figure 6.6: Assembly of the V-shaped optimized truss.

Nowadays, the use of robots during manufacturing and assembly of structures is becoming more and more popular. This aims to decrease the erection time and to eliminate dangerous erection practices by reducing human assistance during construction [50]. The robotic aid to assemble truss structures could be a reality in the near future, as presented in Section 2.2.4, which could be applied on the assembly of the optimized truss presented on this research in Figure 6.4.

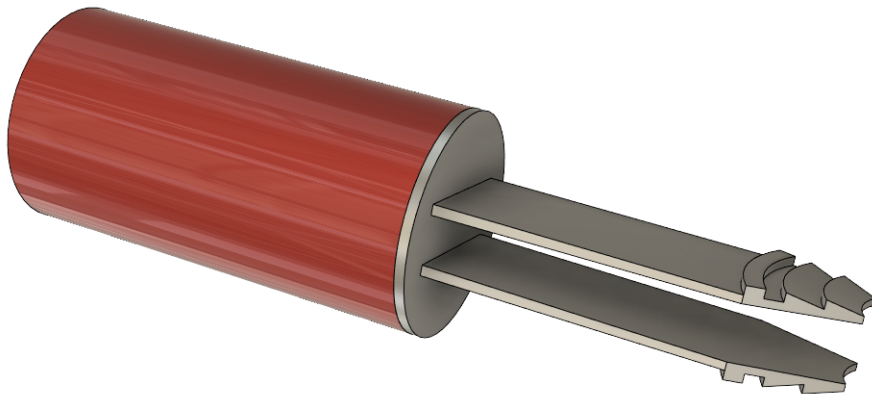
#### 6.3.4 Member - Tip connection

How the inserting unit and the steel member are connected has not been addressed yet on this report. The connection between both elements needs to be strong enough to allow load-transfer without experience any damage. Although the connection between these two components has not been calculated, two conventional connecting procedures are proposed:





(a) Bolted connection



(b) Welded connection

Figure 6.7: Possible connections between the inserting unit and the steel member.

- **Bolted connection:** a circular flange connection could be used to connect the base-plate of the inserting unit with the steel tubular member. This type of connection is very efficient and provides easy and fast installation [51]. This connection will be design for tensile forces only. Besides the ease of installation, with this type of connection the inserting unit could be replaced easily in case of damage or other requirements.
- **Welded connection:** both elements can be connected by welding them together. A fillet weld all round the section is an easy way to connect steel parts, although it disables the disassembly possibility of the tip in case of damage.

Both connecting types can be calculated following the guidelines presented in Eurocode EN 1993-1-8.

## 6.4 CONCLUSION

This innovative connection-concept could be applied at any structure as long as only axial tensile and axial compressive forces are required to resist. Thanks to the unique geometry of the innovative joint, a truss composed of almost any internal geometrical configuration of members could be realised.

Despite the steps developed on this research project are an important progress to the innovation process, additional steps are required. Before this concept can be brought to real practice, validation of the numerical results are required. In addition, it is necessary to the study the manufacturing of the nodes and the general assembly of the optimized truss.

## Part IV

### CONCLUSION & RECOMMENDATIONS

# 7 | CONCLUSION AND DISCUSSION

## 7.1 INTRODUCTION

Based on the results obtained in this research project, this chapter presents conclusions, recommendations and a discussion for future research concerned with the following research question:

---

*How can innovative snap-fit joints help with the implementation of optimized steel trusses in the real engineering practice?*

---

The main research question can now be answered:

The innovative concept design will allow optimized trusses with non-conventional internal nodes and member configurations to be built and used in real engineering practice. The connecting principle based on snap-fitting elements can be implemented on larger scale connections such as structural truss internal joints. Thanks to the non-welded and non-bolted joining technology the innovative connection has, the assembly time could decrease significantly reducing the cost for both the constructor and the client. Additionally, all internal nodes have the same shape which will reduce the manufacturing cost. Nowadays, manufacturing techniques that could be used for the manufacturing of the innovative joint, such as CNC machining techniques, are available and widely used.

## 7.2 CONCLUSIONS

### Part II: Structural design and optimization

- The two-step optimization approach used on this research, in which as starting point the layout with the least possible weight is obtained and then this benchmark is rationalized, was found to be efficient finding an optimized layout that has a good balance between complexity and material efficiency use.
- Layout optimization procedure on steel trusses was found to be more efficient when the structural design is controlled by the stiffness and not by the strength of the structure.
- The engineering optimization-tool Peregrine is useful generating an optimal layout but not to perform a structural design of the resulting

optimized frame structure. For that, a more suitable structural engineering software is required.

- It is very likely that once a layout optimization procedure is applied on a truss structure, internal nodes, that are not neither at the bottom and top chord, will be generated. When truss members are connected to these internal nodes and not to the top or bottom chord, additional checks for the out-of-plane behaviour of the internal nodes should be performed.
- The Wimbledon court No.1 Roof truss was found to be a good example to demonstrate how a structure that is already properly design and that is aesthetically pleasant can be further optimized achieving considerable weight reduction without compromising its functionality.

### Part III: Innovative connection

- Although the shape of Design Concept 1 improves the design tensile and compressive strength of the inserting unit, the deflection is controlled by the vertical plates. Due to the allowable strain properties of steel, achieving the required deflections is not possible without damage. Additionally, the fuse behaviour of the perforation might hinder the insertion of the tip.
- From Design Concept 2 can be concluded that when the joint is connected, tensile forces are not evenly distributed along the tips of the inserting unit. The tip closer to the base carries the most of the load which demonstrate that the use of more than two tips for resisting axial tensile forces is not necessary.
- The final design concept (Design Concept 3) gathers the strengths from the previous design concepts presented on this report.
- The required force (1500 N) to introduce the inserting unit using sliding inserting method can not applied by human hands. Therefore, another mechanism should be used. Additionally, the insertion requires to be performed at a straight movement which demands for great precision. It is expected that in the near future the use of human exoskeletons or robots in constructions will be more common, aiding this task. For now, the proposed manual inserting mechanism is a viable solution.
- While connected and when exposed to axial tensile forces, the joint has a favorable behaviour until 110 kN (two times 55 kN) are applied. After this point, yielding stresses appear at the contact points which generates a small rotation of the inserting unit tips.
- While connected and when exposed to axial compressive forces, the joint has a favorable behaviour until 84 kN (two times 42 kN) are applied. After this point, yielding stresses appear at the contact points in the inserting unit which generates the steel beam-plate to start to buckle.

- It was found that the failure load of the innovative joint under compressive forces is 180 *kN* (90 *kN* per snap-beam).
- It was found that tolerances are required for a correct functioning of the node, specially for the assembly phase of the connection. On the FE models this tolerances are considered and allow a correct assembly and interlocking between the inserting and the retaining unit. Tolerances must consider also small manufacturing errors and creep of steel.
- On this research it was demonstrated that steel can be used for snap-fitting two elements if the insertion phase is performed within elastic range of steel and that snap-fit principle was applied successfully on a large scale connection.
- The snap-fit connecting principle can be used efficiently when assembly a 2D truss. For a V-shaped truss (3D truss) the retaining unit needs to be placed at the same plane of the internal members, which might difficult the truss assembly. Connecting the retaining units from both planes, as shown on this report, will improve the assembly procedure for the V-shaped optimized truss. Additionally, the internal nodes out of plane behavior can be favored.
- Although snap-fit connections are usually design to resist tensile forces only, it was demonstrated that compressive forces can be also taken by adding a resisting block.

## 7.3 DISCUSSION

**Methodology:** The assumptions made in this report due to lack of information regarding to the structural design of the case-study truss might affect its structural design results. Based on the literature, it is know that the original Wimbledon truss weights 93 *tons* whereas the recreated truss on this report weights around 85 *tons*. Although the difference is not negligible, it does not affect the final outcome of this research project.

**Finite element models:** On all FE analyses the retaining unit was modelled with all of its degrees of freedom constrained. This does not represent its real behaviour since during real practice the top a bottom plate of the retaining unit will behave as a short-lever arm cantilever plate. This can be solved by using a fixing-block that connects both retaining unit plates at three or four points at the outer border of the steel plates.

**Applicability:** In order to be applicable, it is required that the top and bottom chord of the steel truss are composed of continuous elements. Otherwise, the total stiffness of the truss will decrease and the innovative joints will not operate as expected.

## 7.4 RECOMMENDATIONS

The recommendations provide a framework for future research on innovative structural connections for frame structures, such as steel trusses, that are based on the snap-fitting principle.

### General recommendations

It would be recommended to:

- Test the behaviour of the node when loads perpendicular to the centroidal axis of the innovate joint are applied.
- Perform technical, economical and value assessments. This report was mainly focused on the technical aspects of the design, based on its structural engineering behavior. Although some aspects such as manufacture and assembly of the optimized truss were briefly addressed, it is important to pay attention to the viability of the concept and a viability study should be performed.
- Conduct mechanical test to validate the Finite Element models. Additionally, FE models can be improved and more accurate results can be obtained by using the true stress-strain material properties that are determined by a coupon test.
- Based on snap-fit connections principle, develop a design concept for all nodes located at the top and bottom chord of the truss. On this research the innovative design concept was developed for the internal nodes only. No design concepts were developed for the nodes located at the top and bottom chord. If not possible, conventional connections such as bolted connections can be used for such nodes.

### Abaqus users

It would be recommended to:

- Spend the necessary time while meshing the FE model in order to obtain a structured meshing. This will improve significantly the required computational time while running the FEA. The required computational time is directly related to the smaller finite element. Furthermore, a finer mesh should be used in surfaces that are in contact with each other.
- Use dynamic steps (either dynamic implicit or dynamic explicit steps) to solve convergence problems in FEA on non-linear problems. It was found to be an efficient strategy. Since effects of inertial forces are considered in the model, the chance of convergence increases.

### Engineers and designers

It would be recommended to:

- Increase the use of optimization procedures during the design phase of any structural design. Material savings and hence costs reductions can be obtained when optimization procedures are applied.
- Consider the use of snap-fit connections as joints for structures that are subjected to tensile and compressive forces, such as truss structures. This joining technology could allow improvements on labour costs and a faster erection process.
- Verify the results obtained from the numerical models. It is highly recommended to use analytical calculations and rules of thumbs after a FE model is performed. Simplified analytical calculations can provide a first result approximation. In this way it is possible to know if the final outcome of a FE model is in good order
- Foster the dialogue with universities, clients and investors in order to develop a prototype to verify the applicability of snap-fit joints into real scale structural connections.

## 7.5 FUTURE OUTLINE AND RESEARCH

Before this innovative connection can be realised in real engineering practice and be used in truss structures, different steps will be required. Although some of the required steps have been presented and discussed briefly on this research project, future studies are required.

The next step within the research topic is investigating and validating the results obtained from the numerical models by developing a prototype and setting up a test in which the results can be compared and validated. Within this step, safety requirement needs to be proven and safety goals need be achieved.

Additionally, some general recommendations are presented below:

- Investigate the out-of-plane behavior of internal nodes of optimized layouts.
- Calibrate the computer material models by performing laboratory tests.
- Prove the feasibility of manufacturing this connection by implementing CNC machining or 3D printing.
- Extensive cost analysis of the manufacturing of the innovative joint.
- Extensive erection-time analysis of the assembly of an optimized truss using the innovative connections developed on this research.
- Comparison between costs and erection-time between an optimized truss composed of convectional connections and one with innovative connections.



## BIBLIOGRAPHY

- [1] H. Fairclough, M. Gilbert, C. Thirion, A. Tyas, and P. Winslow, "Optimisation-driven conceptual design : case study of a large transfer truss," *The Structural Engineer*, pp. 20–26, 2019. [Online]. Available: <http://eprints.whiterose.ac.uk/154501/>
- [2] T. Steel, "Hollow sections: For structural and mechanical application," ., 2013. [Online]. Available: [www.tatasteel.com](http://www.tatasteel.com)
- [3] E. Zurich, "Robotic collaboration in timber construction," ., no. March, pp. 1–3, 2018.
- [4] Gardiner&Theobald, TATA-Steel, and BCSA, "Steel insight - cost planning through design stages," *Steel Insight*, no. January, 2012. [Online]. Available: [www.steelconstruction.org](http://www.steelconstruction.org)
- [5] F. S. K. Bijlaard and J. W. P. M. Brekelmans, "Plug and play type joints in steel and steel – concrete composite constructions : Development guide and design considerations," *The IES Journal Part A : Civil & Structural Engineering*, pp. 37–41, 2008. [Online]. Available: <http://dx.doi.org/10.1080/19373260802228626>
- [6] J. Farkas, "Structural optimization as a harmony of design, fabrication and economy," *Structural and Multidisciplinary Optimization* 30, pp. 66–75, 2005.
- [7] W. Prager, "Optimal layout of trusses with finite numbers of joints." *journal of the Mechanics and Physics of Solids*, vol. 26, no. May, pp. 241–250, 1978.
- [8] Basf, *Snap-Fit Design Manual*. O-Basf, 2007.
- [9] P. R. Bonenberger, *The First Snap-Fit Handbook*, 2nd ed. Hanser, 2005.
- [10] M. J. Throughton, *Handbook of plastics joining : a practical guide*, 2nd ed. Oxford: William Andrew Inc, 2008, ch. Mechanical Fastening, pp. 175–201.
- [11] SCX, "Wimbledon centre court retractable roof," 2017. [Online]. Available: <https://scxspecialprojects.co.uk/case-studies/wimbledon-centre-court-retractable-roof>
- [12] M. Gambhir, *Stability Analysis and Design of Structures*, 1st ed. Springer, 5 2004.
- [13] R. D. Ziemian, *Guide to Stability Design Criteria for Metal Structures*, 6th ed. JOHN WILEY SONS, INC., 2 2010. [Online]. Available: <https://www.wiley.com/en-us/Guide+to+Stability+Design+Criteria+for+Metal+Structures%2C+6th+Edition-p-9780470549087>

- [14] Mazak. Cnc turning. [Online]. Available: <https://english.mazak.jp/machines/process/cnc-turning/>
- [15] E. Zamperini, "Timber trusses in italy: the progressive prevailing of open-joint over closed-joint trusses," *5th International Congress on Construction History*, 2015. [Online]. Available: [https://www.researchgate.net/publication/278036950-Timber\\_trusses\\_in\\_Italy\\_the\\_progressive\\_prevaling\\_of\\_open-joint\\_over\\_closed-joint\\_trusses](https://www.researchgate.net/publication/278036950-Timber_trusses_in_Italy_the_progressive_prevaling_of_open-joint_over_closed-joint_trusses)
- [16] SteelConstruction.info, "Trusses," 2016. [Online]. Available: [https://www.steelconstruction.info/Trusses{#}Types{\\_-}of{\\_-}trusses](https://www.steelconstruction.info/Trusses{#}Types{_-}of{_-}trusses)
- [17] M. Muir C. and A. Julian M., "Utilization of structural steel in buildings," *Proceedings of the royal society A*, no. 2014.0170, pp. 1–14, 2014.
- [18] R. van Mellaert, "Optimal design of steel structures according to the eurocodes using mixed-integer linear programming methods," Ph.D. dissertation, KU LEUVEN, 7 2017.
- [19] Bayer, "Snap-fit joints for plastic: a design guide," *Bayer MaterialScience*, 2013.
- [20] CEN, "Eurocode 3: Design of steel structures - part 1-8: Design of joints," *Eurocode*, vol. 1, no. 2005, 2011.
- [21] V. S. Group, "Msi," 2014. [Online]. Available: <https://www.voortman.net/en/products/solutions/msi>
- [22] R. Ajouz, "Optimising production costs of steel trusses optimising production costs of steel trusses a computational approach of designing cost-effective," Ph.D. dissertation, 2018.
- [23] C. Gibbons, "Economic steelwork design," *The Structural Engineer* 73, no. 15, pp. 1–4, 1995.
- [24] G. N. Vanderplaats, "Structural optimization—past, present, and future," *AIAA Journal*, vol. 20, no. 7, pp. 992–1000, 1982. [Online]. Available: <https://doi.org/10.2514/3.51158>
- [25] R. Van Mellaert, K. Mela, T. Tiainen, M. Heinisuo, and G. Lombaert, "Discrete sizing optimization of trussed steel portal frames according to eurocode 3," *c/e papers 1 (2017)*, vol. 1, no. 2, pp. 3990–3999, 2017. [Online]. Available: <https://doi.org/10.1002/cepa.455>
- [26] W. Dorn, R. Gomory, and M. Greenberg, "Automatic design of optimal structures," *Journal de Mecanique* 3, pp. 25–52, 1964.
- [27] A. G. Weldeyesus, J. Gondzio, L. He, M. Gilbert, P. Shepherd, and A. Tyas, "Adaptive solution of truss layout optimization problems with global stability constraints," *Structural and Multidisciplinary Optimization*, pp. 25–52, 2019. [Online]. Available: <https://doi.org/10.1007/s00158-019-02312-9>

- [28] H. Fairclough and M. Gilbert, "Layout optimization of simplified trusses using mixed integer linear programming with runtime generation of constraints," *Structural and Multidisciplinary Optimization*, pp. 25–52, 2020. [Online]. Available: <https://doi.org/10.1007/s00158-019-02449-7>
- [29] L. L. Beghini, J. Carrion, A. Beghini, A. Mazurek, and W. F. Baker, "Structural optimization using graphic statics," *Structural and Multidisciplinary Optimization*, 2013. [Online]. Available: [https://architecture.mit.edu/sites/architecture.mit.edu/files/attachments/lecture/StructuralOptUsingGraphicStatics\\_r.pdf](https://architecture.mit.edu/sites/architecture.mit.edu/files/attachments/lecture/StructuralOptUsingGraphicStatics_r.pdf)
- [30] A. Michell and M. Melbourne, "Lviii. the limits of economy of material in frame-structures," *The London, Edinburgh, and Dublin Philosophical Magazine and Journal of Science*, vol. 8, no. 47, pp. 589–597, 1904. [Online]. Available: <https://doi.org/10.1080/14786440409463229>
- [31] MOOG, "Electrical motion control retractable roof," ., vol. 2, p. 2, 2012. [Online]. Available: [www.moog.co.uk](http://www.moog.co.uk)
- [32] Severfield, "Wimbledon no . 1 court retractable roof," 2019.
- [33] M. Lacey and ANSYS, "Win , set and match at wimbledon," ., p. 2010, 2010.
- [34] EN 1992-1-1 Eurocode 1: Actions on structures - Part 1-4: General actions - Wind actions, EN. Brussels: CEN, 2005.
- [35] CEN, "Eurocode 1: Actions on structures – part 1–3: General actions – snow loads," *Eurocode*, vol. 3, no. 2003, 2011.
- [36] T. P. Kelmartin, "A new membrane material for fabric structures frankfurt am main," ., no. April, pp. 1–11, 2003.
- [37] S. Krenk and J. Høgsberg, *Truss Structures*. Dordrecht: Springer Netherlands, 2013, pp. 39–89. [Online]. Available: [https://doi.org/10.1007/978-94-007-6113-1\\_2](https://doi.org/10.1007/978-94-007-6113-1_2)
- [38] C. Preisinger, "Linking structure and parametric geometry," *Architectural Design*, 2013. [Online]. Available: <https://manual.karamba3d.com/>
- [39] T. Zegard and G. H. Paulino, "Grand - ground structure based topology optimization for arbitrary 2d domain using matlab," *Structural and Multidisciplinary Optimization*, vol. 50, pp. 861–882, 2014. [Online]. Available: <https://link.springer.com/article/10.1007/s00158-014-1085-z>
- [40] H. L., P. T., G. M., and L. h., *Peregrine User Manual*, LimitState Limited, 2019, sheffield.
- [41] W. F. Baker, A. Mazurek, and A. Beghini, "Applications of structural optimization in architectural design," *Research Gate*, 2012. [Online]. Available:

[https://www.researchgate.net/publication/268589888\\_Applications\\_of\\_Structural\\_Optimization\\_in\\_Architectural\\_Design/citations](https://www.researchgate.net/publication/268589888_Applications_of_Structural_Optimization_in_Architectural_Design/citations)

- [42] W. F. Baker, L. L. Beghini, A. Mazurek, J. Carrion, and A. Beghini, "Structural innovation: Combining classic theories with new technologies," *Engineering Journal (New York)*, vol. 52(3), pp. 203–217, 2015. [Online]. Available: <https://www.aisc.org/globalassets/aisc/awards/tr-higgins/past-winners/structural-innovation--combining-classic-theories-with-new-technologies.pdf>
- [43] T. Spahr, "Snap-fits for assembly and disassembly," *TICONA*, 1991. [Online]. Available: [http://www.gotstogo.com/misc/engineering-info/Snap\\_Fitsres72dpi.PDF](http://www.gotstogo.com/misc/engineering-info/Snap_Fitsres72dpi.PDF)
- [44] M. Smith, *ABAQUS/Standard User's Manual, Version 6.9*. United States: Dassault Systèmes Simulia Corp, 2009.
- [45] M. S. Pavlovic, "Resistance of bolted shear connectors in prefabricated steel-concrete composite decks," Ph.D. dissertation, 2013.
- [46] D. E. Lee and T. Hahn, "Integral fit joint technologies for composites," *Journal of Thermoplastic Composite Materials*, vol. 11, pp. 1–26, March 1998. [Online]. Available: <https://journals.sagepub.com/doi/10.1177/089270579801100206>
- [47] *EN 1993-1-6 Eurocode 3: Design of steel structures - Part 1-6: Strength and Stability of Shell Structures*, EN. Brussels: CEN, 2007.
- [48] ALL3DP. What is cnc milling? – simply explained. [Online]. Available: <https://all3dp.com/2/what-is-cnc-milling-simply-explained/>
- [49] R. Ronquillo. Understanding cnc milling. [Online]. Available: <https://www.thomasnet.com/articles/custom-manufacturing-fabricating/understanding-cnc-milling/>
- [50] F. Bijlaard and A. M. Girao, "Innovative joints in steel construction," vol. 2, no. 4, pp. 243–247, 2009.
- [51] M. Emara, E. Sayed-Ahmed, and E. Soliman, "Numerical analysis of chs unstiffened bolted circular flange connection," *Al-Azhar University Civil Engineering Research Magazine (CERM)*, vol. 41(1), pp. 49–61, 2019. [Online]. Available: <http://www.azharcermjournal.com/CERMF1901/P19-01-04.pdf>

## A.1 WIND LOAD

## A.1.1 Wind load coefficients

Wind coefficients and loads								
Zone	C <sub>pe</sub>	C <sub>pi 1</sub>	C <sub>pi 2</sub>	Load C <sub>pe</sub> kN/m	Load C <sub>pi 1</sub> kN/m	Load C <sub>pi 2</sub> kN/m	Sum1 kN/m	Sum2 kN/m
F	-1.8	0.2	-0.3	-9.576	1.064	-1.596	-8.512	-11.172
G	-1.2	0.2	-0.3	-6.384	1.064	-1.596	-5.32	-7.98
H	-0.7	0.2	-0.3	-3.724	1.064	-1.596	-2.66	-5.32
I	-0.2	0.2	-0.3	-1.064	1.064	-1.596	0	-2.66
I	0.2	0.2	-0.3	1.064	1.064	-1.596	2.128	-0.532

Figure A.1: Wind coefficients and wind loads calculations.

## A.1.2 Load combinations

LC 1: Permanent load						
Load (kN/m)	ULS			SLS		
	Zones			Zones		
	G	H	I	G	H	I
Permanent	12.83	12.83	12.83	9.50	9.50	9.50
F <sub>d</sub>	12.83	12.83	12.83	9.50	9.50	9.50

Table A.1: Loads for load combination 1.

LC 2: Permanent + Wind Situation 1						
Load (kN/m)	ULS			SLS		
	Zones			Zones		
	G	H	I	G	H	I
Permanent	11.40	11.40	11.40	9.50	9.50	9.50
Wind	-9.58	-3.99	3.19	-6.38	-2.66	2.13
F <sub>d</sub>	1.82	7.41	14.59	3.12	6.84	11.63

Table A.2: Loads for load combination 2.

<b>LC 3: Permanent + Wind Situation 2</b>		
	<b>ULS</b>	<b>SLS</b>
	<b>Zone</b>	<b>Zone</b>
<b>Load (kN/m)</b>	<b>I</b>	<b>I</b>
<b>Permanent</b>	11.40	9.50
<b>Wind 2</b>	3.19	2.13
<b>F<sub>d</sub></b>	<b>14.59</b>	<b>11.63</b>

Table A.3: Loads for load combination 3.

<b>LC 4: Permanent + Imposed load</b>						
	<b>ULS</b>			<b>SLS</b>		
	<b>Zones</b>			<b>Zones</b>		
<b>Load (kN/m)</b>	<b>G</b>	<b>H</b>	<b>I</b>	<b>G</b>	<b>H</b>	<b>I</b>
<b>Permanent</b>	11.40	11.40	11.40	9.50	9.50	9.50
<b>Imposed</b>	9.98	9.98	9.98	6.65	6.65	6.65
<b>F<sub>d</sub></b>	<b>21.38</b>	<b>21.38</b>	<b>21.38</b>	<b>16.15</b>	<b>16.15</b>	<b>16.15</b>

Table A.4: Loads for load combination 4.

<b>LC 5: Permanent + Snow</b>						
	<b>ULS</b>			<b>SLS</b>		
	<b>Zones</b>			<b>Zones</b>		
<b>Load (kN/m)</b>	<b>G</b>	<b>H</b>	<b>I</b>	<b>G</b>	<b>H</b>	<b>I</b>
<b>Permanent</b>	11.40	11.40	11.40	9.50	9.50	9.50
<b>Snow</b>	7.13	7.13	7.13	4.75	4.75	4.75
<b>F<sub>d</sub></b>	<b>18.53</b>	<b>18.53</b>	<b>18.53</b>	<b>14.25</b>	<b>14.25</b>	<b>14.25</b>

Table A.5: Loads for load combination 5.

# B | DESIGN

## B.1 STRUCTURAL DESIGN

### B.1.1 Grasshopper model definition

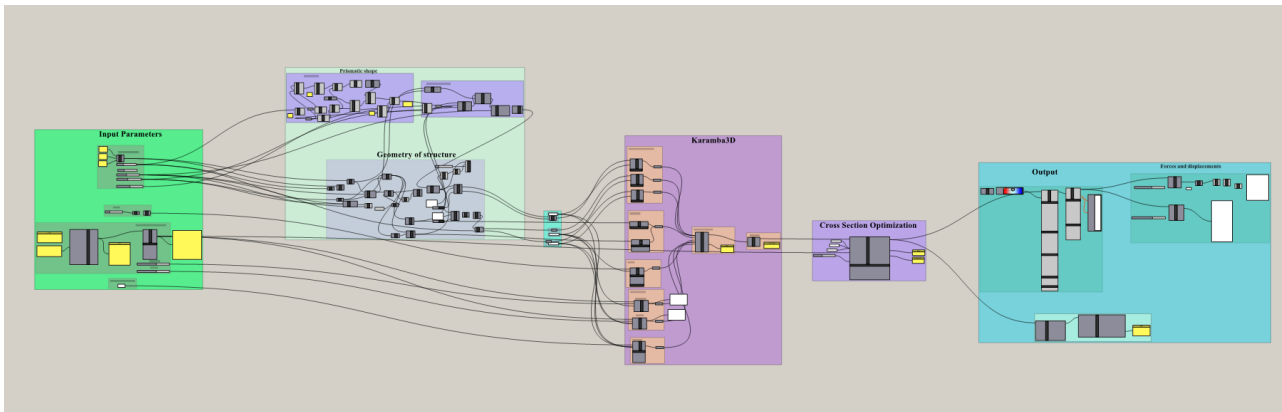


Figure B.1: Case study truss Grasshopper script.

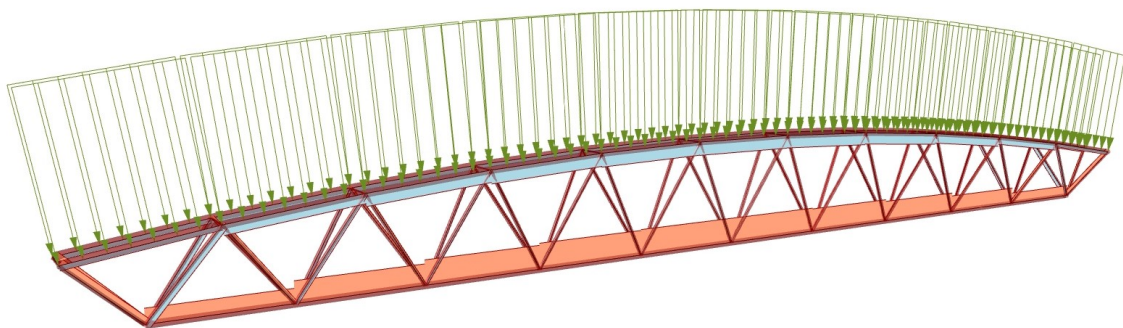


Figure B.2: 3D model of the case-study truss.

### B.1.2 Forces Case-study truss

Element ID	N1 (kN)	N2 (kN)	Vz_1 (kN)	Vz_2 (kN)	My_1 (kN/m)	My_2 (kN/m)
0	468.52	468.52	2.53	2.53	-8.27	3.98
1	469.18	469.18	2.47	2.47	-8.12	3.88
2	254.14	254.14	0.49	0.49	-1.47	1.29
3	-404.97	-404.97	0.14	0.14	-0.75	0.04
4	253.88	253.88	0.49	0.49	-1.45	1.29
5	-404.65	-404.65	0.14	0.14	-0.71	0.05
6	157.33	157.33	0.41	0.41	-1.80	0.79
7	-237.83	-237.83	-0.42	-0.42	0.83	-1.82
8	157.27	157.27	0.41	0.41	-1.80	0.80
9	-237.78	-237.78	-0.42	-0.42	0.83	-1.80
10	91.50	91.50	0.22	0.22	-1.18	0.36
11	-150.02	-150.02	-0.15	-0.15	0.06	-0.94
12	91.47	91.47	0.22	0.22	-1.17	0.37
13	-149.99	-149.99	-0.15	-0.15	0.05	-0.93
14	42.69	42.69	0.13	0.13	-0.89	0.06
15	-89.29	-89.29	-0.09	-0.09	-0.12	-0.74
16	42.69	42.69	0.13	0.13	-0.88	0.06
17	-89.29	-89.29	-0.09	-0.09	-0.12	-0.73
18	-0.02	-0.02	0.06	0.06	-0.61	-0.20
19	-42.18	-42.18	-0.01	-0.01	-0.38	-0.44
20	-0.02	-0.02	0.06	0.06	-0.61	-0.20
21	-42.18	-42.18	-0.01	-0.01	-0.38	-0.44
22	-42.18	-42.18	-0.01	-0.01	-0.38	-0.44
23	-0.02	-0.02	0.06	0.06	-0.61	-0.20
24	-42.18	-42.18	-0.01	-0.01	-0.38	-0.44
25	-0.02	-0.02	0.06	0.06	-0.61	-0.20
26	-89.29	-89.29	-0.09	-0.09	-0.12	-0.74
27	42.69	42.69	0.13	0.13	-0.88	0.06
28	-89.29	-89.29	-0.09	-0.09	-0.12	-0.73
29	42.69	42.69	0.13	0.13	-0.88	0.06
30	-150.01	-150.01	-0.15	-0.15	0.06	-0.94
31	91.49	91.49	0.22	0.22	-1.17	0.36
32	-150.01	-150.01	-0.15	-0.15	0.06	-0.94
33	91.49	91.49	0.22	0.22	-1.17	0.36
34	-237.80	-237.80	-0.42	-0.42	0.83	-1.82
35	157.30	157.30	0.41	0.41	-1.79	0.79
36	-237.80	-237.80	-0.42	-0.42	0.84	-1.82
37	157.30	157.30	0.41	0.41	-1.79	0.79
38	-404.84	-404.84	0.13	0.13	-0.71	0.03
39	254.02	254.02	0.48	0.48	-1.44	1.28
40	-404.80	-404.80	0.13	0.13	-0.71	0.03
41	253.99	253.99	0.48	0.48	-1.44	1.28
42	468.79	468.79	2.48	2.48	-8.13	3.91
43	468.88	468.88	2.48	2.48	-8.12	3.89
44	-340.16	-340.16	-31.71	41.53	8.41	42.06
45	-752.45	-752.45	-38.39	34.85	42.93	30.80
46	-972.61	-972.61	-36.65	36.59	33.55	33.34



### B.1.3 Forces Case-study truss

47	-1096.64	-1096.64	-36.83	36.40	34.64	33.16
48	-1160.94	-1160.94	-36.68	36.56	33.96	33.53
49	-1180.96	-1180.96	-36.62	36.62	33.78	33.78
50	-1160.94	-1160.94	-36.56	36.68	33.53	33.96
51	-1096.64	-1096.64	-36.40	36.83	33.16	34.64
52	-972.62	-972.62	-36.59	36.65	33.34	33.55
53	-752.49	-752.49	-34.85	38.38	30.80	42.90
54	-340.35	-340.35	-41.53	31.70	42.03	8.36
55	-340.61	-340.61	-31.71	41.53	8.36	41.97
56	-752.54	-752.54	-38.38	34.86	42.85	30.80
57	-972.64	-972.64	-36.65	36.59	33.54	33.34
58	-1096.64	-1096.64	-36.83	36.40	34.63	33.16
59	-1160.94	-1160.94	-36.68	36.56	33.96	33.53
60	-1180.96	-1180.96	-36.62	36.62	33.78	33.78
61	-1160.94	-1160.94	-36.56	36.68	33.53	33.96
62	-1096.64	-1096.64	-36.40	36.83	33.16	34.64
63	-972.63	-972.63	-36.59	36.65	33.34	33.55
64	-752.51	-752.51	-34.85	38.38	30.80	42.89
65	-340.41	-340.41	-41.53	31.71	42.01	8.36
66	1149.62	1149.62	-3.84	-3.84	8.07	-18.09
67	1715.99	1715.99	-0.18	-0.18	-11.61	-12.82
68	2037.21	2037.21	-0.60	-0.60	-9.19	-13.29
69	2214.05	2214.05	-0.20	-0.20	-11.00	-12.38
70	2293.95	2293.95	-0.09	-0.09	-11.33	-11.92
71	2293.95	2293.95	0.09	0.09	-11.92	-11.33
72	2214.05	2214.05	0.20	0.20	-12.38	-11.00
73	2037.21	2037.21	0.60	0.60	-13.29	-9.19
74	1715.99	1715.99	0.18	0.18	-12.82	-11.61
75	1149.62	1149.62	3.83	3.83	-18.08	8.05
76	0.00	0.00	0.04	0.04	-0.03	0.06
77	27.38	27.38	0.01	0.01	0.00	0.02
78	13.27	13.27	0.00	0.00	0.01	0.01
79	8.73	8.73	0.00	0.00	0.01	0.01
80	6.55	6.55	0.00	0.00	0.00	0.01
81	5.73	5.73	0.00	0.00	0.00	0.00
82	5.73	5.73	0.00	0.00	0.00	0.00
83	6.55	6.55	0.00	0.00	0.00	0.00
84	8.73	8.73	0.00	0.00	0.01	0.01
85	13.28	13.28	0.00	0.00	0.01	0.01
86	27.45	27.45	0.00	0.00	0.02	0.02
87	0.00	0.00	0.00	0.00	0.02	0.03

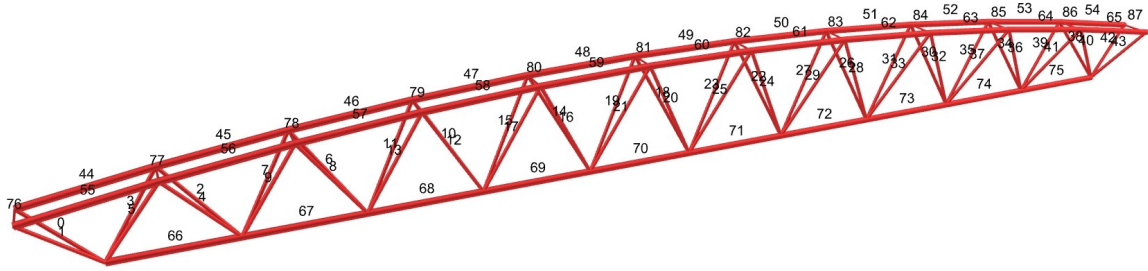
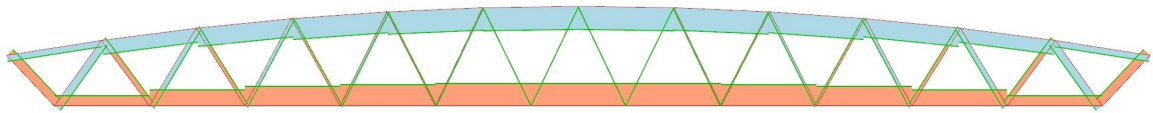
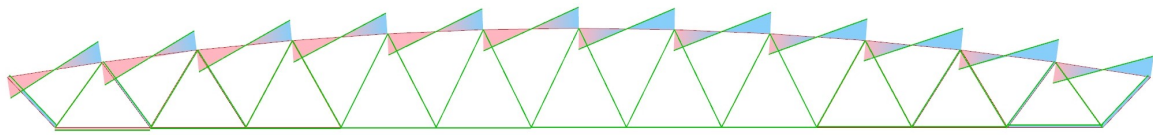


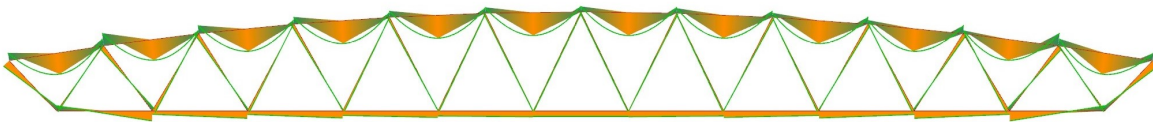
Figure B.3: Case-study truss elements ID.



(a) Normal force (N) diagram.



(b) Shear force (V) diagram



(c) Moment (M) diagram

Figure B.4: Forces diagrams from the design case study truss

#### B.1.4 Forces Optimized truss

Element ID	N1 (kN)	N2 (kN)	Vz_1 (kN)	Vz_2 (kN)	My_1 (kN/m)	My_2 (kN/m)
0	-419.60	-419.60	-53.35	61.12	56.44	98.02
1	-419.60	-419.60	-53.35	61.12	56.44	98.02
2	-884.84	-884.84	-47.76	39.12	81.52	46.40
3	-884.84	-884.84	-47.76	39.12	81.52	46.40
4	-1068.61	-1068.61	-42.00	34.94	46.95	21.54
5	-1068.61	-1068.61	-42.00	34.94	46.95	21.54
6	-1160.55	-1160.55	-51.61	72.79	21.54	144.78
7	-1160.55	-1160.55	-51.61	72.79	21.54	144.78
8	-1160.55	-1160.55	-51.61	72.79	21.55	144.79
9	-1160.55	-1160.55	-51.61	72.79	21.55	144.79
10	-1068.60	-1068.60	-42.00	34.94	46.95	21.54
11	-1068.60	-1068.60	-42.00	34.94	46.95	21.54
12	-884.81	-884.81	-47.74	39.13	81.39	46.41
13	-884.81	-884.81	-47.74	39.13	81.39	46.41
14	-419.70	-419.70	-53.39	61.08	56.78	97.93
15	-419.70	-419.70	-53.39	61.08	56.78	97.93
16	1282.08	1282.08	-7.78	-7.78	39.83	-17.89
17	1769.09	1769.09	-3.54	-3.54	-15.70	-39.25
18	2062.36	2062.36	3.41	3.41	-38.71	-9.26
19	2366.81	2366.81	-1.66	-1.66	-10.36	-20.10
20	2363.55	2363.55	0.00	0.00	-19.89	-19.89
21	2366.81	2366.81	1.66	1.66	-20.10	-10.36
22	2062.36	2062.36	-3.40	-3.40	-9.26	-38.69
23	1769.03	1769.03	3.53	3.53	-39.24	-15.79
24	1282.09	1282.09	7.85	7.85	-17.99	40.22
25	-58.13	-58.13	0.03	0.03	-0.34	-0.05
26	-58.13	-58.13	0.03	0.03	-0.34	-0.05
27	0.10	0.10	-0.02	-0.02	-0.07	-0.22
28	0.10	0.10	-0.02	-0.02	-0.07	-0.22
29	0.10	0.10	-0.02	-0.02	-0.07	-0.22
30	0.10	0.10	-0.02	-0.02	-0.07	-0.22
31	-58.13	-58.13	0.03	0.03	-0.34	-0.05
32	-58.13	-58.13	0.03	0.03	-0.34	-0.05
33	-60.98	-60.98	-0.20	-0.20	0.31	-0.42
34	120.29	120.29	-0.06	-0.06	0.16	-0.16
35	212.68	212.68	0.14	0.14	-0.44	0.38
36	506.93	506.93	-14.38	-14.38	20.72	-56.81
37	132.43	132.43	-0.02	-0.02	0.03	-0.14
38	-374.73	-374.73	0.43	0.43	0.56	2.04
39	-113.54	-113.54	0.24	0.24	-0.69	-0.08
40	-60.98	-60.98	-0.20	-0.20	0.31	-0.42
41	120.29	120.29	-0.06	-0.06	0.16	-0.16
42	212.68	212.68	0.14	0.14	-0.44	0.38
43	506.93	506.93	-14.38	-14.38	20.72	-56.81
44	132.43	132.43	-0.02	-0.02	0.03	-0.14
45	-374.73	-374.73	0.43	0.43	0.56	2.04
46	-113.54	-113.54	0.24	0.24	-0.69	-0.08
47	39.62	39.62	-0.02	-0.02	0.04	-0.03
48	-161.11	-161.11	0.13	0.13	-0.28	0.59
49	-464.44	-464.44	4.11	4.11	-16.52	2.55
50	39.62	39.62	-0.02	-0.02	0.04	-0.03
51	-161.11	-161.11	0.13	0.13	-0.28	0.59
52	-464.44	-464.44	4.11	4.11	-16.52	2.55
53	-126.73	-126.73	0.12	0.12	-0.43	0.32
54	81.16	81.16	-0.06	-0.06	0.06	-0.13

### B.1.5 Forces Optimized truss

55	-126.73	-126.73	0.12	0.12	-0.43	0.32
56	81.16	81.16	-0.06	-0.06	0.06	-0.13
57	-62.02	-62.02	-0.40	-0.40	0.57	-0.61
58	-62.02	-62.02	-0.40	-0.40	0.57	-0.61
59	-60.97	-60.97	-0.20	-0.20	0.32	-0.42
60	120.26	120.26	-0.06	-0.06	0.16	-0.16
61	212.73	212.73	0.14	0.14	-0.43	0.38
62	132.43	132.43	-0.02	-0.02	0.03	-0.14
63	-62.02	-62.02	-0.40	-0.40	0.57	-0.61
64	-113.53	-113.53	0.24	0.24	-0.69	-0.08
65	-60.97	-60.97	-0.20	-0.20	0.32	-0.42
66	120.26	120.26	-0.06	-0.06	0.16	-0.16
67	212.73	212.73	0.14	0.14	-0.43	0.38
68	132.43	132.43	-0.02	-0.02	0.03	-0.14
69	-62.02	-62.02	-0.40	-0.40	0.57	-0.61
70	-113.53	-113.53	0.24	0.24	-0.69	-0.08
71	-126.73	-126.73	0.12	0.12	-0.43	0.32
72	81.16	81.16	-0.06	-0.06	0.06	-0.14
73	-126.73	-126.73	0.12	0.12	-0.43	0.32
74	81.16	81.16	-0.06	-0.06	0.06	-0.14
75	39.60	39.60	-0.02	-0.02	0.04	-0.04
76	-161.08	-161.08	0.13	0.13	-0.28	0.60
77	-464.60	-464.60	4.10	4.10	-16.47	2.57
78	39.60	39.60	-0.02	-0.02	0.04	-0.04
79	-161.08	-161.08	0.13	0.13	-0.28	0.60
80	-464.60	-464.60	4.10	4.10	-16.47	2.57
81	506.78	506.78	-14.20	-14.20	20.47	-56.06
82	-374.86	-374.86	0.46	0.46	0.51	2.09
83	506.78	506.78	-14.20	-14.20	20.47	-56.06
84	-374.86	-374.86	0.46	0.46	0.51	2.09
85	-1.81	-1.81	0.00	0.00	0.00	-0.01
86	-1.81	-1.81	0.00	0.00	0.00	-0.01
87	-37.90	-37.90	0.17	0.17	-0.44	0.28
88	-37.90	-37.90	0.17	0.17	-0.44	0.28
89	-1.81	-1.81	0.00	0.00	0.00	-0.01
90	-1.81	-1.81	0.00	0.00	0.00	-0.01
91	-37.90	-37.90	0.17	0.17	-0.44	0.28
92	-37.90	-37.90	0.17	0.17	-0.44	0.28
93	0.00	0.00	0.00	0.00	0.00	0.00
94	16.84	16.84	0.00	0.00	0.00	0.00
95	12.48	12.48	0.00	0.00	0.00	0.00
96	13.63	13.63	0.00	0.00	0.00	0.00
97	22.40	22.40	0.00	0.00	0.00	0.00
98	13.64	13.64	0.00	0.00	0.00	0.00
99	12.34	12.34	0.00	0.00	0.00	0.00
100	17.35	17.35	0.00	0.00	0.00	0.00
101	0.00	0.00	0.00	0.00	0.00	0.00

### B.1.6 Cross sections Optimized truss

ID	Cross Section	Member
0	CHSC610x23.8	Top cords
1	CHSC610x23.8	Top cords
2	CHSC610x23.8	Top cords
3	CHSC610x23.8	Top cords
4	CHSC610x23.8	Top cords
5	CHSC610x23.8	Top cords
6	CHSC610x23.8	Top cords
7	CHSC610x23.8	Top cords
8	CHSC610x23.8	Top cords
9	CHSC610x23.8	Top cords
10	CHSC610x23.8	Top cords
11	CHSC610x23.8	Top cords
12	CHSC610x23.8	Top cords
13	CHSC610x23.8	Top cords
14	CHSC610x23.8	Top cords
15	CHSC610x23.8	Top cords
16	CHSC508x30.0	Bottom cords
17	CHSC508x30.0	Bottom cords
18	CHSC508x30.0	Bottom cords
19	CHSC508x30.0	Bottom cords
20	CHSC508x30.0	Bottom cords
21	CHSC508x30.0	Bottom cords
22	CHSC508x30.0	Bottom cords
23	CHSC508x30.0	Bottom cords
24	CHSC508x30.0	Bottom cords
25	CHSC168.3x10.0	Diagonals2
26	CHSC168.3x10.0	Diagonals2
27	CHSC168.3x10.0	Diagonals2
28	CHSC168.3x10.0	Diagonals2
29	CHSC168.3x10.0	Diagonals2
30	CHSC168.3x10.0	Diagonals2
31	CHSC168.3x10.0	Diagonals2
32	CHSC168.3x10.0	Diagonals2
33	CHSC114.3x8.0	Diagonals
34	CHSC114.3x6.3	Diagonals
35	CHSC139.7x10.0	Diagonals
36	CHSC273x16.0	Diagonals
37	CHSC114.3x8.0	Diagonals
38	CHSC219.1x16.0	Diagonals
39	CHSC139.7x8.0	Diagonals
40	CHSC114.3x8.0	Diagonals
41	CHSC114.3x6.3	Diagonals
42	CHSC139.7x10.0	Diagonals
43	CHSC273x16.0	Diagonals
44	CHSC114.3x8.0	Diagonals
45	CHSC219.1x16.0	Diagonals
46	CHSC139.7x8.0	Diagonals
47	CHSC48.3x5.0	Diagonals
48	CHSC193.7x12.0	Diagonals
49	CHSC273x16.0	Diagonals
50	CHSC48.3x5.0	Diagonals

ID	Cross Section	Member
51	CHSC193.7x12.0	Diagonals
52	CHSC273x16.0	Diagonals
53	CHSC168.3x10.0	Diagonals
54	CHSC88.9x6.0	Diagonals
55	CHSC168.3x10.0	Diagonals
56	CHSC88.9x6.0	Diagonals
57	CHSC114.3x8.0	Diagonals
58	CHSC114.3x8.0	Diagonals
59	CHSC114.3x8.0	Diagonals
60	CHSC114.3x6.3	Diagonals
61	CHSC139.7x10.0	Diagonals
62	CHSC114.3x8.0	Diagonals
63	CHSC114.3x8.0	Diagonals
64	CHSC139.7x8.0	Diagonals
65	CHSC114.3x8.0	Diagonals
66	CHSC114.3x6.3	Diagonals
67	CHSC139.7x10.0	Diagonals
68	CHSC114.3x8.0	Diagonals
69	CHSC114.3x8.0	Diagonals
70	CHSC139.7x8.0	Diagonals
71	CHSC168.3x10.0	Diagonals
72	CHSC88.9x6.0	Diagonals
73	CHSC168.3x10.0	Diagonals
74	CHSC88.9x6.0	Diagonals
75	CHSC48.3x5.0	Diagonals
76	CHSC193.7x12.0	Diagonals
77	CHSC273x16.0	Diagonals
78	CHSC48.3x5.0	Diagonals
79	CHSC193.7x12.0	Diagonals
80	CHSC273x16.0	Diagonals
81	CHSC273x16.0	Diagonals
82	CHSC219.1x16.0	Diagonals
83	CHSC273x16.0	Diagonals
84	CHSC219.1x16.0	Diagonals
85	CHSC114.3x6.3	Diagonals3
86	CHSC114.3x6.3	Diagonals3
87	CHSC114.3x6.3	Diagonals3
88	CHSC114.3x6.3	Diagonals3
89	CHSC114.3x6.3	Diagonals3
90	CHSC114.3x6.3	Diagonals3
91	CHSC114.3x6.3	Diagonals3
92	CHSC114.3x6.3	Diagonals3
93	CHSC21.3x2.0	Cross Bars
94	CHSC33.7x3.0	Cross Bars
95	CHSC26.9x3.0	Cross Bars
96	CHSC26.9x3.0	Cross Bars
97	CHSC42.4x3.2	Cross Bars
98	CHSC26.9x3.0	Cross Bars
99	CHSC26.9x3.0	Cross Bars
100	CHSC33.7x3.0	Cross Bars
101	CHSC21.3x2.0	Cross Bars

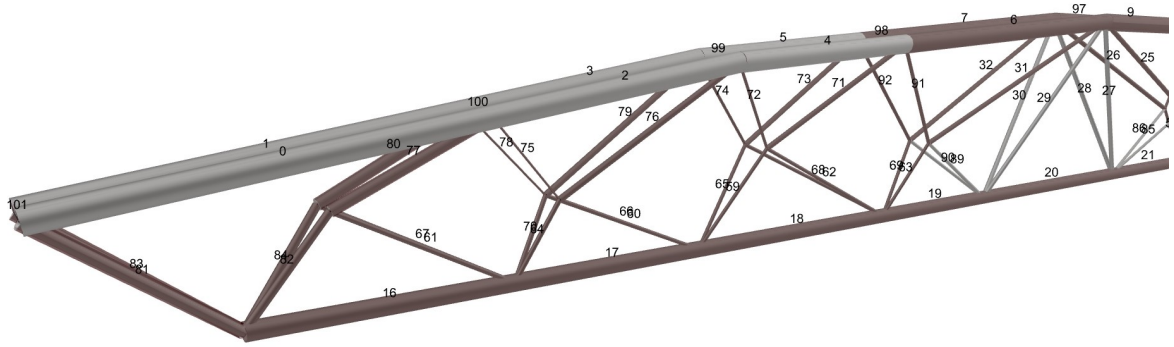


Figure B.5: Optimized truss elements ID.

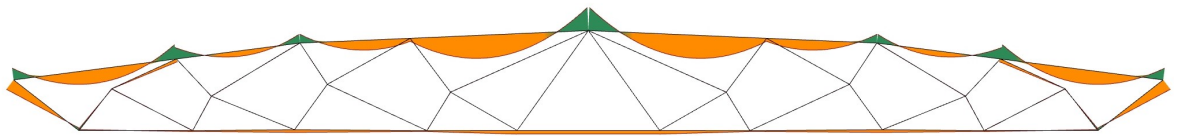


Figure B.6: Bending moment diagram on optimized truss

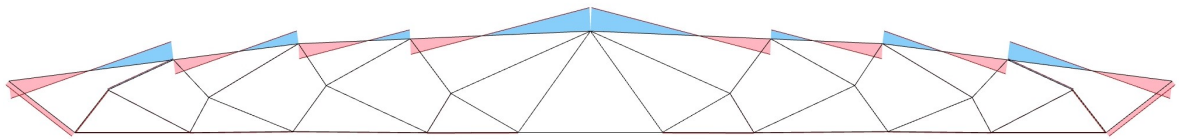


Figure B.7: Shear forces diagram on optimized truss

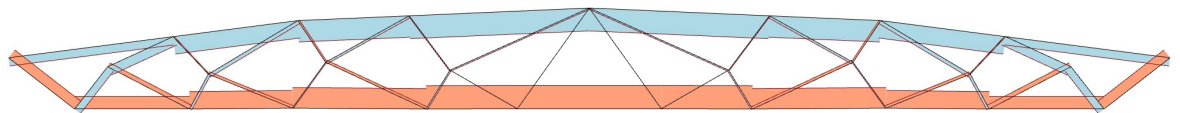


Figure B.8: Normal forces diagram on optimized truss

## B.2 OPTIMIZATION

The following figures (Figure B.9 and Figure B.10) present the grasshopper script and workflow of the optimization process performed with Peregrine.

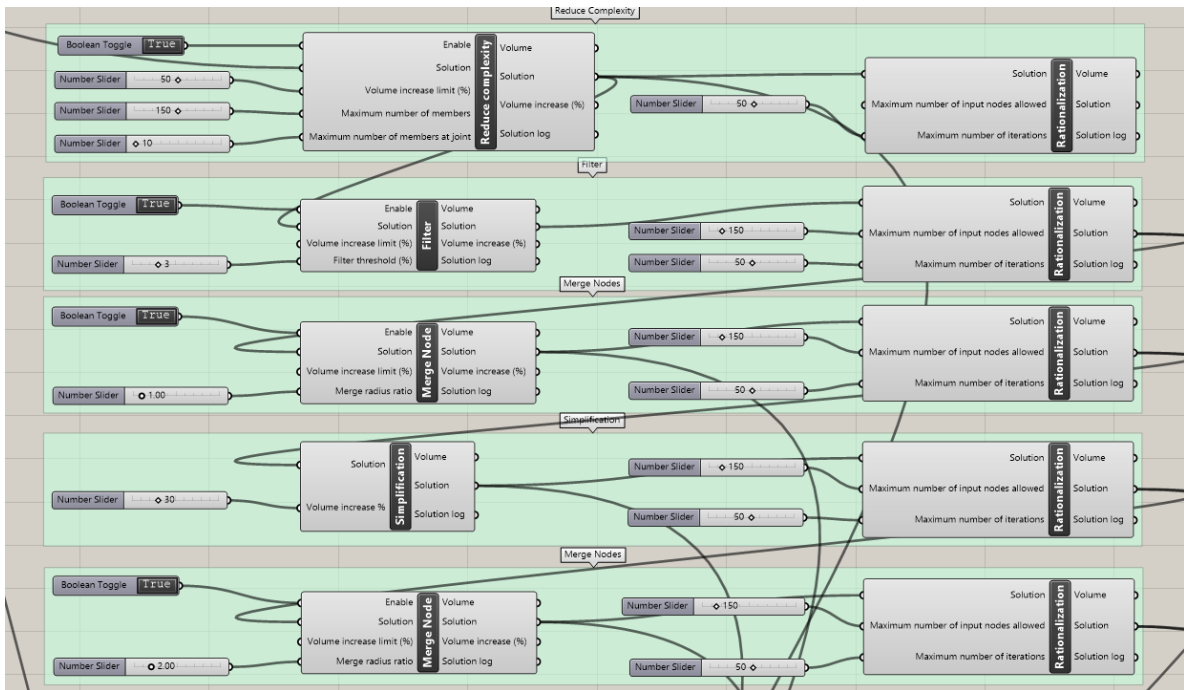


Figure B.9: Post-process workflow on Grasshopper.

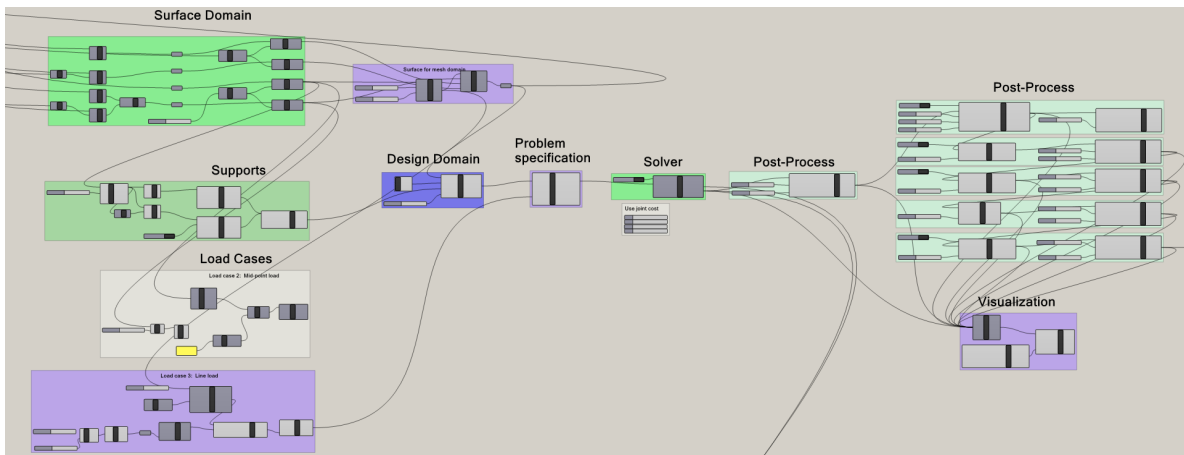


Figure B.10: Complete optimization process on Grasshopper.

The following figures (Figure B.11 and Figure B.12) present the grasshopper script and workflow of the structural design process performed with Karamba3D.

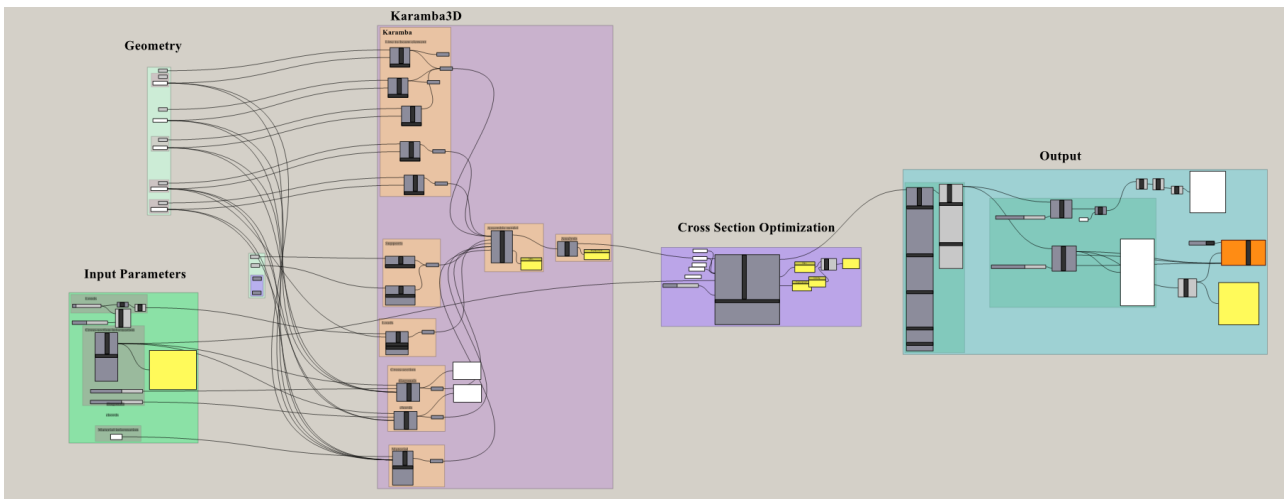


Figure B.11: Grasshopper script for the structural design of the optimized truss.

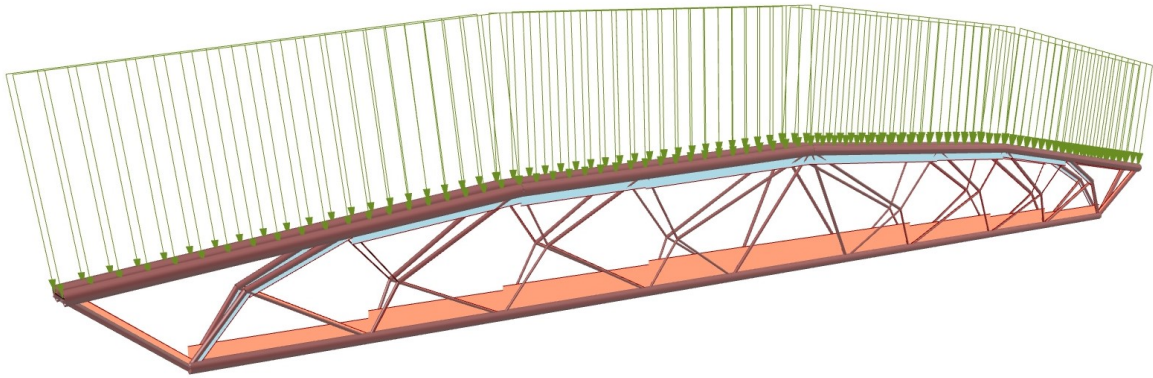


Figure B.12: 3D model of the optimized truss.



## C.1 DESIGN CONCEPT 1

The following Figure C.1 shows the stress distribution around the perforation for Design Concept 1, shown in Section 5.6.1.

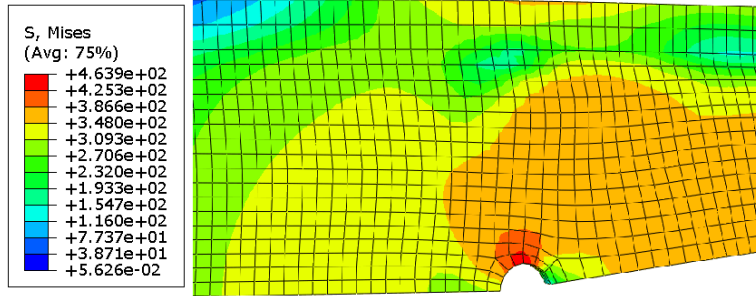


Figure C.1: Stress concentration ( $N/mm^2$ ) at the perforation in design concept 1.

The deflected shape of the inserting unit from Design Concept 1 can be observed at Figure C.2.

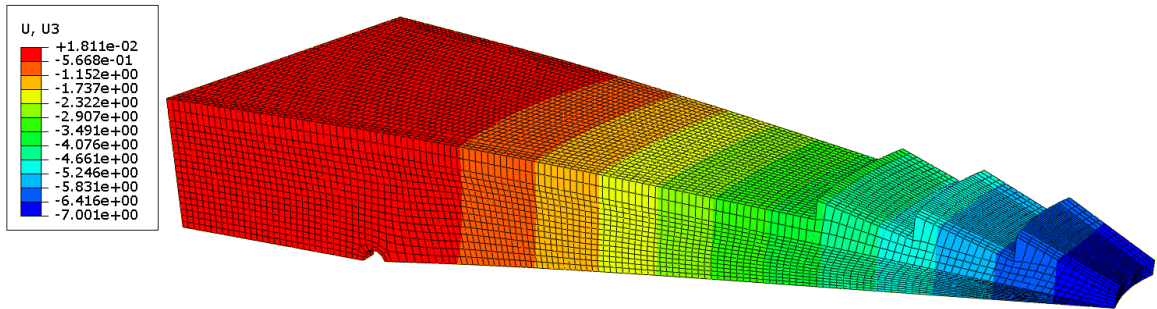


Figure C.2: Vertical displacement ( $mm$ ) of the inserting unit from design concept 1.

Figure C.3 presents the stress distribution along the duration of the FE analysis. It can be observed that after 0.2 sec the yielding stress is reached and after thi point stresses around the perforation keep growing until reach-  
ing  $450 kN/mm^2$



Figure C.3: Stress vs time curve at the perforation in design concept 1.

The following figure (Figure C.4) shows a cut view of Design Concept 1 and presents how the stress concentrates around the perforation. It also can be seen how the stresses at the horizontal plate are concentrated on the top surface, contrary to a conventional snap-fit, as shown in Figure 5.25 and Figure 5.3.

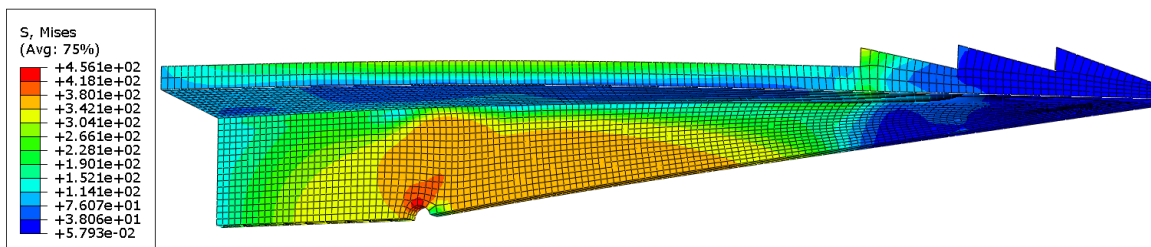


Figure C.4: Von Mises stresses ( $N/mm^2$ ) at a cut-view plane of inserting unit from design concept 1.

## C.2 DESIGN CONCEPT 2

As presented in Section 5.6.2 the inserting unit is composed of three tips at the end of the beam. Figure C.5 shows how the reaction forces are distributed between the tips. It is clear that the first tip carries most of the load while the last tip does carries a small percentage of the load.

Chart C.6 illustrates the reaction force to an applied tensile force at certain nodes from all three tips during the duration of the analysis presented in Section 5.6.2. This clearly shows the load bearing distribution each tip has.

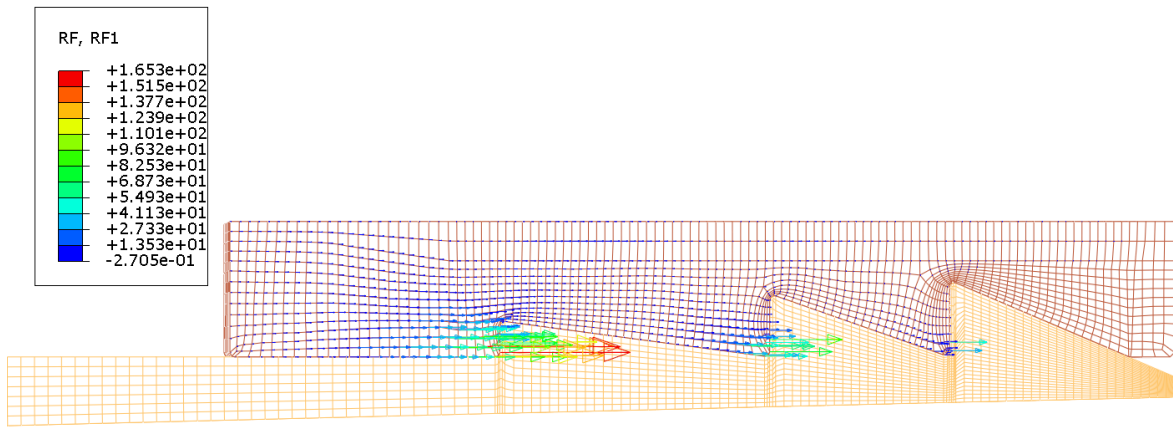


Figure C.5: Reaction forces (N) at each tip of design concept 2.

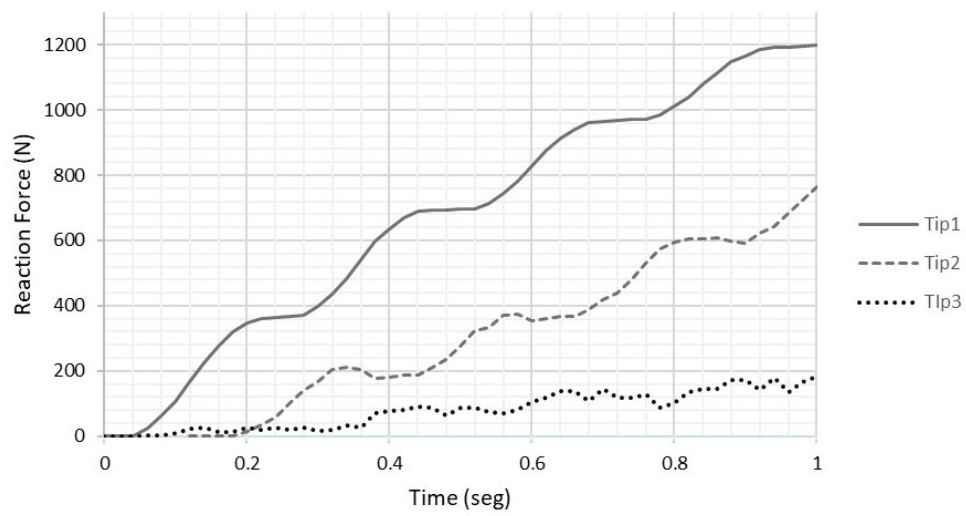
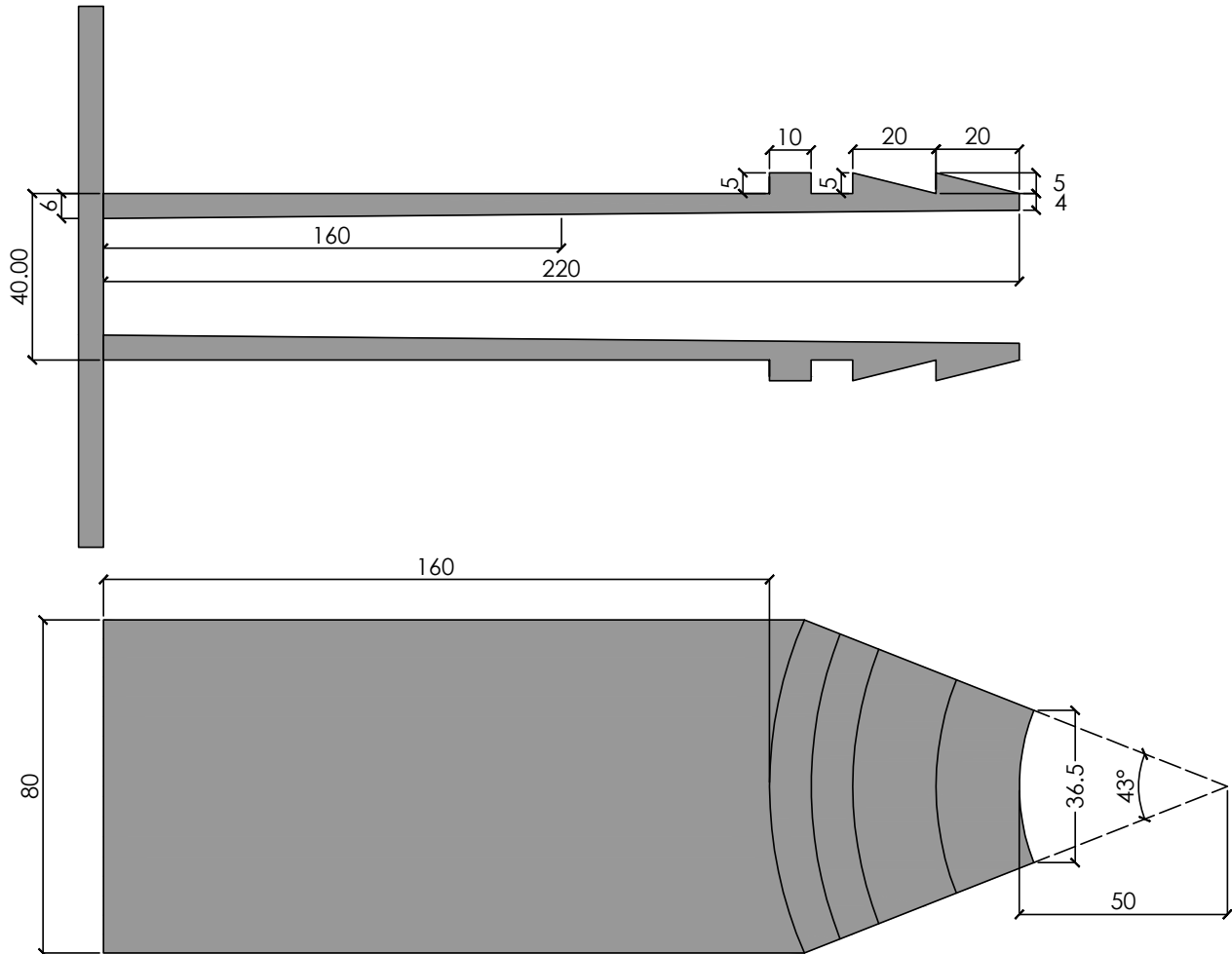


Figure C.6: Reaction forces at each tip of design concept 2.

### C.3 DESIGN CONCEPT 3: FINAL DESIGN

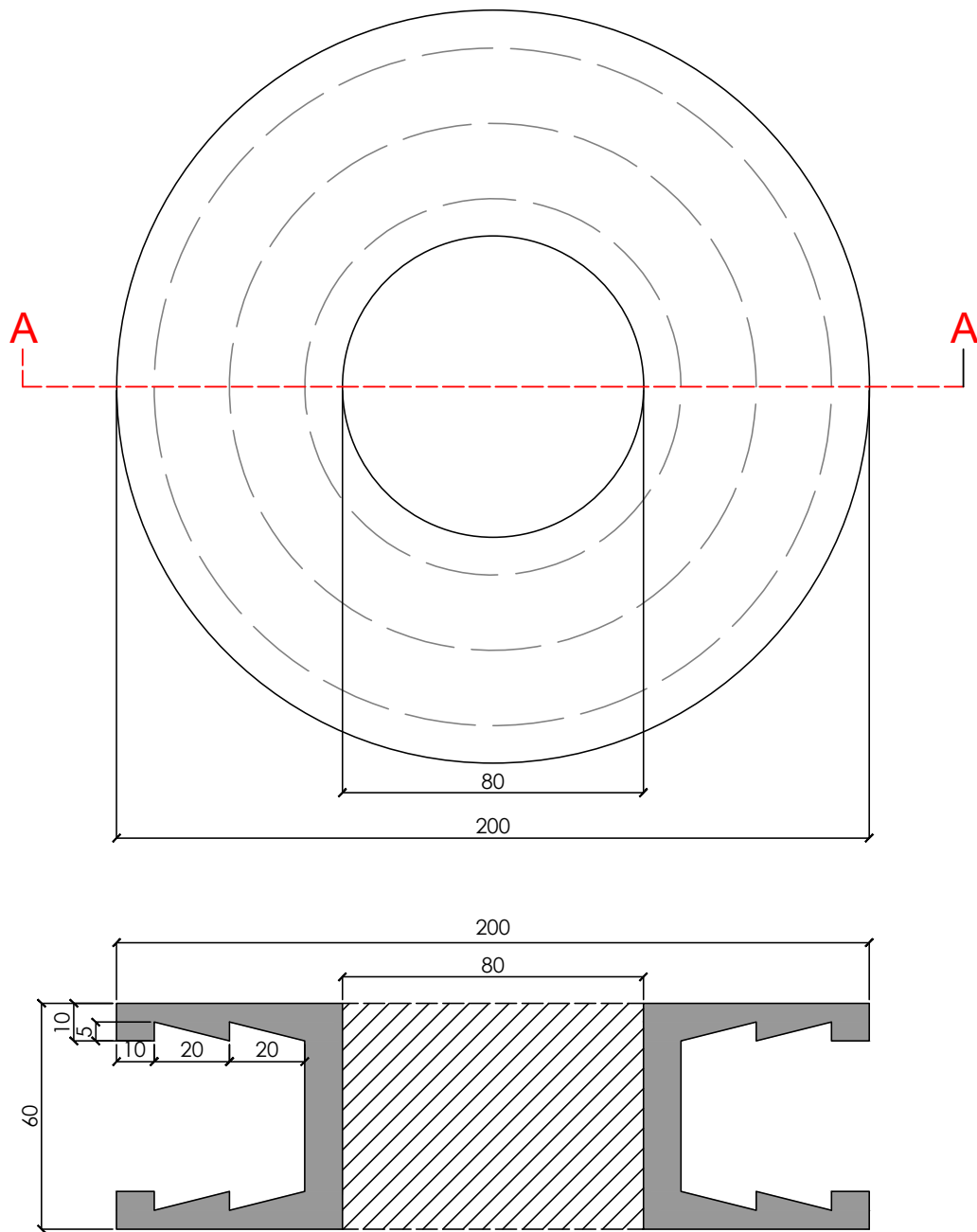
#### C.3.1 Innovative joint dimensions

This section presents the final geometrical dimensions of the inserting unit and the retaining unit



Inserting Unit  
Dimensions (mm)

Figure C.7: Insertion tip dimensions.



Retaining Unit  
Dimensions (mm)

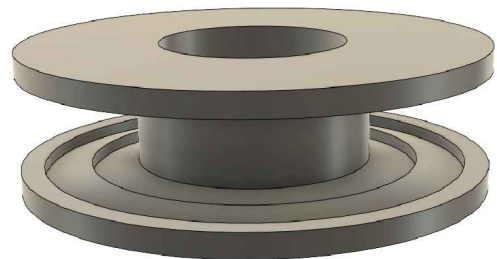


Figure C.8: Retaining unit dimensions.

## C.4 ASSEMBLY PHASE

From Figure C.9a it can be observed that plastic strains appear at the edge of the last tip due to contact with the retaining unit. Figure C.9b shows the contact stresses in  $kN/mm^2$  of the edges of the inserting unit.

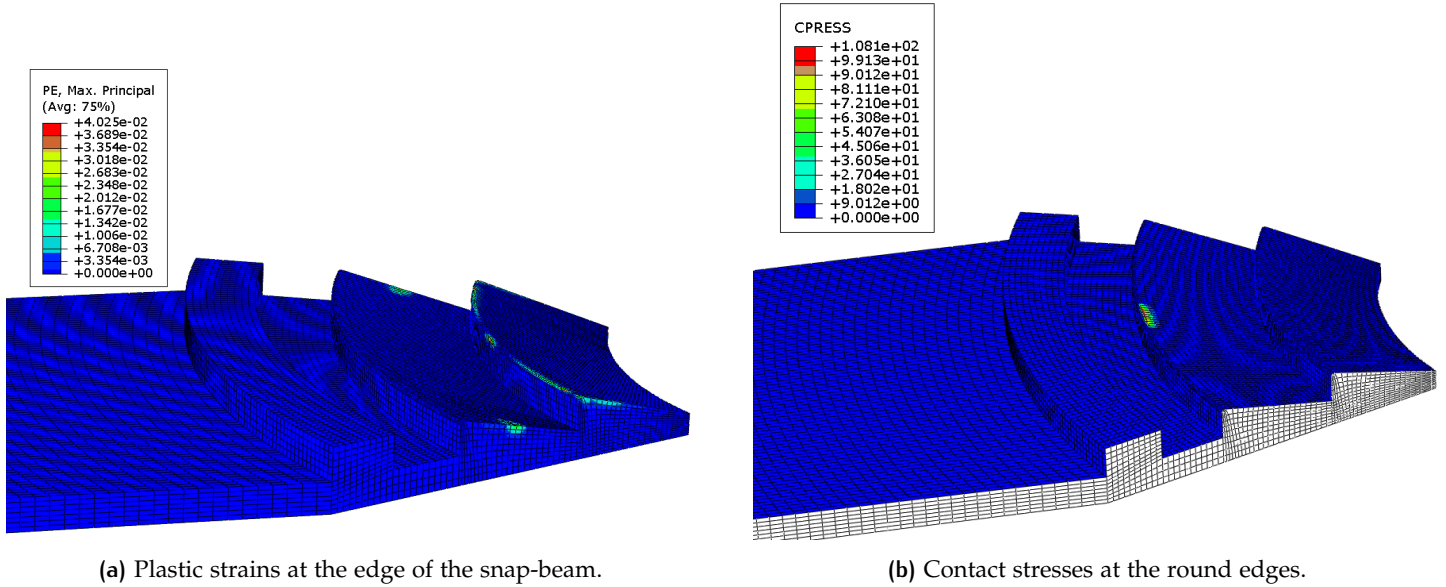


Figure C.9: Plastic strains and contact stresses of the snap-beam.

The following charts show how the stress and strain develops during the time specified of the FE analysis.

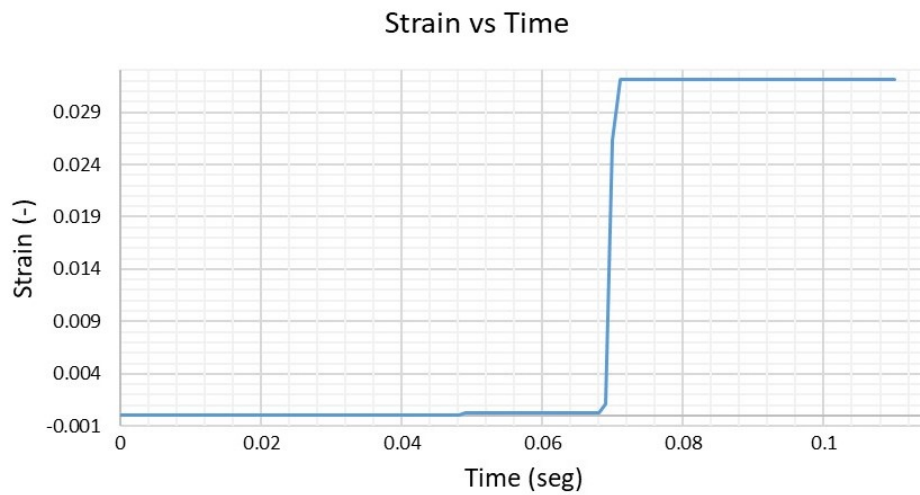


Figure C.10: Node at the round-edge: Strain vs time

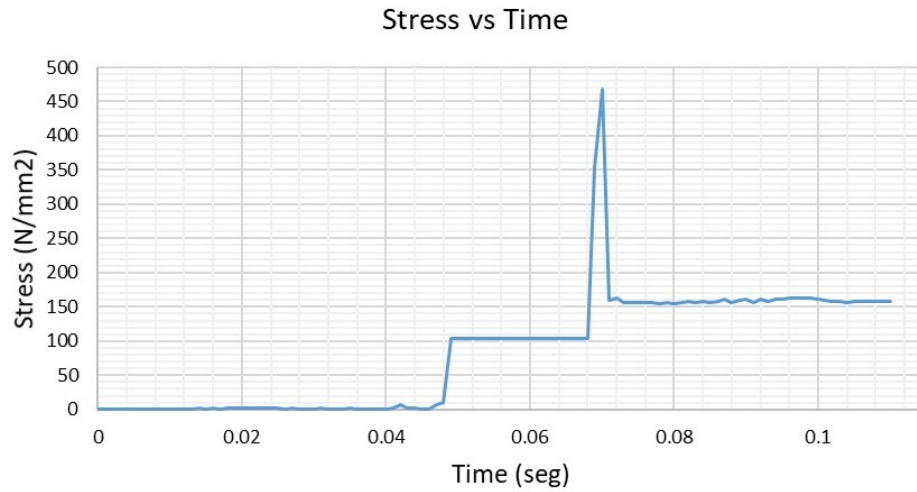


Figure C.11: Von Mises stress at node at the round edge.

Figure C.12 presents the deflection behaviour of each of the three tips from the inserting unit while being connected through the sliding inserting mechanism.

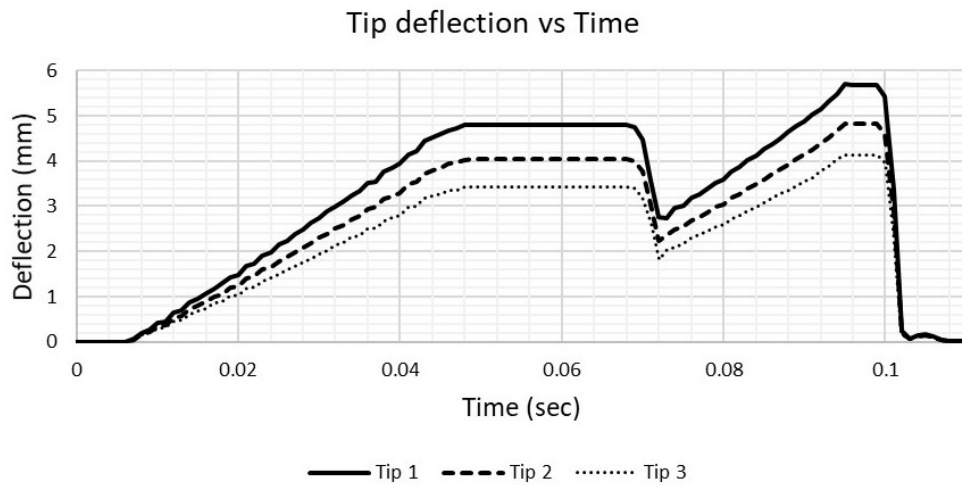


Figure C.12: Vertical displacement of each tip during the assembly phase.

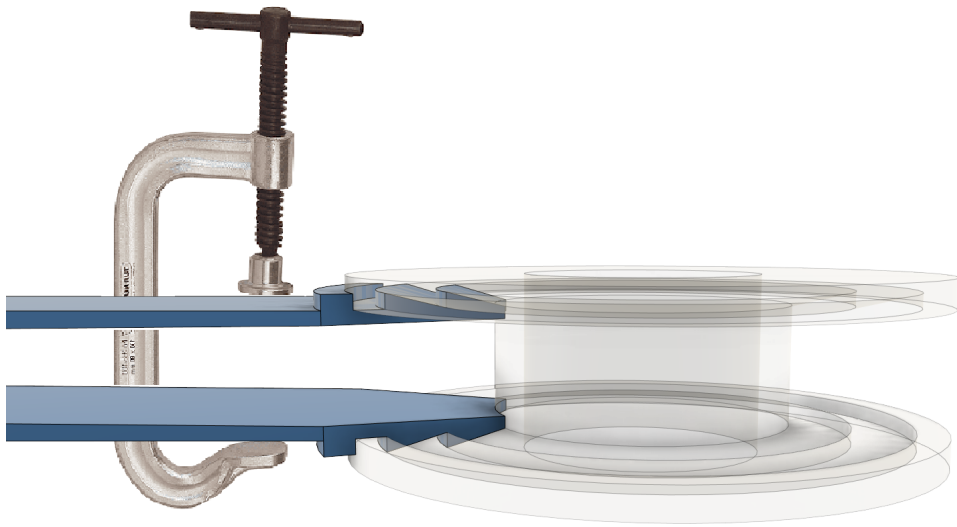


Figure C.13: Manual disassembly procedure.

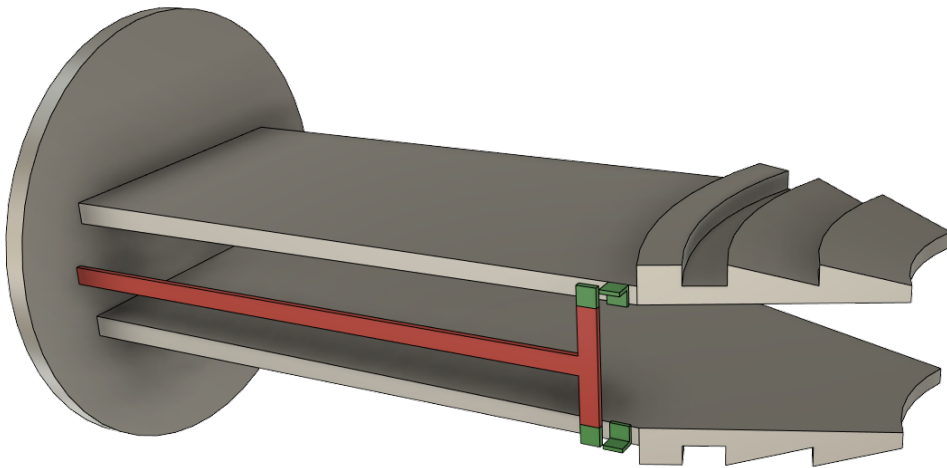


Figure C.14: Safety mechanism for the manual disassembly procedure.



#### c.4.o.1 Deflection Study: Constant height and width

restart :  
with(plots) :

### ▼ Euler beam

```

IB :=  $\frac{1}{12} \cdot b \cdot (h)^3$ ; DE1 := E·IB·diff(w1(x), x$4) = 0 :
DE2 := E·IB·diff(w2(x), x$4) = 0 :
sol1 := dsolve( {DE1, DE2}, {w1(x), w2(x)}); assign(sol1) :
w1 := w1(x) :

w2 := w2(x) :
phi1 := -diff(w1, x) : M1 := E·IB·diff(phi1, x) : V1 := diff(M1, x) :
phi2 := -diff(w2, x) : M2 := E·IB·diff(phi2, x) : V2 := diff(M2, x) :
x := 0 : eq1 := w1 = 0 : eq2 := phi1 = 0 :
x := Lx : eq3 := w1 = w2 : eq4 := phi1 = phi2 : eq5 := V1 - V2 = P : eq6 := M1 = M2 :
x := L : eq7 := V2 = 0 : eq8 := M2 = 0 :
x := 'x':
sol2 := solve( {eq1, eq2, eq3, eq4, eq5, eq6, eq7, eq8}, {_C1, _C2, _C3, _C4, _C5, _C6, _C7,
_C8}); assign(sol2) :
simplify(w1);
# Input Data:
L := 220 :
Lx := 160 :
b := 80 :
h := 6 :
P := 1000 :
E := 210000 :
IB
x := Lx; evalf(w1);
Stressmax := evalf( $\frac{(P \cdot Lx) \cdot h}{2 \cdot I_B}$ );
x := L; evalf(w2);
x := Lx; evalf(w1);
x := 180; evalf(w1);
x := 'x':
w1plot := plot( -w1, x=0..Lx, color=[red], legend=[typeset("w1")] ) :
w2plot := plot( -w2, x=Lx..L, color=[blue], legend=[typeset("w2")] ) :
display( [w1plot, w2plot]);

```

#### c.4.o.2 Deflection Study: variable height

restart :  
with(plots) :

### ▼ Euler Beam: variable h

```

I_B := 1/12 * b * ( ( (h_tip - h_base) / L ) * x + h_base )^3;
expand(I_B)
dI_B := diff(I_B, x) :
ddI_B := diff(I_B, x$2) :
DE1 := E * ( (ddI_B * diff(w1(x), x$2)) + 2 * (dI_B * diff(w1(x), x$3)) + (I_B * diff(w1(x), x$4)) ) = 0;

DE2 := E * ( (ddI_B * diff(w2(x), x$2)) + 2 * (dI_B * diff(w2(x), x$3)) + (I_B * diff(w2(x), x$4)) ) = 0;

sol1 := dsolve( {DE1, DE2}, {w1(x), w2(x)} ) : assign(sol1) :
w1 := w1(x) :

w2 := w2(x) :
phi1 := -diff(w1, x) : M1 := -E * I_B * diff(w1, x$2) : V1 := -E * ( (dI_B * diff(w1, x$2)) + (I_B * diff(w1,
x$3)) ) :
phi2 := -diff(w2, x) : M2 := -E * I_B * diff(w2, x$2) : V2 := -E * ( (dI_B * diff(w2, x$2)) + (I_B * diff(w2,
x$3)) ) :
x := 0 : eq1 := w1 = 0 : eq2 := phi1 = 0 :
x := Lx : eq3 := w1 = w2 : eq4 := phi1 = phi2 : eq5 := V1 - V2 = P : eq6 := M1 = M2 :
x := L : eq7 := V2 = 0 : eq8 := M2 = 0 :
x := 'x':
sol2 := solve( {eq1, eq2, eq3, eq4, eq5, eq6, eq7, eq8}, {_C1, _C2, _C3, _C4, _C5, _C6, _C7,
_C8} ) : assign(sol2) :

simplify(w1);
# Input Data:
L := 220 :
Lx := 160 :
b := 80 :
h_base := 6 :
h_tip := 4 :
P := 1000 :
E := 210000 :

Stress_max := evalf( ( 6 * P * Lx / ( b * (h_base)^2 ) );
Strain_base := evalf( ( Stress_max / E );
x := Lx; evalf(w1);

```

### c.4.o.3 Deflection Study: variable width

restart :  
with(plots) :

#### ▼ Euler Beam: variable h

```

I_B := 1/12 * (( (b_tip - b_base) / L ) * x + b_base ) * (h)^3;
expand(I_B)
dI_B := diff(I_B, x) :
ddI_B := diff(I_B, x$2) :
DE1 := E * ( (ddI_B * diff(w1(x), x$2)) + 2 * (dI_B * diff(w1(x), x$3)) + (I_B * diff(w1(x), x$4)) ) = 0;

DE2 := E * ( (ddI_B * diff(w2(x), x$2)) + 2 * (dI_B * diff(w2(x), x$3)) + (I_B * diff(w2(x), x$4)) ) = 0;

soll := dsolve( {DE1, DE2}, {w1(x), w2(x)} ) : assign(soll) :
w1 := w1(x) :

w2 := w2(x) :
phi1 := -diff(w1, x) : M1 := -E * I_B * diff(w1, x$2) : V1 := -E * ( (dI_B * diff(w1, x$2)) + (I_B * diff(w1,
x$3)) ) :
phi2 := -diff(w2, x) : M2 := -E * I_B * diff(w2, x$2) : V2 := -E * ( (dI_B * diff(w2, x$2)) + (I_B * diff(w2,
x$3)) ) :
x := 0 : eq1 := w1 = 0 : eq2 := phi1 = 0 :
x := Lx : eq3 := w1 = w2 : eq4 := phi1 = phi2 : eq5 := V1 - V2 = P : eq6 := M1 = M2 :
x := L : eq7 := V2 = 0 : eq8 := M2 = 0 :
x := 'x':
sol2 := solve( {eq1, eq2, eq3, eq4, eq5, eq6, eq7, eq8}, {_C1, _C2, _C3, _C4, _C5, _C6, _C7,
_C8} ) : assign(sol2) :

simplify(w1);
# Input Data:
L := 220 :
Lx := 160 :
#b := 80 :
h := 6 :
b_base := 60 :
b_tip := 40 :
#h_base := 6 :
#h_tip := 4 :
P := 800 :
E := 210000 :

Stress_max := evalf( ( 6 * P * Lx / (b_base * (h)^2) );

```

## C.5 USAGE PHASE: TENSILE FORCES

### C.5.1 Resistance to tensile forces

On the following figures the Von Mises stresses and the strains distribution are presented while subjected to axial tensile forces. It can be observed that the most prominent concentration occurs at the contact edge between the inserting and retaining unit.

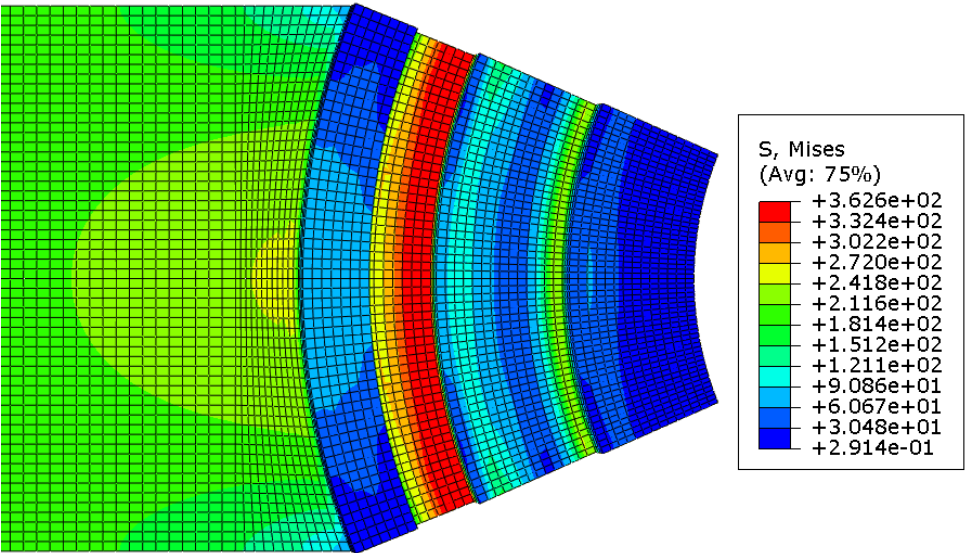


Figure C.15: Von Mises stresses ( $kN/mm^2$ ) on the inserting unit tip. Top view.

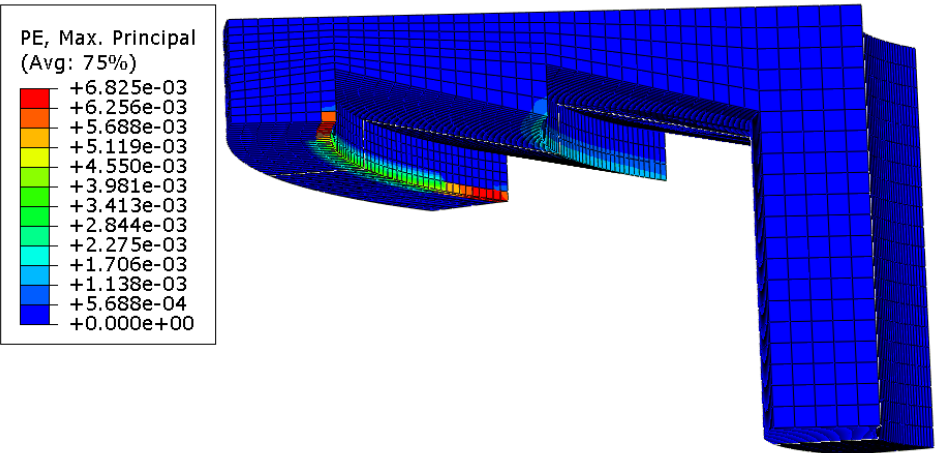


Figure C.16: Plastic strains (-) at the retaining unit.

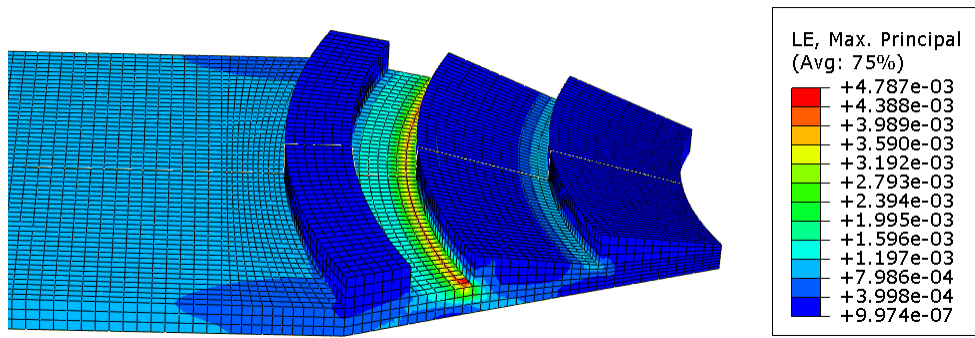


Figure C.17: Plastic strains (-) at the inserting unit.

The following chart presents the stress-tensile force relationship for both, the inserting and retaining unit.

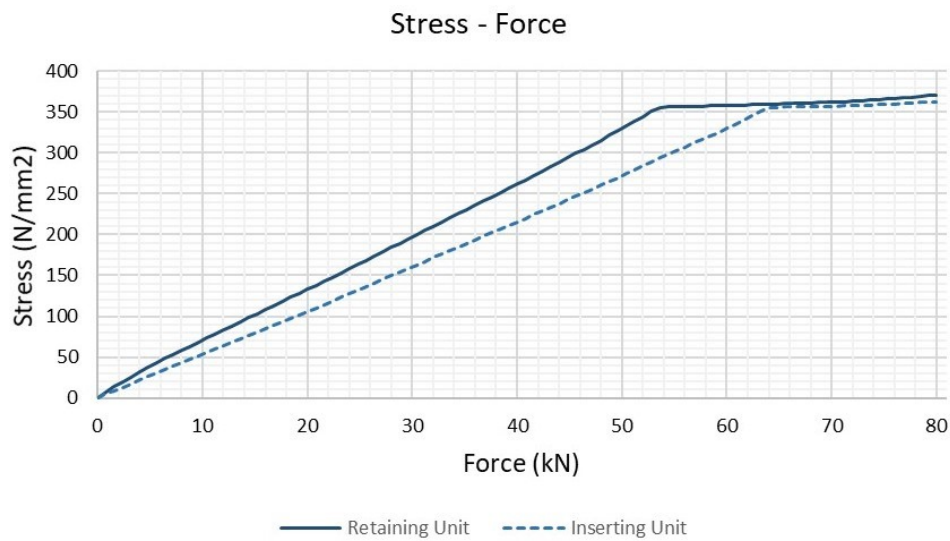


Figure C.18: Von Mises stresses ( $kN/mm^2$ ) vs applied force ( $kN$ ).

### c.5.2 Resistance to compressive forces

On the following figures the Von Mises stresses and the strains distribution are presented while subjected to axial compressive forces. It can be observed that the most prominent concentration occurs at the contact edge between the inserting and retaining unit. Additionally, the deflecting behavior of the snap-beam can be observed on Figure C.19. This illustrates the buckling shape of inserting unit under the action of compressive loads.

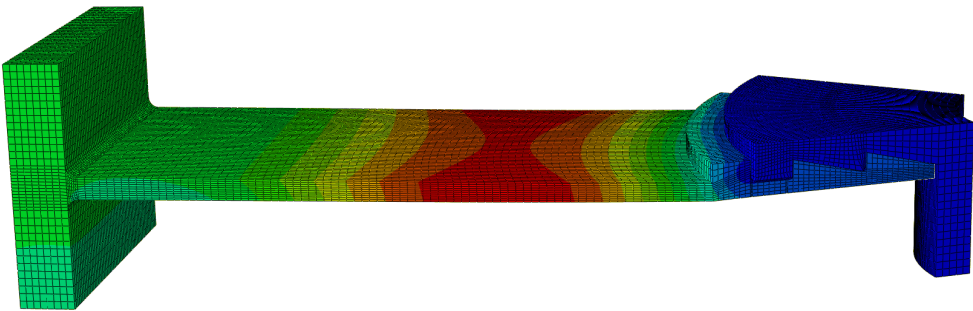


Figure C.19: Buckling shape for a compressive force.

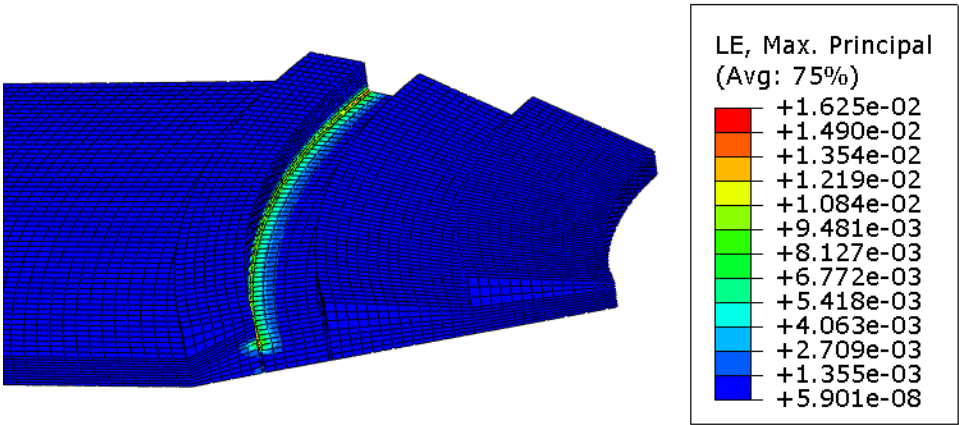


Figure C.20: Strain at the inserting unit.

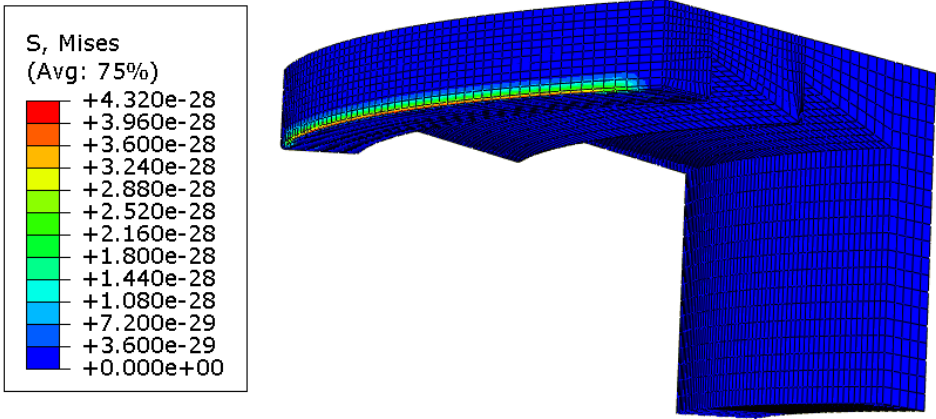


Figure C.21: Stresses at retaining unit

The following chart (Figure 5.47) presents the force-displacement relationship at one point at the red zone shown on Figure C.19. This shows that the relation is not-linear.

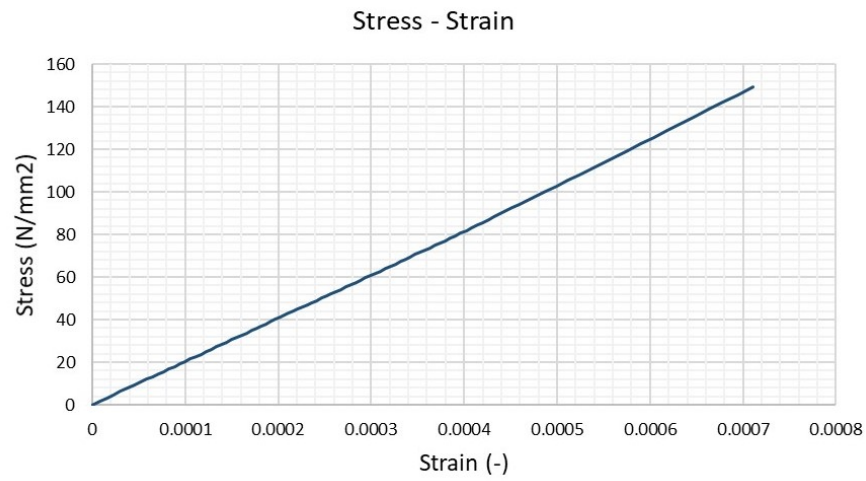


Figure C.22: Von Mises stresses vs strain at retaining unit.

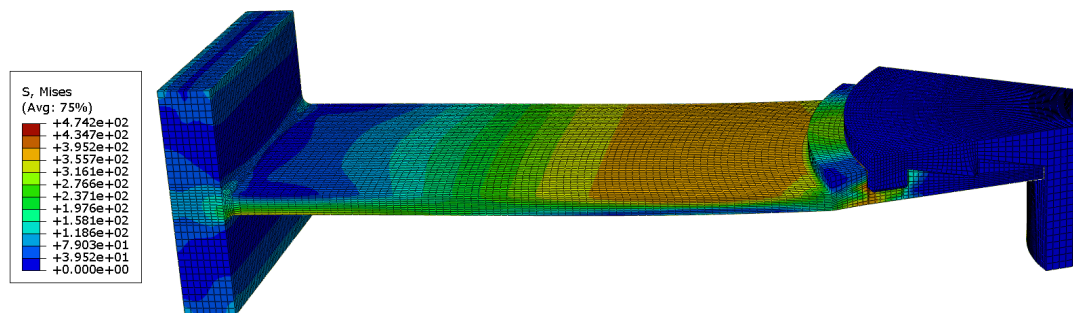


Figure C.23: Von Mises stress distribution ( $kN/m^2$ ) of the innovative connection at a compressive load of 92 kN.

## C.6 INPUT DATA FOR MATERIAL MODELS IN ABAQUS

### c.6.1 Assembly phase: sliding insertion

#### Assembly phase: Sliding insertion

```

** MATERIALS

*Material, name="Steel Bilinear"

*Density

7.85e-09,

*Elastic

210000., 0.3

*Plastic

355., 0.

547.6, 0.0686

** INTERACTION PROPERTIES

*Surface Interaction, name=IntProp-1

1.,

*Friction, slip tolerance=0.005

0.4,

*Surface Behavior, pressure-overclosure=HARD

** INTERACTIONS

** Interaction: Int-1

*Contact Pair, interaction=IntProp-1, type=SURFACE TO SURFACE

SlaveSurf, MasterSurf

** -----

** STEP: Step-1

*Step, name=Step-1, nlgeom=YES, inc=1000

*Dynamic,application=QUASI-STATIC,initial=NO

0.001,0.11,1.1e-06

** BOUNDARY CONDITIONS

** Name: BC-4 Type: Displacement/Rotation

*Boundary, amplitude=Amp-1

_PickedSet15, 1, 1, 50.02

```



### c.6.2 Usage phase: retention to axial tensile forces

#### Usage Phase: Axial tensile forces retention

```

** MATERIALS

*Material, name="Steel Bilinear"

*Density

7.85e-09,

*Elastic

210000., 0.3

*Plastic

355.6, 0.

547.6, 0.0686

** INTERACTION PROPERTIES

*Surface Interaction, name=IntProp-1

1.,

*Friction, slip tolerance=0.005

0.4,

*Surface Behavior, pressure-overclosure=HARD

** STEP: Step-1

*Step, name=Step-1, nlgeom=YES, inc=300

*Dynamic,application=QUASI-STATIC,initial=NO

0.01,1.,1e-05

** LOADS

** Name: Load-1 Type: Concentrated force

*Cload

_PickedSet13, 1, -40000.

```

### c.6.3 Usage phase: retention to axial compressive forces

#### Usage Phase: Axial compressive forces retention

```

** MATERIALS

*Material, name="Steel Bilinear"

*Density

7.85e-09,

*Elastic

210000., 0.3

*Plastic

355., 0.

547.6, 0.0686

** INTERACTION PROPERTIES

*Surface Interaction, name=IntProp-1

*Friction, slip tolerance=0.005

0.4,

*Surface Behavior, pressure-overclosure=HARD

** INTERACTIONS

** Interaction: Int-1

*Contact

*Contact Inclusions, ALL EXTERIOR

*Contact Property Assignment, , IntProp-1

*Surface Property Assignment, property=GEOMETRIC CORRECTION

** STEP: Step-1

*Step, name=Step-1, nlgeom=YES, inc=1000

*Static

0.01, 1., 1e-05, 0.01

** LOADS

** Name: Load-1 Type: Concentrated force

*Clload, amplitude=Amp-1

_PickedSet12, 1, 80000.

```

